



universität
wien

MASTERARBEIT / MASTER'S THESIS

Titel der Masterarbeit / Title of the Master's Thesis

„Dissecting the molecular mechanism of the KLMT-1/KSS-1 TA element in the nematode *C. tropicalis*“

verfasst von / submitted by

Daniel Ciro Krogull, BSc

angestrebter akademischer Grad / in partial fulfilment of the requirements for the degree of
Master of Science (MSc)

Wien, 2021 / Vienna, 2021

Studienkennzahl lt. Studienblatt /
degree programme code as it appears on
the student record sheet:

UA 066 877

Studienrichtung lt. Studienblatt /
degree programme as it appears on
the student record sheet:

Masterstudium Genetik und
Entwicklungsbiologie

Betreut von / Supervisor:

Dr. Alejandro Burga

Table of contents

1. Abstract	4
1.1. Abstract (in german)	5
2. Introduction	6
2.1. Toxin-Antidote Elements	6
2.2. Discovery of <i>klmt-1/kss-1</i> TA element in <i>C. tropicalis</i>	7
2.3. <i>klmt-1</i> evolved from a highly conserved essential gene	10
2.4. <i>kss-1</i> is a putative F-box protein	11
2.5. Working model for the <i>klmt-1/kss-1</i> TA element	12
2.6. Aims	12
3. Methods	15
3.1. Strains	15
3.2. Generation of transgenic lines	15
3.3. Crosses and genotyping	15
3.4. Single-molecular Fluorescence <i>in situ</i> Hybridization	16
3.5. Immunofluorescence	17
3.6. Imaging	17
3.7. Synchronization of <i>fars-1::FLAG C. tropicalis</i>	17
3.8. Protein extraction	18
3.9. Western blotting	19
3.10. Plasmid construction	19
3.11. Yeast transformation	20
3.12. Galactosidase assay	20
3.13. Serial dilution – Spot assay	21
3.14. Growth analysis of <i>klmt-1</i> expression in yeast	21
3.15. Heat-shock induction for <i>klmt-1</i> overexpression in <i>C. elegans</i>	21
4. Results & Discussion	22
4.1. Expression pattern and protein interaction network of <i>klmt-1/kss-1</i> TA element	22
4.1.1. Expression pattern of KLMT-1 <i>in vivo</i>	22

4.1.2. Expression pattern of KSS-1 <i>in vivo</i>	31
4.1.3. FARS-1 short-isoform is sufficient for KLMT-1 to fulfil its toxic effect	32
4.1.4. KSS-1 might be involved in KLMT-1 degradation	35
4.1.5. Characterization of protein-protein interaction using a Yeast-2-Hybrid system	38
4.2. Aim 2: Specificity and evolutionary conservation of KLMT-1 toxicity	42
4.2.1. Can KLMT-1 kill <i>C. elegans</i>	42
4.2.2. Can KLMT-1 kill <i>Saccharomyces cerevisiae</i>	44
5. Conclusion & future directions	48
6. Acknowledgement	52
7. References	53
8. Supplementary Data	57

1. Abstract

Selfish genetic elements are genomic regions that promote their own transmission despite being neutral or even harmful to the individual. Toxin-antidote (TA) elements are a class of selfish elements that cause post-segregation distortion, subverting the Mendelian laws of segregation. TA elements comprise two tightly linked genes: a toxin and its cognate antidote. The toxin is expressed in a gamete (either oocyte or sperm) whereas the antidote is only zygotically expressed. In a maternal-effect TA element, the toxin is deposited into all the oocytes prior to fertilization irrespective of their genotype. However, only embryos that inherit at least one copy of the TA element can express the antidote and counteract the deadly effect of the toxin. Thus, a single maternal-effect TA element can cause embryonic lethality in up to 25% of the F2 progeny and selectively eliminate homozygous non-carriers (Fig. 1). In this way, TA elements quickly spread in natural populations, a phenomenon known as gene drive activity.

TAs are common in prokaryotes, but only a few examples are known in animals. For almost a decade, only two TAs have been dissected in animals, a paternal-effect element in *Caenorhabditis elegans* and a maternal-effect element in the beetle *Tribolium* (1)(2). Recently, we identified five novel maternal-effect TA elements in *Caenorhabditis tropicalis* that were characterized in depth using Near-Isogenic Lines (NILs). Unfortunately, the molecular underpinnings of all known eukaryotic TAs are still largely unknown, which limits our understanding of this class of selfish elements.

To investigate the molecular mechanism of TA elements, I focussed on one of the five TA elements recently discovered in *C. tropicalis* which is called *klmt-1/kss-1*. In this thesis, I provide first insight into the expression pattern, subcellular localization and protein-protein interactions of the *klmt-1/kss-1* TA in *in vivo*. Additionally, I investigate the specificity of KLMT-1 toxicity in *C. elegans* and *Saccharomyces cerevisiae*.

Keywords: selfish genetic element, toxin-antidote, maternal-effect TA

1.1. Abstract (german Version)

Egoistische genetische Elemente sind genomische Regionen, die ihre eigene Übertragung fördern, obwohl sie neutral oder sogar schädlich für das Individuum sind. Toxin-Antidot (TA)-Elemente sind eine Klasse egoistischer Elemente, die eine Verzerrungen in der Segregation verursachen und die Mendelschen Segregationsgesetze untergraben. TA-Elemente umfassen zwei eng miteinander verbundene Gene: ein Toxin und sein verwandtes Gegenmittel. Das Toxin wird in einem Gameten (entweder Eizelle oder Sperma) exprimiert, während das Gegenmittel nur zygotisch exprimiert wird. In einem TA-Element mit maternaler Wirkung wird das Toxin vor der Befruchtung unabhängig von ihrem Genotyp in allen Eizellen abgelagert. Nur Embryonen, die mindestens eine Kopie des TA-Elements erben, können das Gegenmittel exprimieren und der tödlichen Wirkung des Toxins entgegenwirken. Somit kann ein einzelnes TA-Element mit maternaler Wirkung bei bis zu 25% der F2-Nachkommen embryonale Letalität verursachen und homozygote Nicht-Träger selektiv eliminieren (Abb. 1). Auf diese Weise breiten sich TA-Elemente schnell in natürlichen Populationen aus, ein Phänomen, das als Gen-Drive-Aktivität bekannt ist.

TAs sind bei Prokaryoten häufig, bei Tieren sind jedoch nur wenige Beispiele bekannt. Seit fast einem Jahrzehnt wurden nur zwei TAs bei Tieren präpariert, ein väterlich wirkendes Element in *C. elegans* und ein mütterlich wirkendes Element im Käfer *Tribolium* (1,2). Kürzlich haben wir fünf neuartige TA-Elemente mit maternaler Wirkung in *C. tropicalis* identifiziert, die mithilfe von Near-Isogenic Lines (NILs) eingehend charakterisiert wurden. Leider sind die molekularen Grundlagen aller bekannten eukaryotischen TAs noch weitgehend unbekannt, was unser Verständnis dieser Klasse egoistischer Elemente einschränkt.

Um den molekularen Mechanismus von TA-Elementen zu untersuchen, habe ich mich auf eines der fünf kürzlich in *C. tropicalis* entdeckten TA-Elemente konzentriert, das *klmt-1/kss-1* genannt wird. In dieser Arbeit gebe ich erste Einblicke in das Expressionsmuster, die subzelluläre Lokalisation und die Protein-Protein-Interaktionen der *klmt-1/kss-1* TA *in vivo*. Zusätzlich untersuche ich die Spezifität der KLMT-1-Toxizität in *C. elegans* und *Saccharomyces cerevisiae*.

Stichwörter: Egoistische genetische Elemente, Toxin-Antidot Element, TA-Element mit maternaler Wirkung

2. Introduction

2.1. Toxin-Antidote Elements

Selfish genetic elements are genomic regions that can enhance their own transmission at the expense of other genes in the genome, despite being neutral or harmful to the individuals fitness (3)(4)(5). Among them are autonomously replicating elements (transposons), segregation distorters (meiotic drive chromosomes) and post-segregation distorters, such as the *Medea* locus of many insect which kills its progeny that do not inherit the allele (6)(7)(8)(2). As a consequence of their selfish behaviour, they create a genetic conflict that causes hybrid dysgenesis, sterility, and genetic incompatibility in the wild (9)(10)(11). Selfish elements are a universal feature of genomes, yet we know surprisingly little about their molecular diversity, molecular mechanisms and their contribution to evolution.

Toxin-antidote elements (TAs) are an extreme example of selfish elements, subverting the laws of Mendelian segregation by killing non-carrier individuals. TAs comprise two tightly linked genes: a toxin and its cognate antidote. The toxin is expressed in a gamete (either oocyte or sperm) whereas the antidote is only expressed zygotically. In a maternal-effect TA element, the toxin is deposited into all the oocytes prior to fertilization irrespective of their genotype and kills or impairs the development of individuals. However, only embryos that inherit at least one copy of the TA element can express the antidote and counteract the deadly effect of the toxin. Thus, a single maternal-effect TA element can cause embryonic lethality in up to 25% of the F2 progeny and selectively eliminate homozygous non-carriers (Fig.1). Thus, TA elements quickly spread in natural populations, a phenomenon known as gene drive activity (12)(4).

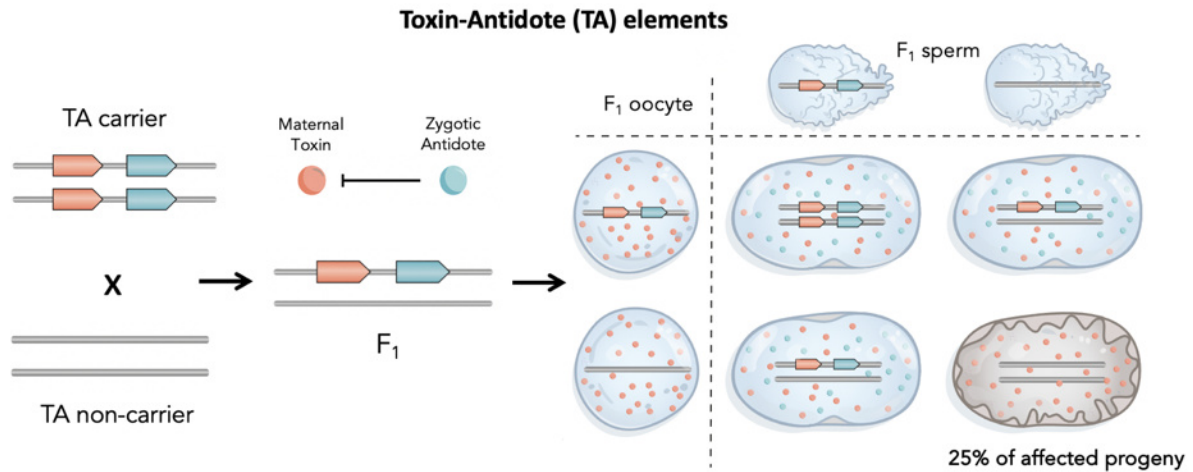


Figure 1. Inheritance model for a maternal-effect Toxin-Antidote element (TA). (A) Parental carrier and noncarrier strains and their F₁ hybrid are perfectly healthy. (B) The genetic incompatibility only becomes visible in homozygous non-carriers in the F₂ generation. Punnett square depicting a cross between heterozygous individuals. The toxin (orange circle) is expressed in the germline and deposited into all eggs, whereas its antidote (cyan circle) is only expressed zygotically. Up to 25% of F₂ progeny is affected because they do not express the antidote.

Although TAs have long been recognized in prokaryotes (Toxin-Antitoxin), only a few examples are known in animals (13). For almost a decade, only two TAs were known in animals, a paternal-effect element in *C. elegans*, *peel-1/zeel-1*, and a maternal-acting element in the beetle *Tribolium* (14)(2)(15). The idea that TAs were rare in animals was recently challenged by our group (16)(17). First, we identified a second TA in *C. elegans*, the maternal-effect *sup-35/pha-1* TA, which was mischaracterized as an developmental gene for over 25 years because *pha-1*, the zygotic antidote, was proposed to be an organ-specific differentiation gene (16)(1). Second, we discovered a total of five maternal-effect TAs in *C. tropicalis* and one in *C. briggsae*, two hermaphroditic relatives of *C. elegans* (16)(17). Based on these recent discoveries, we hypothesize that this largely uncharacterized class of selfish elements may in fact be common in nature and play important roles in evolution (18).

2.2. Discovery of *klmt-1/kss-1* TA element in *C. tropicalis*

In this study, we focus on one particular TA element, consisting of the toxin *klmt-1* (for Killer of embryos and Larvae Maternal Toxin) and the antidote, *kss-1* (for Klmt rescue by zygotically expreSsed antidote), being one of the five TA elements found in the nematode species, *C. tropicalis*. *C. tropicalis* is found exclusively in tropical regions worldwide and is distantly related to *C. elegans* (Fig. 2A). The genome sequences of the two species are as divergent as

those of humans and mice (20). Although the development of *C. tropicalis* is comparable to *C. elegans*, it prefers a temperature of 25°C and only takes ~48h to develop from egg to adult stage. Like *C. elegans*, *C. tropicalis* has independently evolved hermaphrodites that self-fertilize but can also mate with males, which makes them a good genetic model system to study in the lab (19). Previous research found that *C. tropicalis* isolates from different geographical locations are more likely to generate defective offspring compared to those between isolates from the same location (21). In a cross between two wild isolates of *C. tropicalis*, NIC203 (Guadalupe) and EG6180 (Puerto Rico) (Fig. 2B), the *klmt-1/kss-1* TA was identified together with four additional TAs and fine-mapped using Near-Isogenic Lines (NILs) (16). NILs are strains which genetic makeups are identical except for one or a few specific locations or genetic loci (22) and can be created by multigenerational backcrosses (Fig. 2C). Using the advantage of the inherent gene-drive activity of selfish elements, the locus of the *klmt-1/kss-1* TA was mapped by backcrossing hybrid hermaphrodites of a cross between NIC203 and EG6180 to EG6180 males (17)(23). This backcross was performed for 19 generations, before the genome of the resulting strain was sequenced (Fig. 2B) (17). As a result, a NIL was obtained with the genetic background of EG6180 but with the exception of three introgressions on three different chromosomes (Chr. II; III; V) coming from the strain NIC203 (17). In order to test whether multiple TAs are present in the cross, additional NILs were generated, each NIL carrying only one of the introgressions of NIC203 (NIL-Chr. II; NIL-Chr. III; NIL-Chr. V), which was confirmed by whole-genome sequencing (17). To identify the genes underlying the TA in the NIL-Chr. V (QX2343), knockouts of specific candidate genes were performed that were missing in EG6180 using CRISPR-Cas9 (unpublished results) (24). Mutant NIL hermaphrodites were then crossed to EG6180 males and their F2 progeny characterized. We found that introducing a frameshift mutation in a single gene (which we named *klmt-1*) was sufficient to abolish the toxic activity of the TA, resulting in the reduction of affected worms from 27.7% to 0% (Fig. 3A cross 3 & 4). Finally, by knocking out candidate genes for the antidote in the background of the *klmt-1* mutant, we found a gene which we named *kss-1* that turns the NIC203 allele into a EG6180-like susceptible allele (cross 5) (17). The *klmt-1/kss-1* TA is located on the left arm of NIC203 Chr. V (qqIR47 (V:1.3-1.8 Mb; NIC203 > EG6180)) and induces embryonic lethality and early larval arrest in ~25% of F2 worms, which indicates a fully penetrant TA element (27.7% lethality, n=542; Fig. 3A, cross 3) (Fig. 2D, 3) (17). Genotyping of the F2 progeny confirmed that only homozygous individuals for the

EG6180 allele were affected by the toxin (Fig. 3A). As a negative control, only background levels of lethality were observed in both parental strains (2.5% for NIL, n=120, and 3.4% for EG6180; Fig. 3A, cross 1 & 2). Additionally, by performing maternal and paternal backcrosses, the NIL carrying the *klmt-1/kss-1* TA was found to be a maternal-effect TA (17).

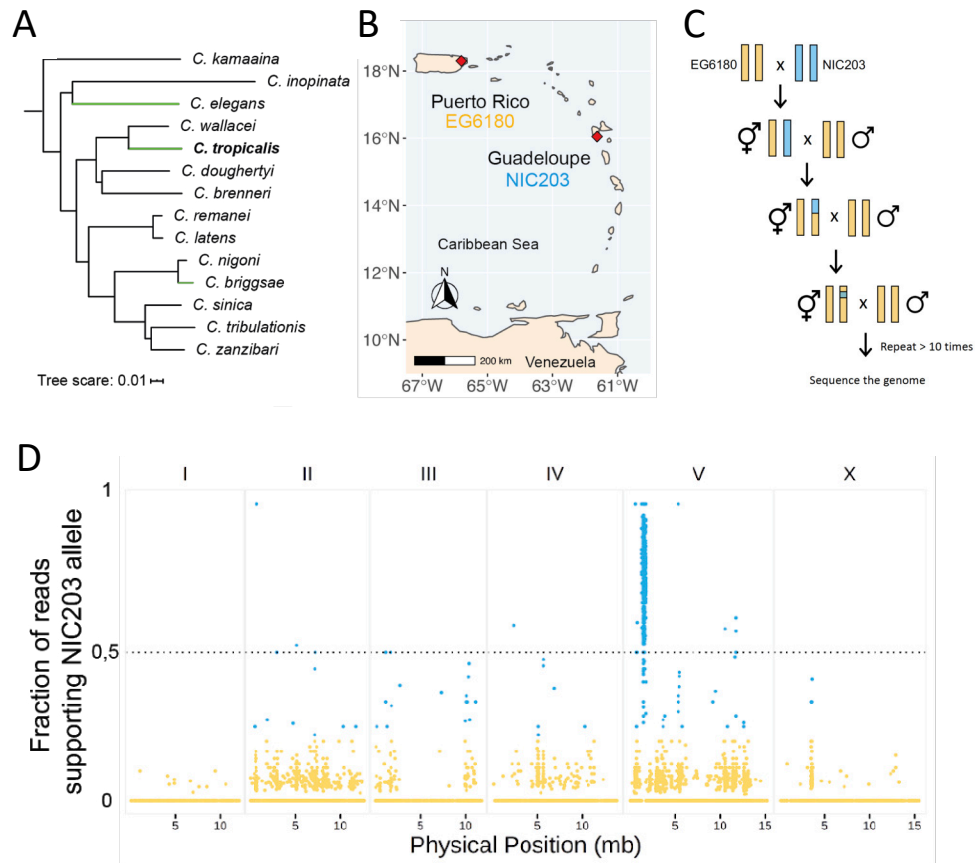


Figure 2. (A) Phylogenetic tree of *Ceanorhabditis* species (20). (B) Geographical localization of two neutral *C. tropicalis* isolates: NIC203 and EG6180. (C) Schematic representation of the multigenerational backcross between EG6180 and NIC203, resulting in a NIL. (D) Whole genome sequencing of the Near-Isogenic Line (NIL) carrying a 500kb Chr. V introgression of NIC203 (blue) into EG6180 background (yellow). Adapted from Ben-David et. al. 'Ubiquitous Selfish Toxin-Antidote Elements in *Caenorhabditis* Species'.

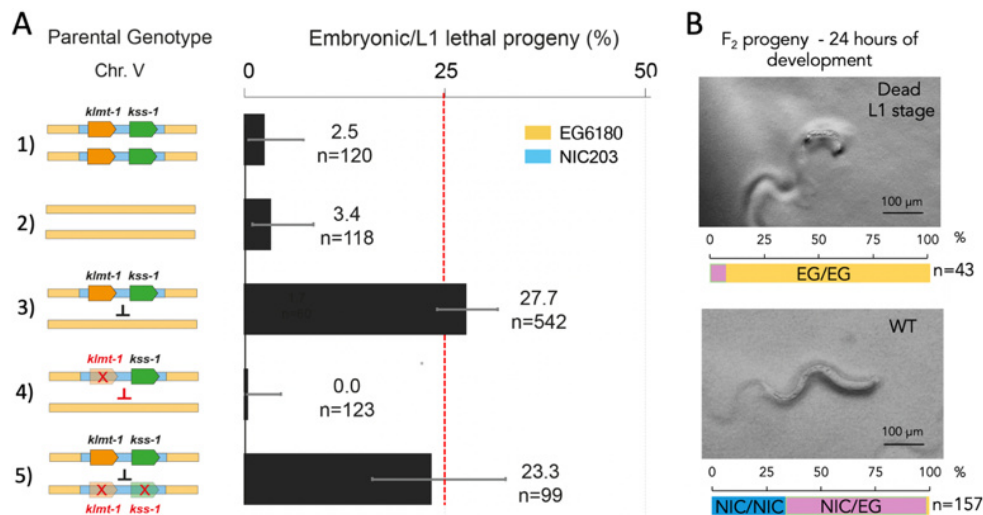


Figure 3. Genetic dissection of the *klmt-1/kss-1* locus in *C. tropicalis*, a novel maternal-effect TA element. (A) NIL carrying introgression of NIC203 (blue) into EG6180 background (yellow) shows only background levels of embryonic/L1 lethality (cross 1). No lethality is observed in the EG6180 strain either (cross 2), but ~25% of their F₂ cross- progeny is affected (cross 3). A knockout of *klmt-1* in the NIL background is sufficient to completely abrogate the toxicity (cross 4). Knocking out *kss-1* in the background of the *klmt-1* mutant turns the NIC203 allele into a EG6180-like susceptible allele (cross 5). Dotted red line denotes expected lethality (25%) for a TA element. (B) Genotyping of F₂ progeny (cross 3) confirmed that homozygous (NIC/NIC) and heterozygous (NIC/EG) carriers are healthy and the vast majority of homozygous non-carriers (EG/EG) die (17).

2.3. *klmt-1* evolved from a highly conserved essential gene

To investigate if the toxin *klmt-1* has homology to known proteins, we performed a protein sequence conservation analysis using BLAST (504-aa). We found that *klmt-1* shows homology to *fars-3* (Supplementary Fig. 1). The gene *fars-3* codes for the beta subunit of the phenylalanine tRNA synthetase (PheRS) complex. The PheRS belongs to the family of aminoacyl tRNA synthetases (aaRS), which are important enzymes that charge tRNAs with their cognate amino acid, a key process for protein translation. While most aaRS are monomeric, the cytoplasmic PheRS is a heterotetrameric protein consisting of two alpha (α) and two beta (β) subunits responsible for charging tRNA^{Phe} during translation (25). The α -subunit is the catalytic core of the PheRS, and the β -subunit has structural modules with a wide range of functions, including tRNA anti-codon binding, hydrolysing mis-activated amino acids and editing of misaminoacylated tRNA^{Phe} (25)(26)(27). Importantly, both subunits are needed for aminoacylation of tRNA^{Phe} and are remarkably conserved in evolution (28). In nematodes the two subunits are encoded by the genes *fars-1* and *fars-3*, respectively (Fig. 4), which are known as *FARSA* and *FARSB* in vertebrates while in yeast they are known as *FRS1* and *FRS2* (29)(30).

The homologous region to *fars-3* is located in the central region of KLMT-1 with 52% identity. We additionally used a protein structure prediction tool (IUPred2A) to gain further insights into its structure. We found that both the N-terminal sequence from 1-51 amino acids (aa) residues based on ANCHOR2 or 1-82-aa based on IUPred and the C-terminal sequence from 430-504-aa based on ANCHOR2 or 457-504-aa based on IUPred of KLMT-1 protein sequence are predicted to be intrinsically disordered (Fig. 5A). IUPred2A is a combined prediction tool designed to discover intrinsically disordered or conditionally disordered proteins and protein regions (31)(32). While IUPred is a tool used to predict protein disorder based on the assumption that disordered regions are composed of amino acids that cannot form favourable interactions with each other, the ANCHOR method recognizes specific regions that undergo disorder-to-order transition upon binding (33)(34). These Intrinsic disordered protein regions (IDPR) usually lack a fixed or ordered three-dimensional structure (35) but may play an important role for the function of the toxin KLMT-1. Many IDPRs can adopt a fixed three-dimensional structure after binding to other macromolecules, being targets for post-translational modifications (PTMs), resulting in protein degradation or allow their binding partner to induce larger conformational changes by a long-range allosteric interaction (36)(37). How this affects the enzymatic properties of KLMT-1 is still unknown. Given the sequence similarity to *fars-3*, our hypothesis is that *klmt-1* exerts its toxic activity by interfering with the correct function of the PheRS complex (Fig. 5C, Supplementary Fig. 1), and this may involve modifications on the IDPRs.

2.4. *kss-1* is a putative F-box protein

The antidote gene *kss-1*, codes for a 389-aa protein. Domain conservation analysis using Phyre² analysis revealed the presence of a F-box domain on the N-terminal region (Fig. 5B). In addition, we performed an InterPro analysis which predicted the presence of an F-box-associated (FBA) domain in the central region of the protein, which is commonly associated to F-box proteins in nematodes (Fig. 5). F-box proteins play an important role as components of the SCF ubiquitin-ligase (E3) complex (Fig. 5D), which is named after their main components, Skp1, Cullin, and a F-box protein (38). F-box proteins have a dual function: they interact with substrates and bind to the protein Skp1 through their F-box motif, resulting in ubiquitin-mediated proteolysis of the substrate in the SCF complex (39).

2.5. Working model of the *klmt-1/kss-1* TA element

Taken together, our working model is that the toxin KLMT-1 is maternally deposited into the oocytes and after fertilization its toxicity is driven by disrupting the PheRS enzymatic activity. The antidote, KSS-1, binds KLMT-1 as part of the SCF complex and mediates its ubiquitination, which then triggers proteasomal degradation (Fig. 4, 5D). The fact that *klmt-1/kss-1* evolved from a highly conserved and well characterized enzyme and that the antidote is potentially involved in the ubiquitin-mediated degradation pathway, makes this TA element a suitable system to dissect the molecular mechanism of a eukaryotic TA for the first time.

2.6. Aims

The recent discoveries of TA elements in fungi, insects, plants and nematode, including the TA elements found by our group, indicate that TA elements could be common in nature and could play important evolutionary roles (18). Unfortunately, the molecular underpinnings of all known eukaryotic TAs are still largely or completely unknown, which severely limits our understanding of this fascinating class of selfish elements. Specially the lack of homology to well-studied proteins makes them a very challenging subject to study. Therefore, it is important to understand the molecular mechanism, which will greatly facilitate our understanding of their ability to induce developmental defects, gene drive activity and contributions to evolution of genes and speciation. The aim of this thesis was to gain insight and delineate the expression pattern and protein interaction network of the *klmt-1/kss-1* TA element. We expect that our experiments will make a significant contribution towards a detailed molecular understanding of an animal TA element and paves the way for future investigations. The second aim of this thesis was to investigate the specificity of the toxin *klmt-1* in different species. Together with the ability of selfish elements to spread in populations, this could serve as a fundament of a new synthetic drive element that controls vector-borne diseases, such as malaria.

To validate our TA model for the *klmt-1/kss-1* TA element and gain insights into its molecular mechanism, we set out to examine its expression pattern, subcellular localization and protein-protein interaction in *C. tropicalis in vivo*. To do so, we implemented single molecular

fluorescence in situ hybridization (smFISH), immunofluorescence (IF) staining and time-lapse imaging to dissect the spatiotemporal expression pattern of the toxin KLMT-1 in embryos and the mechanism of its cognate antidote KSS-1. Furthermore, using yeast-two-hybrid assay (Y2H) we investigated the interactome and important protein domains of the TA element with its putative targets FARS-1 and SCF complex, respectively. In addition, we provide first insights into the specificity of KLMT-1 toxicity in other species by inducing overexpression of KLMT-1 in *S. cerevisiae* and *C. elegans*.

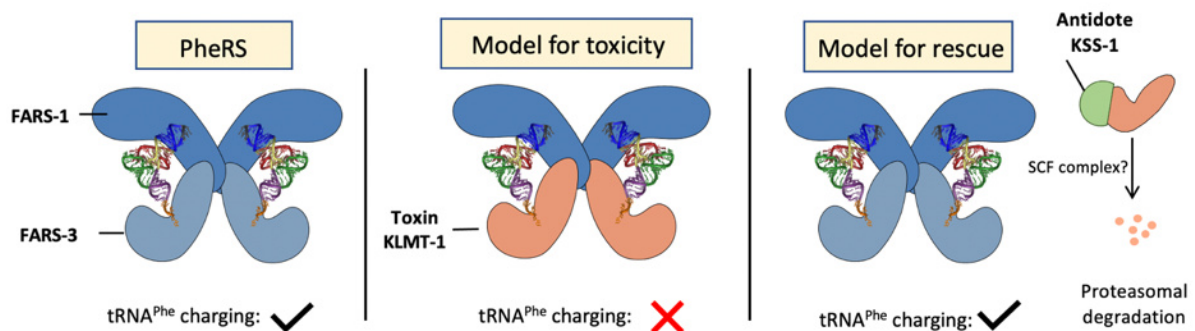
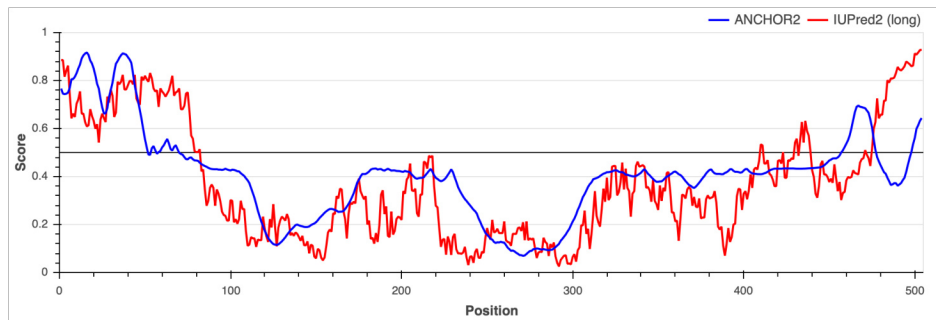


Figure 4. Working model for the molecular mechanism of *klmt-1/kss-1*. The native *PheRS* is a heterotetramer made up of two *FARS-1* and two *FARS-3* subunits (left). We hypothesize that in the presence of the toxin *KLMT-1*, a *FARS-3* paralog, the activity of the native *PheRS* is compromised, likely due at least in part to interactions between *KLMT-1* and *FARS-1*. As a consequence, charging of $tRNA^{Phe}$ with its cognate amino acid could be impaired or alternatively, it could cause a drastic increase of miss charging errors (middle). We propose that the antidote, *KSS-1*, binds to *KLMT-1* and targets it for ubiquitin-mediated protein degradation (right). *KSS-1* is predicted to have an F-box domain at its N-terminus, which likely links it to the SCF ubiquitin complex.

A**B****Phyre² domain prediction of KSS-1**

#	Template	Alignment Coverage	3D Model	Confidence	% i.d.	Template Information
1	c5vztB_	Alignment		88.5	22	PDB header: cell cycle Chain: B; PDB Molecule: f-box only protein 31; PDBTitle: crystal structure of the skp1-fbx31 complex
2	d2ovrb1	Alignment		88.0	11	Fold: F-box domain Superfamily: F-box domain Family: F-box domain
3	d1p22a1	Alignment		86.1	11	Fold: F-box domain Superfamily: F-box domain Family: F-box domain

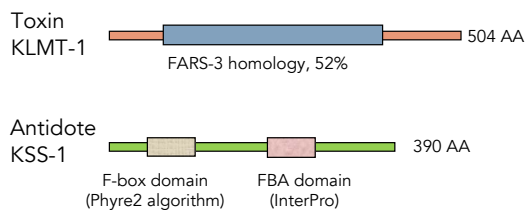
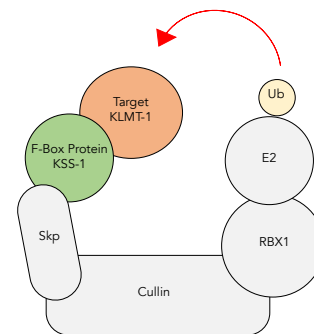
InterPro prediction of KSS-1**C****D**

Figure 5. (A) The toxin, KLMT-1 is homologous to FARS-3, a beta-subunit of Phenylalanine-tRNA-Synthetase complex (PheRS). A score higher than 0.5 indicates predicted intrinsically disordered regions (IDRs) (y-axis) across the amino acid sequence length of the protein (x-axis). (B) Screenshot showing the results of Phyre² and InterPro domain prediction of KSS-1 which is predicted to have a F-box associated (FBA) domain in the center and a predicted F-box domain located at its N-terminus, which is a common feature of E3 ubiquitin ligase adaptors. (C) Schematic representation of the sequence conservation analysis of KLMT-1. Schematic representation of the protein domain prediction analysis of KSS-1. (D) Schematic representation of SCF ubiquitin ligase (E3) complex which mediates ubiquitination of KLMT-1, which is targeted for degradation through KSS-1.

3. Methods

3.1. Strains

All experiments were carried out at 20°C for *C. elegans* and 25°C *C. tropicalis* unless specified in the text. Strains were grown on modified nematode growth medium (NGM) containing *E. coli* OP50, and 1% agar/0.7% agarose to prevent burrowing of wild isolates using standard culturing techniques developed for *C. elegans*. A list of all the strains used and generated in this study is available in Supplementary Table 1 and 9. Some of the strains were provided by the CGC, which is funded by the NIH Office of Research Infrastructure Programs (P40 OD010440).

3.2. Generation of transgenic lines

To generate *C. tropicalis* mutants (Supplementary Table 1), we used the CRISPR/Cas9 ribonucleoprotein (RNP) complex injection protocol developed by Dokshin et al for *C. tropicalis*. We incubated 15 pmol of Cas9 (0.5 µl of Alt-R Cas9 from IDT) with 4.45 nM modified synthetic single guide RNA (sgRNA) (Synthego) for 10 minutes in 37°C for 10 minutes. To the assembled RNP we then added 2.5 ng/µl of pCFJ90 plasmid as a co-injection marker and injected young adult hermaphrodites. For ORF010079 we also included 2.2 ng/µl of a single-stranded oligonucleotide donor (ssODN) repair template that introduced a stop-codon and a frameshift. We singled F1 mCherry positive fluorescent worms and screened their progeny for random frameshift deletions or homology-directed repair events by Sanger sequencing.

3.3. Crosses and genotyping

We set up crosses in 12-well plates. Typically, 5 hermaphrodites were mated with at least 5-fold excess males. After 3 days, 10 F1 L4 hermaphrodites were placed into individual 5 cm plates. On day 4, once F1 hermaphrodites were fully gravid, they were transferred into fresh 5-cm plates and allowed to lay eggs for 4-5 hours. Then, we collected 10 F2 embryos per F1 hermaphrodites. Each embryo was placed in a single 5 cm plate, which allowed us to reliably score post-embryonic phenotypes. Once F2 embryos were collected, we genotyped their mothers, and only included in our final analysis true F1 mothers and their progeny and not those that originated from self-fertilization of the original hermaphrodite. We scored the phenotype of F2 progeny every 24 hours typically for 5-9 days depending on the cross. Plates

that initially contained a single phenotypically WT F2 hermaphrodite starved after 6-7 days. Following phenotyping, we genotyped each worm by PCR using indels (Supplementary Table 13).

3.4. Single-molecule Fluorescence in situ Hybridization

With the help of the Stellaris RNA FISH Probe Designer (Biosearch Technologies, Inc., Petaluma, CA), custom Stellaris FISH Probes were designed against *klmt-1* by, available online at www.biosearchtech.com/stellarisdesigner. Following the manufacturer's instructions available online at www.biosearchtech.com/stellarisprotocols the samples were hybridized with the *klmt-1*. The protocol was adapted from Raj et al (40).

One plate of gravid hermaphrodites was used for fixation. Worms were washed with M9 buffer (3 g KH₂PO₄, 6 g Na₂HPO₄, 5 g NaCl, 1 M MgSO₄ in 1l H₂O) and transferred to a 15 ml conical tube. After centrifugation (1000 rpm for 1 min) and aspiration of the M9, bleaching solution (250 ul 1M NaOH and 250 ul bleach) was added. The tubes were approximately 4 min incubated and frequently vortexed until the worms dissolved, and only embryos remained. After centrifugation and aspiration of the supernatant, the samples were washed twice with M9 before fixation buffer (3.7% formaldehyde in 1X PBS) was added. The samples were incubated for 15 min at room temperature, followed by freezing in liquid nitrogen for at least 2 min. The samples were thawed in water and incubated for 20 min on ice. After two washes with 1X PBS, the remaining PBS was discarded, and 70% ethanol was added. The samples were incubated overnight at 40C. The next day, the ethanol was removed and followed by a 5 min wash with Wash Buffer A (10% formamide in 1X Stellaris RNA FISH Wash Buffer A). Then, Wash Buffer A was aspirated and 100 ml Hybridization Buffer (10% formamide in Stellaris RNA FISH Hybridisation Buffer) containing 125 nM probe was added to the samples. These samples were incubated for 16 hours at 37°C. The following day, samples were incubated for 30 min with Wash Buffer A at 37°C. To stain the nuclei, we used DAPI solution (Wash Buffer A consisting of 5 ng/mL DAPI (D9542, Sigma-Aldrich)) which was added to the samples and incubated for 30 min at 37°C. After removing the DAPI solution one additional wash-step was performed using Wash Buffer B for 5 min. Finally, the embryos were added onto a microscopy slide containing a drop of mounting medium (Fluoroshield F6182, Sigma-Aldrich) and sealed with a coverslip.

3.5. Immunofluorescence

To stain embryos and gonads, adult hermaphrodites were dissected and embryos/gonads were transferred into a drop of M9 buffer on poly-l-lysine coated slides, freeze-cracked in liquid nitrogen, and fixed by incubating slides in ice cold methanol for 15min and acetone for 10min. Embryos and gonads were rehydrated in a series of ethanol dilutions (95%, 70%, 50%, 30%, PBS), each step for 5 min. Slides were blocked with PBST (PBS + 0.1% Triton-X 100) containing 3% BSA for 1 hour at RT, and subsequently incubated overnight on 4°C either with monoclonal anti-FLAG (F1804 - Monoclonal ANTI-FLAG® M2 antibody, Sigma-Aldrich) antibody, diluted (1:1000) in PBST+ 3% BSA or monoclonal anti-KLMT-1 antibody, diluted (1:100) in PBST+ 3% BSA. After primary antibody incubation, slides were washed three times in PBST and incubated with Alexa568-labeled anti-mouse (1:1000) (Jackson ImmunoResearch) for 2 h, diluted in PBST+3% BSA. Slides were washed again three times in PBST. Before the last washing step, 1,5 ul DAPI was added into 150ml PBST washing buffer. Finally, slides were mounted in Vectashield mounting media.

3.6. Imaging

To image Immunofluorescence labeled probes, an Axio Imager.Z2 (upright) with sCMOS camera (Hamamatsu Orca Flash 4), AxioCam colour camera and a 63x/1.4 plan-apochromat Oil DIC objective was used (lenses used: Ex 470/40nm, Em 525/50nm; Ex 436/25nm, Em 480/40nm). Quantification was performed using R-studio.

Time-lapse imaging was performed by dissecting adult hermaphrodites to extract embryos. Embryos were transferred into an 8-well chambered cover-glass (Thermo Fisher), containing M9 buffer. Within the Celldiscoverer 7 (ZEISS), worms were incubated at 25°C and images were taken using 25x magnification for 12 hours.

3.7. Synchronization of *fars-1::FLAG C. tropicalis*

The bleaching technique is used for synchronizing *C. elegans* cultures at the first larval stage (L1). After treatment with alkaline hypochlorite solution, embryos are incubated in liquid media without food, which allows hatching but prevents further development. Worms were collected in 15 ml tubes by washing plates with M9 Buffer. Afterwards worms were pelleted by centrifuging for 1 minutes 1000 rpm at room-temperature and the supernatant was discarded. The wash steps were performed 2 additional times until the buffer appears clear

of bacteria. To start the bleaching reaction, 750 ul M9 buffer, 250 ul 1M NaOH and 250 ul bleaching solution (3:1:1 ratio) were added, shortly mixed by vortexing and incubated for 4 minutes (destruction of the adult tissue should be monitored under the dissecting microscope and the reaction stopped when traces of adults are still visible, which typically takes between 3 and 9 minutes depending on several issues, such as the volume of worm pellet). Bleached worms were quickly centrifuged (since treatment may still be active) for 1 minute at 1000 rpm and the supernatant was discarded. To stop the reaction, M9 buffer was added to fill the tube. Eggs were washed as previously described for three more times with M9 buffer. To start starvation, we incubated the eggs in M9 Buffer for several hours in 15ml falcons. The falcon tube was only filled up to 6-7ml with M9 buffer to leave room for oxygen. Nearly all eggs hatched after incubation for 18 h, on 20°C, shaking 170rpm. 2000-3000 synchronized L1 worms were seeded on plates. Their growth was monitored and samples from different timepoints (5h, 14h, 24h, 40h) after seeding were taken.

3.8. Protein extraction

Worms were grown as previously described. To extract protein from embryos, worms were first synchronized and grown until gravid adult stage. After collecting worms in 15ml tubes they were washed three times with M9 buffer to minimize OP50 contamination. Washing was performed by centrifuging worms for 1min at 1000rpm, discarding the supernatant and adding M9 Buffer to fill the 15ml tube. Then, worms were treated with Alkaline Hypochlorite Solution (Bleach) (41) for 3-5min, depending on the size of pellet. The principle of the method lies in the fact that worms are sensitive to bleach while the eggshell protects embryos from it. Reaction was stopped by adding M9 buffer and subsequently three washing steps were performed. After worms were centrifuged one last time, all but 1ml of the supernatant was discarded and protease inhibitors (Complete EDTA free, 25x) were added. Finally, worms were frozen at -80°C. For a mixed staged population extract, worms were collected in 15ml tubes and washed off from bacteria with M9 buffer as previously described. Then the supernatant was discarded and protease inhibitors (Complete EDTA free, 25x) were added before freezing at -80°C. To disrupt the tissues, worms were unfrozen and transferred to a 1.5ml microcentrifuge tube. Approximately 10 zirconium oxide beads 1.4mm were added to each probe. Homogenization was accomplished by using the Precellys Evolution homogenization (Bertin Instruments). After homogenization, 0,3-1ml protein lysis buffer (20mM Tris pH8.0,

100mM NaCl, 0.05% NP-40, 10% glycerol) was added to each probe, depending on the initial number of worms and incubated for 30min on 4°C using a rotating shaker (15rpm). After lysis buffer incubation, probes were centrifuged at 14000rpm on a table-top centrifuge at +4C for 10min and the supernatant was transferred to new epis. After centrifugation, the supernatant was collected and protein concentration was measured by Bradford method (Bradford 1976) using bovine serum albumin as standard.

Yeast total protein lysate was extracted using a modified version of the technique developed for denatured protein extraction (42). From a fresh yeast culture, cells equivalent of 0.5 to 1 OD600 units were harvested by centrifugation (5000rpm, 3min) and washed with ice-cold water (500 µL). After discarding the supernatant, cell pellets were resuspended with 100 µL water. Then, 100 µL NaOH 0,2M was added following incubation of 10 min at RT. Cells were Centrifuged for 30s at 13000 rpm, supernatant was carefully removed and 200µL of 1x Leammli Buffer was added. Cells were immediately heated at 95°C and 6ul was used for further analysis.

3.9. Western blotting

Between 10-20 µg of proteins were loaded on a 4-16% Bis-Tris protein gel (Thermo Fisher) before they were transferred onto nitrocellulose membrane (BIO-RAD, Hercules, CA). Membranes were blocked for 1 h at room temperature in blocking buffer (TBS + 0.1% Tween-20 + 4% nonfat dry milk), then incubated overnight at 4°C with primary antibodies in blocking buffer. For primary antibodies either monoclonal anti-flag (F1804 - Monoclonal ANTI-FLAG® M2 antibody, Sigma-Aldrich) diluted 1:1000 in blocking buffer or monoclonal anti-KLMT-1 produced in mouse and diluted 1:100 in blocking buffer were used. After extensive washes in 0.1% TBST, membranes were incubated for 1 h at room temperature with goat anti-mouse HRP-conjugated secondary antibody (ThermoFisher Scientific) diluted 1:5000 in blocking buffer. After extensive washes, membranes were processed with chemiluminescent reagent (ECL KIT).

3.10. Plasmid construction

Total RNA was extracted from *C. tropicalis* using and treated with *DNaseI* to eliminate contaminated genomic DNA. To generate cDNA, the region of interests were reverse transcribed using primers shown in Supplementary Table 13. The purified cDNA was

subsequently amplified with corresponding Gibson primers and cloned into respective plasmids (Supplementary Table 7, 8, 11). After Gibson cloning, plasmids were transformed into competent *Escherichia coli*. Dilutions of transformed mixture from 1:10 and 1:100 were spread on LB media (Amp) and incubated at 37°C until colonies appeared. Colonies were genotyped by PCR using primers from Supplementary Table 13 and subsequently checked for their insert sizes using 1% agarose gel electrophoresis. Simultaneously, colonies were inoculated into LB Amp over-night. Over-night cultures were used for Plasmid preparation (MBS facility). Plasmids were sequenced using sanger sequencing.

3.11. Yeast transformation

For Y2H assay, plasmids from Supplementary Table 7 & 8 were transformed into Yeastmaker Gold strain using Matchmaker Gold Yeast Two-Hybrid System (Tanaka Bio USA). Transformed yeast colonies were streaked on synthetically defined (SD) medium lacking tryptophan and leucine (SD/-Trp/-Leu/) and incubated at 30 °C for 3–5 days. Colonies were genotyped using primers shown in Supplementary Table 13 and used for Galactosidase Assay.

Temperature sensitive FRS1-1/FRS1-2 (*YLR060W*) or FRS2 (*YFLO22C*) strains (Supplementary Table 10) were transformed with *pCEV-G2-Km::fars1::fars3* or with *pCEV-G2-Km::fars1::fars3* and *p42Nat::pGal1-10::KLMT-1* and spread on selective YPDA plates (200ug/ml G418; 100ug/ml CloNat) at 30°C for 3-5 days (Supplementary Table 11, 12). Then, colonies were genotyped using primers shown in Supplementary Table 13 and used for serial dilution growth assay.

3.12. Galactosidase assay

6 different colonies were streaked for each transformation. Transformed yeast colonies were streaked on SD/-Trp/-Leu medium but containing X-Gal and Aureobasidin A (SD/-Trp/-Leu/X-Gal/AbA). In terms of measuring a positive or negative interaction, we discriminated between three states. First, the colony shows no blue coloration, therefore no interaction was observed, which we indicated with the symbol '-'. Second, a weak blue coloration was observed but not on the level of the control coloration. Therefore, an interaction between proteins takes place, which was indicated with '+'. Third, a blue coloration was observed similar to the level of the control, which we indicated with '+++'.

3.13. Serial dilution - Spot assay

Yeast cultures were prepared by streaking freshly transformed strains onto YPD agar plates containing antibiotics (CloNat 100ug/ml; G418 200ug/ml). After incubating the cells at 25°C in YPD supplemented with 2% Glucose overnight, cultures were resuspended in autoclaved H₂O to a final OD₆₀₀ of 1.0. Serial dilutions (10⁻¹ to 10⁻⁶) were prepared by mixing 10 µl of culture into 90 µl sterile H₂O. From each dilution, 5 µl was spotted in sequence onto solid agar plates with varying composition depending upon the strain and experimental design. Plates were incubated at 25°C or at 37°C for 48 h and scanned for growth comparison.

3.14. Growth analysis of *klmt-1* expression in *Saccharomyces cerevisiae*

Synthetic defined minimal media (SDMM) was made using drop out base powder (SC-Phe, Sunrise Science) and M9 minimal broth. For M9 minimal broth 200ml 5x M9 Salts (5x M9 Salts compose of 64g Na₂HPO₄, 15g KH₂PO₄, 2,5 g NaCl, 5g NH₄Cl per Liter) was prepared and the following filter sterilized solutions were added: 2ml 1 M MgSO₄ Solution, 0,1ml 1 M CaCl₂ Slution and 100 ml 20% Glucose, and filled up to 1000ml with sterile MonoQ. For SDMM containing 2% Raffinose and 2% Raffinose / 2% Galactose, 100ml of 20% Raffinose or 50ml of 40% Raffinose/Galactose was added. Tyrosine stress media (SDMM + Phe:Tyr) was made with SDMM and varying concentrations of Phe:Tyr where [Phe] was kept at either 0.003 mM or 1.2mM and [Tyr] at 1.2 mM. For all growth assays, *S. cerevisiae* strains and derivatives were streaked on YPDA and grown at 25°C for 72 h. Single colonies were suspended YPD 2% Glucose for overnight culture. Overnight were regrown in fresh YPD 2% Glucose media for several hours until an OD₆₀₀ of 0.1-0.3. Cultures were washed with sterile MonoQ and used to inoculate 200 µl of media in a microtiter plate to a final OD₆₀₀ of 0.01. Growth was monitored using an Synergy H1 (BioTek) absorbance spectrophotometer by measuring the absorbance at 600 nm every five minutes for 72 h. Rescue of FRS1/FRS2 strains was achieved through transformation of plasmid pCEV containing a WT copy of FARS-1 and FARS-3 of *C. tropicalis*.

3.15. Heat-shock induction for *klmt-1* overexpression in *C. elegans*

20 to 30 adult worms were transferred into a 20ul drop of M9 worm media onto a slide. Embryos were extracted by cutting the adult in half by using two syringe needles. Embryos were transferred onto an agar plate in small patches of 20 to 30 individuals. Heat-shock was

applied by transferring the agar plates into an Air-incubator on 37°C for 1 hour, immediately or after 3 hours of incubation at 25°C. After heat-shock, embryos that did not hatch were counted every 24 hours, for three days. Embryos that managed to hatch but showed the typical larval arrested phenotype were separated into a new agar plate and monitored for several days. Initially, embryos were staged directly by collecting and mounting four-cell embryos. Experiment was performed in triplicates. To extract protein from heat-shocked worms and embryos, they were given 4 hours of recovery after heats-hock before proceeding with protein extraction as described previously.

4. Results & Discussion

4.1. Aim 1: Expression pattern and protein interaction network of *klmt-1/kss-1* TA element

4.1.1. Expression pattern of KLMT-1 *in vivo*

Our TA model predicts that the toxin KLMT-1 is maternally deposited into unfertilized eggs. In order to investigate the molecular mechanism of *klmt-1*, we have generated transgenic lines by using a CRISPR/Cas9 based protocol. This method uses the site-specific DNA cutting activity of the Cas9/gRNA ribonucleoprotein (RNP) complex, which generates a double strand break in the target gene. The DNA break is then repaired by homologous recombination using a template that incorporates either a small protein tag (FLAG) or in-frame fluorescent protein (mNeonGreen) (43)(24). Exploiting this method, we have successfully generated strains carrying an endogenously *klmt-1* tagged with a FLAG-tag either on its N- or C-terminus in *C. tropicalis*. This allows us to study the expression pattern, cellular and subcellular localization of KLMT-1 during embryonic development. A FLAG-tag is a short peptide (DYKDDDDK) recognized by an antibody and commonly used to study proteins (44). Although its short peptide sequence and hydrophilic nature makes it less likely to denature or inactivate proteins it is attached to, the addition of a tag comes with the risk that the native function of the protein may be abolished or compromised. To test if the FLAG-tagged KLMT-1 protein is expressed and translated in the strains, we performed a Western blot by using either an anti-FLAG or anti-KLMT-1 antibody on whole worm or only embryo protein lysates. In all Western blots, we observed a strong band of the expected molecular weight of 59.3 kDa for the FLAG-tagged strains and 56.9 kDa for the positive control strains (NIC203, QX2343), respectively

(Fig. 6B, 6C, 6D). Interestingly, next to the expected fragment, we occasionally observed two additional smaller and less prominent fragments running between 55 kDa and 60 kDa (Fig. 6B, 6C, 6D). We hypothesize that the presence of the three differently sized fragments could be the result of PTMS or cleavage, which makes it very likely that KLMT-1 could potentially have different activities depending on its modifications. Whether these fragments originate from a technical variation or from biological modifications remains elusive.

To check if the tagged KLMT-1 protein is functional and can apply its toxic effect, we performed crosses of the *klmt-1* FLAG-tagged strains to a non-carrier strain (EG6180) and scored the phenotypes of their F2 progeny. In the C-terminally tagged strain 21.2% (n = 99) and in the N-terminally tagged strain 26.2% (n = 80) of their F2 progeny showed developmental defects. As expected for a TA element, all affected progeny were homozygous non-carriers (EG6180 homozygous) (Fig. 6A).

Our results could show that both N-terminal and C-terminal FLAG-tagged strains and the anti-KLMT-1 antibody show the same prominent band with the expected molecular weight, respectively. Moreover, our results indicate that the FLAG-tagged toxin KLMT-1 is expressed and functional, making the transgenic lines suitable for downstream molecular characterization.

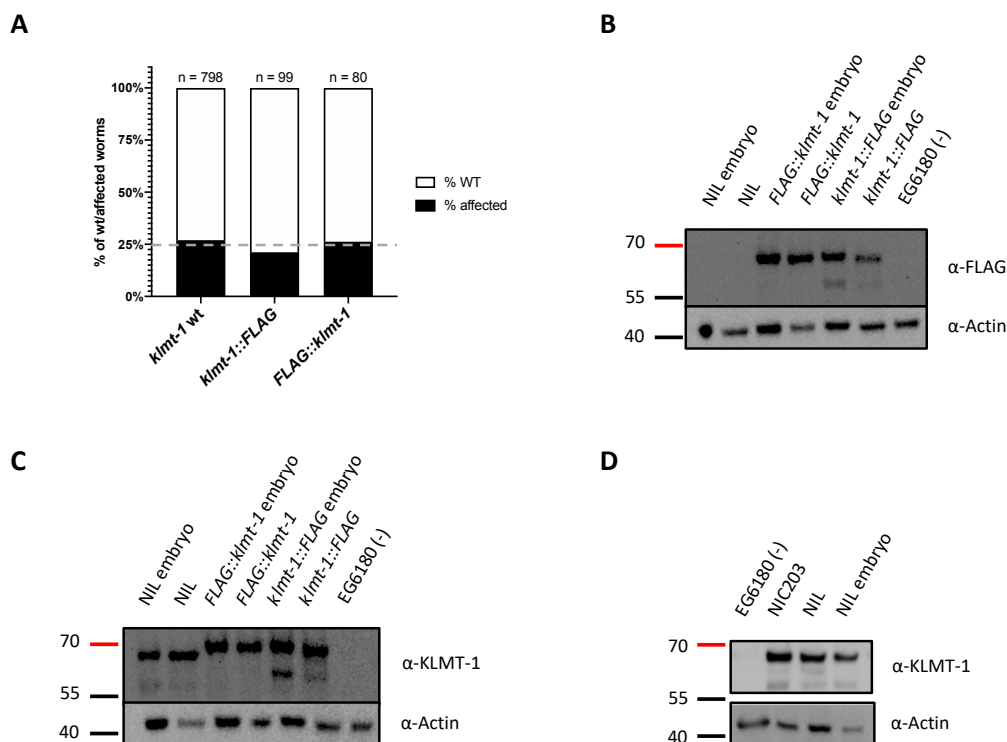


Figure 6. Validation of KLMT-1::FLAG transgenic lines. (A) Cross between either QX2343 (NIL carrying *klmt-1* wt), *klmt-1::FLAG* or *FLAG::klmt-1* hermaphrodites to EG6180 males shows, 27%, 21.2% and 26.3%

developmental defects in their F2 progeny. Dotted line represents the expected number of 25% affected offspring for a single TA element. (B) Western blot using anti-FLAG antibody on whole worm and embryo lysates on *klmt-1::FLAG* and *FLAG::klmt-1* strains show the expected size of 59.3 kDA. Positive control is NIL (QX2343); negative control is the strain EG6180 (-). (C) Western blot using anti-KLMT-1 monoclonal antibody on whole worm and embryo lysates on *klmt-1::FLAG* and *FLAG::klmt-1* strains shows the expected size of 59.3 kDA. NIL (QX2343) (+); EG6180 (-). (D) Western blot using KLMT-1 monoclonal antibody on whole worm and embryo protein extracts of NIC203 (wt) and the NIL (QX2343) shows the expected size of 56.9 kDA. No fragment was detected in the negative control strain EG6180. Additionally, in all Western blots, anti-b-actin antibody was used to control the amount of protein loaded and show the expected fragment sizes of 45 kDA.

To investigate the spatiotemporal expression pattern of the toxin KLMT-1 in embryos, we performed single molecular fluorescence *in situ* hybridization (smFISH) in *C. tropicalis* embryos, which was conducted by Pinelopi Pliota. The result indicates that *klmt-1* mRNA is present in early embryos before the 4-cell stage, in agreement with its maternal-effect (Fig. 7). In later stages of development (after comma stage), *klmt-1* mRNA localizes exclusively in two cells, presumably the germline precursors. This observation suggests that *klmt-1* mRNA is expressed in the germline as early as embryonic development (Fig. 7).

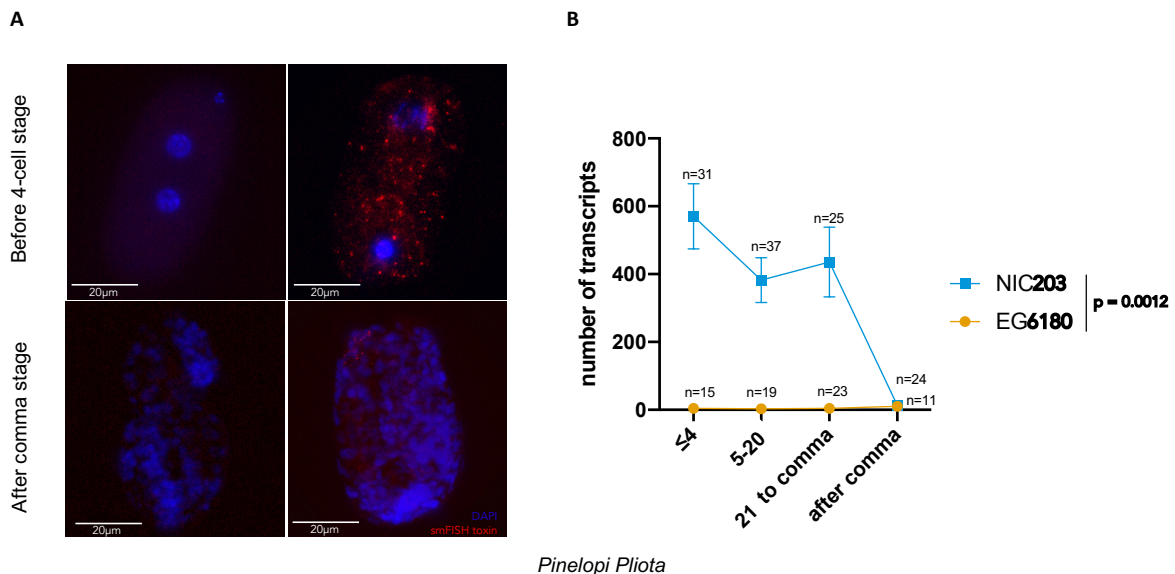


Figure 7. smFISH shows *klmt-1* mRNA is present in early embryos. Representative images of NIC203 and negative control EG6180 embryos hybridized with smFISH probes against *klmt-1* transcripts. Embryos were grouped into four broad developmental categories based on their number of nuclei (DAPI staining) and the total number of *klmt-1* transcripts were quantified using an automatic pipeline (right). All tests are unpaired t-tests, p-values are Bonferroni corrected (** $P \leq 0.01$, **** $P \leq 0.0001$).

Additionally, we tested if the KLMT-1 protein is present in embryos by performing an Immunofluorescence (IF) assay on embryos of the wildtype (NIC203) and negative control strain (EG6180), which naturally does not carry the TA element. In order to detect the toxin KLMT-1, we used an anti-KLMT-1 monoclonal antibody. By comparing the fluorescence

intensity between different stages of embryonic development, we observed that the toxin KLMT-1 is ubiquitously present in the cytoplasm before comma stage and later localizes into two cells, presumably the germline precursors, which is consistent with its maternal-effect (Fig. 8). Moreover, we performed an IF assay on the generated *klmt-1::FLAG* strain and compared it to the negative control strain (EG6180) using anti-FLAG antibody. We observed that KLMT-1::FLAG is ubiquitously present in the cytoplasm before comma stage and later localizes into two cell. This observation, similar to the observation we made in the wildtype (NIC203) when using the anti-KLMT-1 antibody, suggests that the FLAG-tag does not interfere with the subcellular localization of KLMT-1 (Fig. 8).

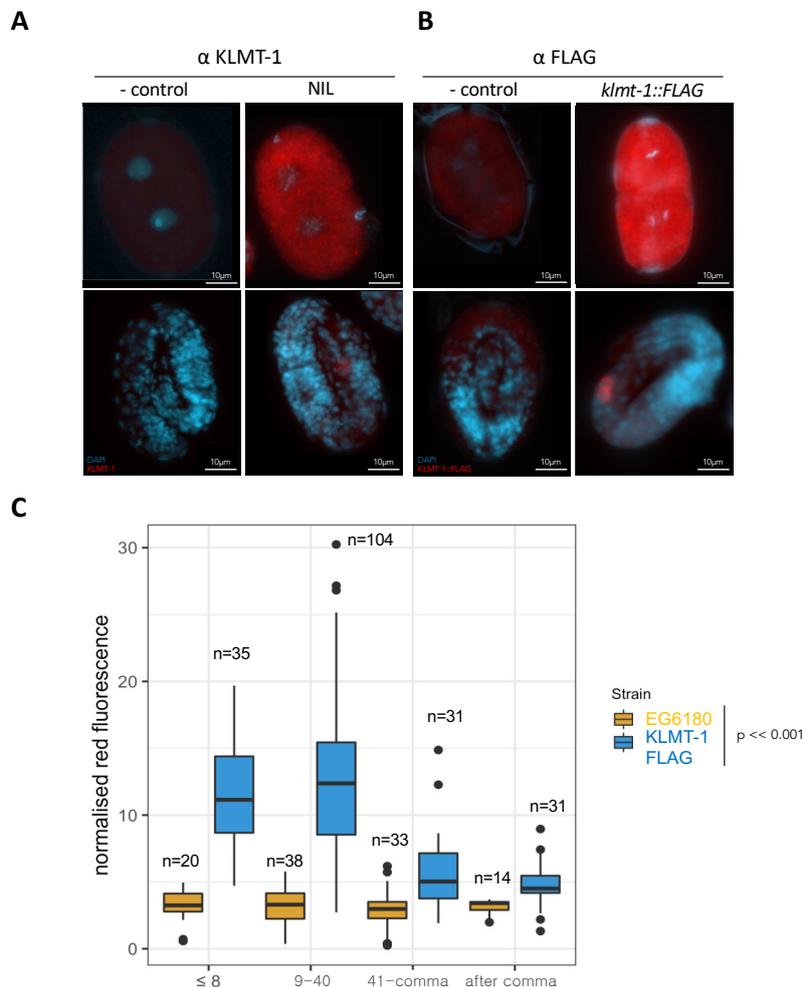


Figure 8. KLMT-1 is present in 2-cell embryos and localizes into two cells later in embryogenesis. (A) Representative images of EG6180 (control) and NIL (QX2343) embryos stained with anti-KLMT-1 monoclonal antibody. (B) Representative images of EG6180 (control) and *klmt-1::FLAG* embryos stained with anti-FLAG antibody. Images show 2-cell stage embryos (top) and 3-fold embryos (bottom). Immunofluorescence and DAPI merged images. (C) Embryos were grouped into four broad developmental categories based on their number of nuclei (DAPI staining) and the normalized red fluorescence were quantified using ImageJ. p -values are Bonferroni corrected ($p << 0.001$).

According to our *klmt-1/kss-1* TA model, the toxin is maternally deposited into the oocyte and after fertilization it exerts its toxic effect, if not counteracted by the antidote. In light of the developmental defected worms that we observed in the crosses and our previous IF data on embryos, showing that KLMT-1 is ubiquitously present in early development and later localization into germline precursor cells, we hypothesize that the toxin must be present in the fully developed gonad of an adult. Furthermore, if it is expressed in the fully developed gonad, this raises the question of how KLMT-1 can be present in the germline, without exerting its toxic effect. To investigate the expression pattern and localization of KLMT-1 in gonads, we performed an IF assay on gonads. Our preliminary IF data on gonads using a monoclonal antibody against KLMT-1 in NIL (QX2343) compared to negative control strain (EG6180) shows that KLMT-1 is ubiquitously present in gonads (Fig. 9A, B). Using anti-FLAG antibody in the *klmt-1::FLAG* strain shows that KLMT-1 is ubiquitously present in gonads compared to the control strain (QX2343) (Fig. 9C, D). Our results could show that KLMT-1 is present in the fully developed gonad of an adult, which is in accordance with its maternal-effect.

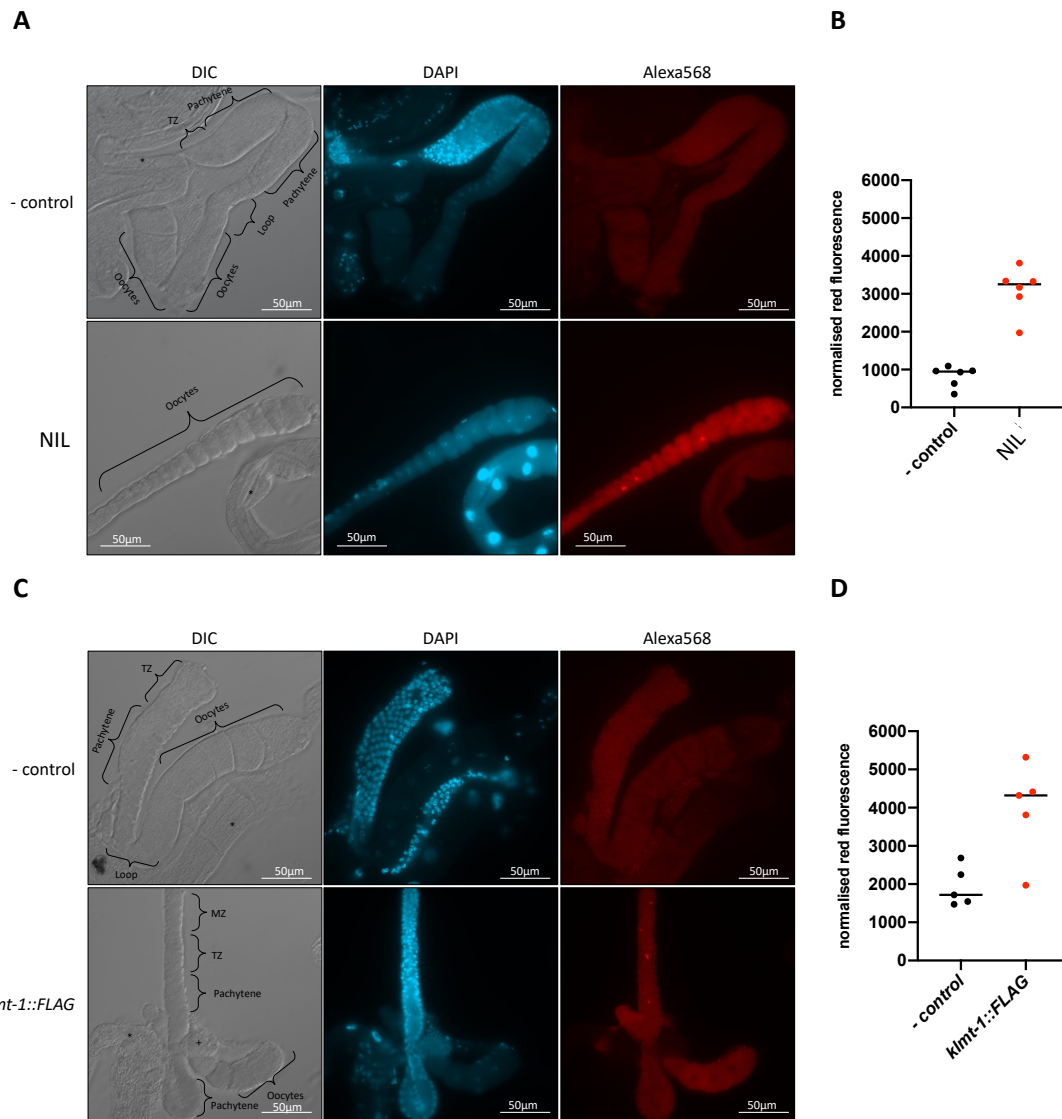


Figure 9. KLMT-1 is ubiquitously present in gonads. (A) Representative images of EG6180 (control) and NIL (QX2343) gonads stained with anti-KLMT-1 monoclonal antibody. (B) Plot shows normalized red fluorescence of EG6180 (control) and NIL (QX2343) gonads (n=5). (C) Representative images of NIL (QX2343) (control) and *klmt-1::FLAG* gonads stained with anti-FLAG antibody. (D) Plot shows normalized red fluorescence of NIL (QX2343) (control) and *klmt-1::FLAG* gonads (n=5). Normalized red fluorescence was calculated using ImageJ. Scale = 50um.

Furthermore, we have decided to genetically attach a fluorescent tag (mNeonGreen) to *klmt-1*, which has the benefit of allowing studies in living organisms. mNeonGreen (mNG) is a 26,6 kDa large monomeric yellow-green fluorescent protein and a brighter alternative to Green Fluorescent Protein (GFP), which is derived from a tetrameric fluorescent protein from the cephalochordate *Branchiostoma lanceolatum* (45)(46). Since fluorescent tags are usually larger than small peptide tags and can pursue the function of the protein, we introduced a linker between KLMT-1 and mNG. 2xTY1 (2Ty) tag is a small peptide sequence which serves as a small flexible linker between KLMT-1 and mNG. Small flexible linkers help to separate

multiple domains in a single protein. They are used to prohibit unwanted interactions between the discrete domains and can be used to preserve the function of the protein by reducing the chance of unwanted side-reactions such as steric hindrance.

To test if the toxin is active, we crossed *klmt-1::2Ty::mNG* strain to a non-carrier strain (EG6180). Unfortunately, we observed only 5% (n = 100) embryonic lethality in the F2 progeny while 95% were wt, indicating that fluorescent tag impairs with the toxic activity of KLMT-1 (Fig. 10A). One hypothesis is that the fluorescent tag interferes with the target recognition of KLMT-1, which could explain the reduced embryonic lethality. To investigate the expression of KLMT-1::2Ty::mNG we performed a Western blot and observed a fragment which is slightly larger than the expected size of KLMT-1::2Ty::mNG. While the estimated molecular weight of KLMT-1::2Ty::mNG is 91,7 kDa large (Supplementary Fig. 3) we observed a fragment running between 100 kDa and 120 kDa (Fig. 10B).

Furthermore, we followed KLMT-1::2Ty::mNG signal throughout the development of *C. tropicalis* and could observe that KLMT-1 is located in cells which later develop into the germline. Although the detailed characterization of germline development in *C. tropicalis* is not available yet, we compared these cells to the well described primordial germ cells of its sister species *C. elegans* and could observe similarities in their position and fate to become the fully developed gonad (Fig. 11). In L1 larvae we observed two fluorescent cells that later in the adult worm develop into the full germline (Fig. 11A).

Despite the fact that the toxic activity is impaired by the fluorescence tag, the observation of the subcellular localization of KLMT-1::2Ty::mNG in the germline, supports our previously described smFISH and IF results, and is in accordance with its maternal effect.

To our surprise, we observed that KLMT-1::2Ty::mNG forms subcellular aggregates or foci (Fig. 11, 12, 16, 17). To investigate if these aggregates are artifacts formed by the mNG tag, we performed IF on *klmt-1::2Ty::mNG* strain embryos using anti KLMT-1 antibody and compared these images to the IF images of the NIL (QX2343) embryos stained with anti-KLMT-1 monoclonal antibody (Fig. 12). We observed that these foci are only present in the *klmt-1::2Ty::mNG strain*. We also observed the same pattern of aggregates in the gonads of *klmt-1::2Ty::mNG strain in vivo* (Fig. 12, 16, 17). Therefore, we think that the formation of aggregates is an artifact produced by the mNG tag and it does not reflect the normal state of KLMT-1.

On top of the validated transgenic lines, we could show that the toxin KLMT-1 is present throughout all stages. Starting from the zygote and early embryonic development, KLMT-1 is ubiquitously present. We could show that KLMT-1 localizes within the cytoplasm of the germline precursor cells, which develop into the gonad of an adult worm later during development. This supports our hypothesis of being a maternally deposited toxin.

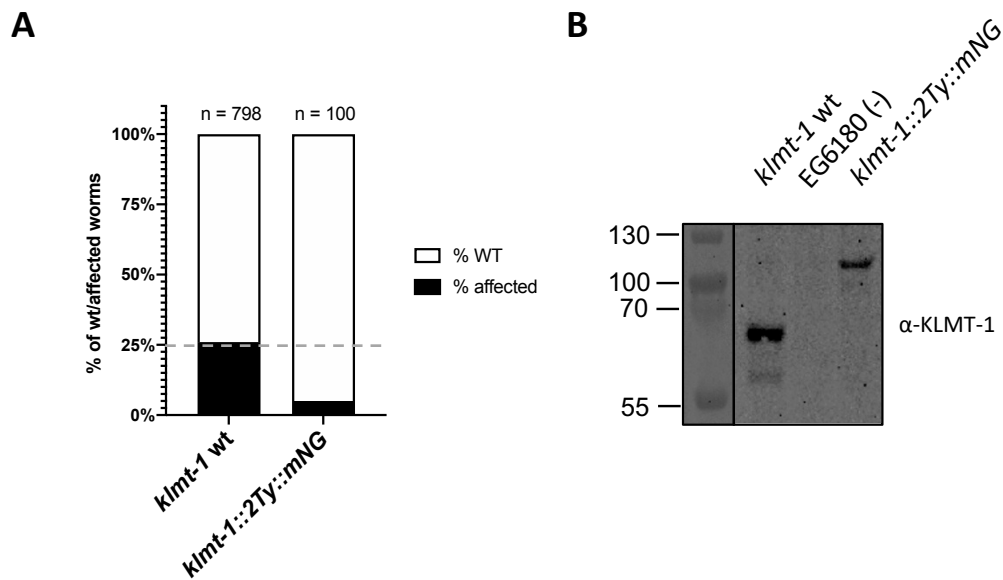


Figure 10. Validation of *klmt::2Ty::mNG* transgenic line. (A) Cross between QX2343 (NIL carrying *klmt-1* wt) or *klmt-1::2Ty::mNG* hermaphrodites to EG6180 males shows, 27% (n=798) and 5% (n=100) affected worms in their F2 progeny. (B) Western blot using monoclonal antibody against KLMT-1 on whole worm lysate of *klmt-1::2Ty::mNG* strain shows a fragment between 100 kDa and 120 kDa. In the positive control *klmt-1* wt (NIC203) (+) fragment of correct size of 56.9 kDa, negative control EG6180 (-) shows no fragment.

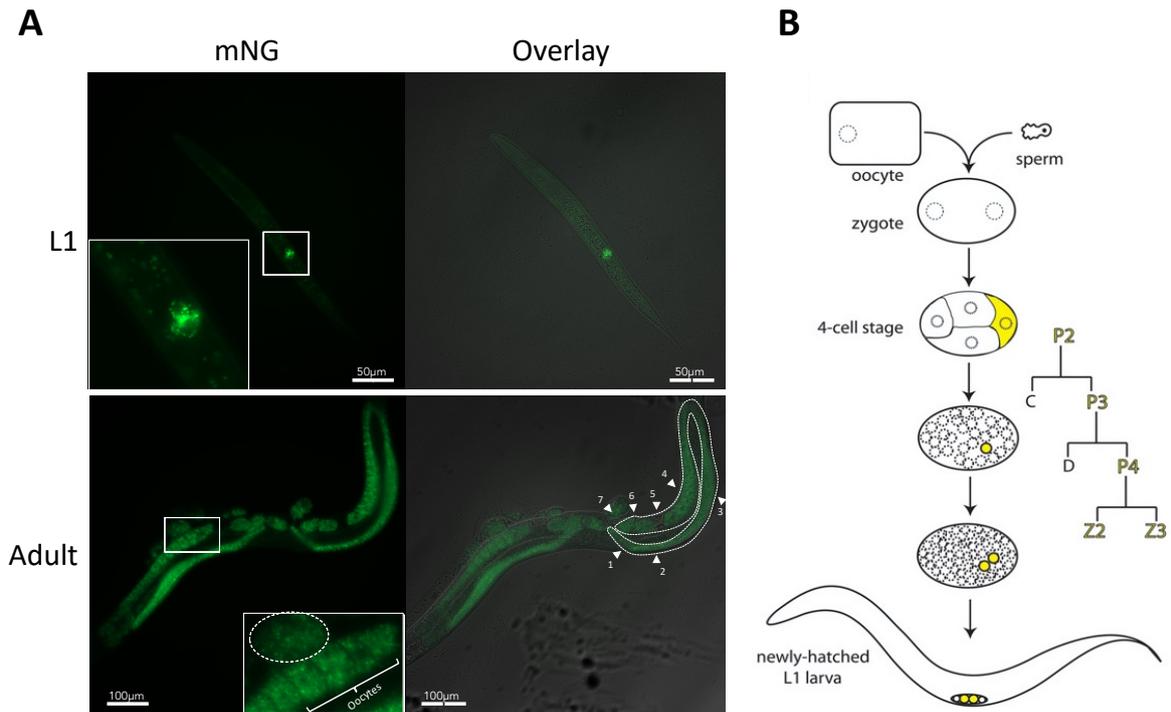


Figure 11. KLMT-1 localizes in the germline. (A) Representative image of L1 (top) and Adult (bottom) *C. tropicalis* expressing *klmt-1::2Ty::mNG*. (top) Inset shows magnification of L1 gonad precursor cells. (bottom) Inset shows one early embryo with ~30 cells highlighted with dashed lines and the cellularized oocytes of one gonad arm. Furthermore, in the overlay image one gonad arm is outlined in white where the distal tip cell caps the distal end (1) and developing oocytes populate the proximal end (6). In the distal half of the gonad, germ cell nuclei are situated along the outer surface of the gonadal tube, sharing the same cytoplasm (3). Overt oocyte development occurs from the loop region into the proximal half of the gonad on the ventral side (4). The spermatheca (5) lies adjacent to the final oocyte. As an oocyte (4) is ovulated into the spermatheca, a sperm fertilizes it and early development initiates in the uterus (6). The developing embryos are then released through the vulva (7). (B) Cartoon representation of fertilization and the embryonic germ line of *C. elegans*. Oocyte and sperm meet, and fertilization initiates embryonic development. Germline lineages are depicted in yellow (34). Yellow color indicates the germline precursor cell lineage. In embryonic development of *C. elegans* the germ line is set aside during the very first cell divisions, and divides into Z2 and Z3, the precursors of all germ cells of the animal, before hatching (47). Z2 and Z3 proliferate in the expanding gonad during L2 and split into two gonad arms during L3. The distal tip cell begins to direct gonad migration inward, and meiosis is initiated in proximal populations of each gonad arm during L3. These early meiotic cells develop as sperm in L4 (48). In young adults, the proliferating cells entering meiosis differentiate into oocytes in the proximal arms of each gonad, where they sit adjacent to mature spermatids. Overall, the reproductive system consists of somatic gonad, the germ line and the egg-laying apparatus. There are two bilaterally symmetric, U-shaped gonad arms that are connected to a central uterus through the spermatheca. The germ line within the distal gonad arms (ovaries) is syncytial with germline nuclei surrounding a central cytoplasmic core. More proximally, germ cells pass sequentially through the mitotic, meiotic prophase and diakinesis stages. As they pass through the bend of the gonad arm (oviduct), oocytes enlarge, detach from the syncytium, and mature as they move to the uterus. The oocytes are fertilized by the sperm in spermatheca. The resulting diploid zygotes are stored in the uterus and laid outside through the vulva, which protrudes at the ventral midline.

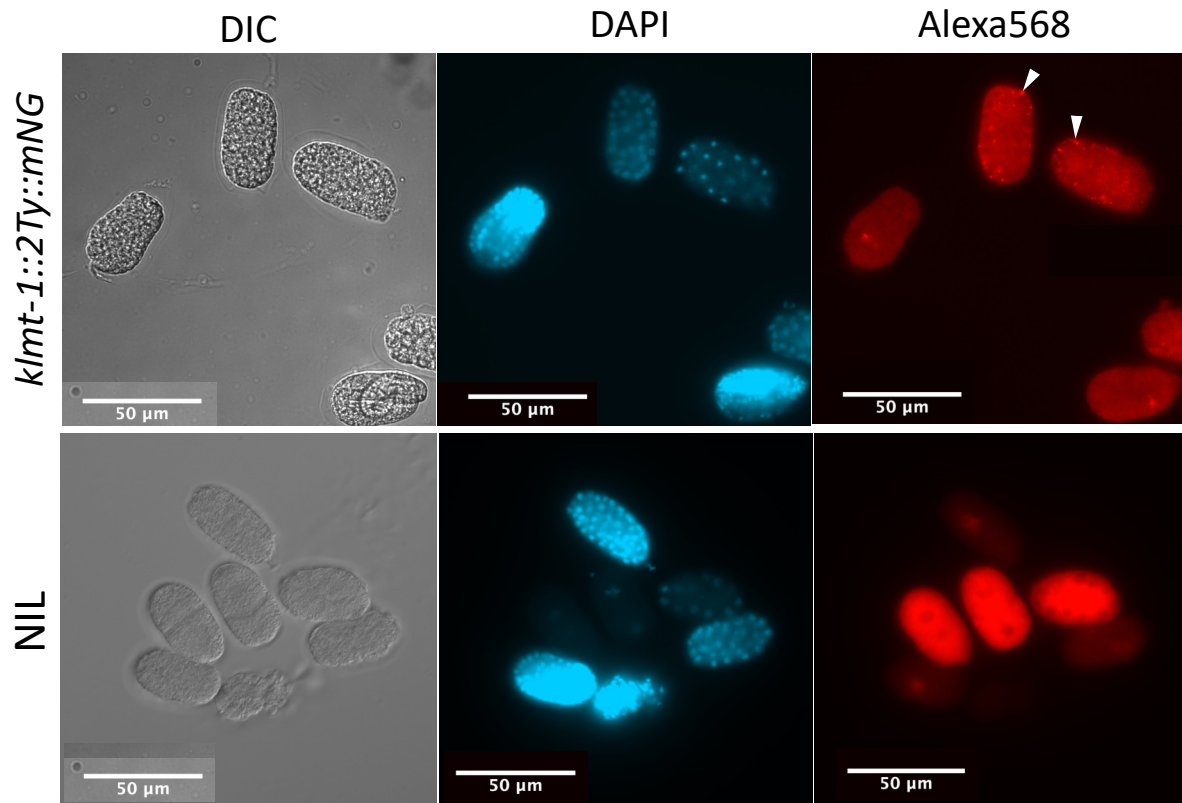


Figure 12. KLMT-1::2Ty::mNG forms aggregates in embryos. Representative images of *klmt-1::2Ty::mNG* and *NIL* (QX2343) embryos stained with anti-KLMT-1 antibody. Two white arrows indicate subcellular aggregations of KLMT-1.

4.1.2. Expression pattern of KSS-1 *in vivo*

To study the expression and localisation of the antidote *kss-1*, we have N-terminally tagged *kss-1* with a Human influenza hemagglutinin tag (HA-tag) in the background of *klmt-1::FLAG*. Similar to the FLAG-tag, the HA-tag (YPYDVPDYA) is a small peptide sequence allowing the detection of the protein it is attached to by common molecular methods e.g. Immunofluorescence or Western blotting. We have verified the expression of *kss-1* by performing a Western blot that shows the correct band of 47kDA using an anti-HA antibody (Fig. 13C).

To test if the antidote KSS-1 is still functioning *in vivo*, we crossed the *HA::kss-1* strain to EG6180. In the F2 progeny, we observed 25.3% (n= 99) affected offspring and 74.7% wt (Fig. 13A). As expected for a TA element, all wt progeny were either heterozygous or homozygous carriers (NIC203/EG8180; NIC203/NIC203), while the affected worms were homozygous-non carriers, indicating that the antidote is still active. In addition, we performed IF on *HA::kss-1* strain using anti-HA antibody (Fig. 13B). Although KSS-1 is active, we could not observe any signal or localization of KSS-1. It is conceivable, that the expression level of KSS-1 is low and

only present in a short time-window to counteract KLMT-1 toxicity, just not enough to be detected by the anti-HA antibody. Similar to KLMT-1, we fused a fluorescent tag mScarlet to KSS-1, which was performed in the background of *klmt-1::2Ty::mNG* to allow the investigation of its subcellular localization. Unfortunately, no fluorescent signal could be detected in either adult worms or embryos.

Our results show, that the N-terminally tagged *kss-1* with a HA-tag is expressed and still functional, making this transgenic line suitable for downstream molecular characterization.

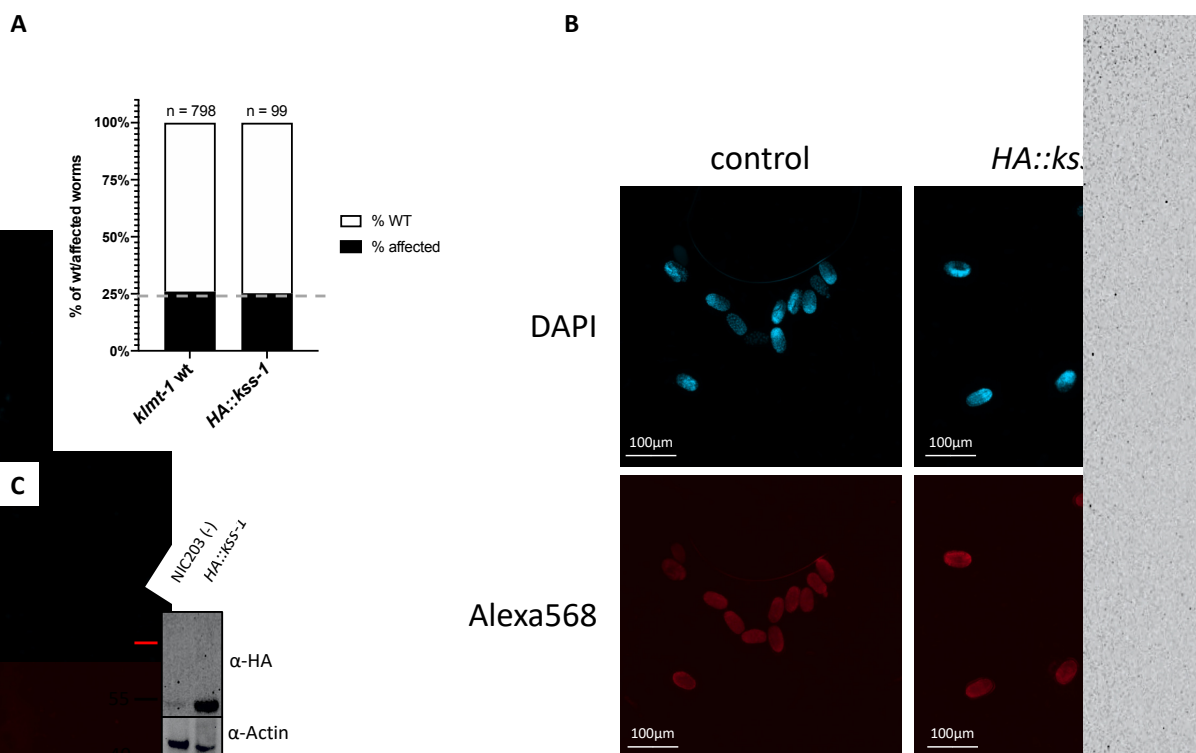


Figure 13. Immunofluorescence of HA::kss-1. (A) Cross between NIL (strain carrying *klmt-1 wt*; QX2343), *HA::kss-1* hermaphrodites and EG6180 males shows, 27% (n=798) and 25,3% (n=99) affected worms in their F2 progeny. (B) Representative images of Qx2343 (control) and *HA::kss-1* embryos stained with anti-HA antibody. Images show early and late developed embryos. The intensities in both images showing the Alexa568 signal were equally adjusted to make the embryos visible. (C) Western blot using anti-HA antibody on whole worm lysate on *HA-KSS-1* strain shows the expected size of 47kDa. In the control (NIC203), no fragment was detected. Additionally, using anti-b-actin antibody was used to control the amount of protein loaded and shows the expected fragment size of 45kDa.

4.1.3. FARS-1 short-isoform is sufficient for KLMT-1 to fulfill its toxic effect

To understand the molecular mechanism of the *klmt-1/kss-1* TA element, we investigated the spatiotemporal expression pattern of the putative target FARS-1. FARS-1 exists in two different isoforms, the full long version (62.5 kDa) and a short version (56 kDa) missing the

first two exons (56 amino acids) at the N-terminus, which is the result of an alternative transcriptional starting site (TSS) and both isoforms are conserved in *Caenorhabditis* nematodes (Supplementary Fig. 2). As previously described, the toxin KLMT-1 has sequence similarity to FARS-3, which is known to bind to FARS-1. Due to the sequence similarity to its paralogue, the toxin could form a complex with FARS-1, thereby executing its toxic effect. In principle, KLMT-1 could interfere with the charging of the tRNA^{Phe} in different ways, such as, charging the tRNA with an incorrect amino acid or charging a different tRNA with phenylalanine.

To investigate whether FARS-1 isoforms play any role in KLMT-1 toxicity, we have generated a transgenic line that exclusively expresses the FARS-1 short isoform which was accomplished by introducing a mutation in the first exon resulting in a premature stop codon (Supplementary Fig. 2). We also tried to generate a transgenic line which would only express the FARS-1 long isoform by introducing a non-synonymous mutation in the start codon of the small isoform (Met -> Ala). Although we were able to generate heterozygous worms carrying this mutation, homozygous mutants were non-viable, which strongly suggests that the short isoform is essential for the survival of worms, whereas the long isoform is dispensable. To investigate if KLMT-1 can possibly exert its toxicity in the background of FARS-1 short isoform transgenic line, we crossed it to EG6180, which also only carries the FARS-1 short isoform transgene. We observed 30% (n = 100) of their F2 progeny showed developmental defects (13,3% embryonic lethal, 86,7% L1 arrest) (Fig. 14A). None of the surviving progeny were homozygous non-carriers (EG6180 homozygous), which suggests that if FARS-1 is the target, then its short isoform is sufficient for KLMT-1 to exert its toxic effect.

In addition, we studied the temporal expression of FARS-1 isoforms during *C. tropicalis* life cycle. To do so, we prepared protein lysates from embryos and synchronised worms which were collected from different timepoints of development (5h, 14h, 24h, 40h). Protein levels were detected by performing a Western blot, showing the fragments with the expected molecular weight of 56 kDa and 62.5 kDa for FARS-1 short-isoform and FARS-1 long-isoform, respectively. Although further repeats need to be made, our preliminary results indicate that both isoforms seem to be expressed during all developmental stages (Fig. 14). It is currently unknown what is the physiological role that the FARS-1 long isoform may play. However, our results clearly show that if FARS-1 is the target of KLMT-1, then, the long

isoform is dispensable for the toxicity of the selfish element. Alternatively, FARS-1 may not be the target of KLMT-1, in which case this would be a trivial result.

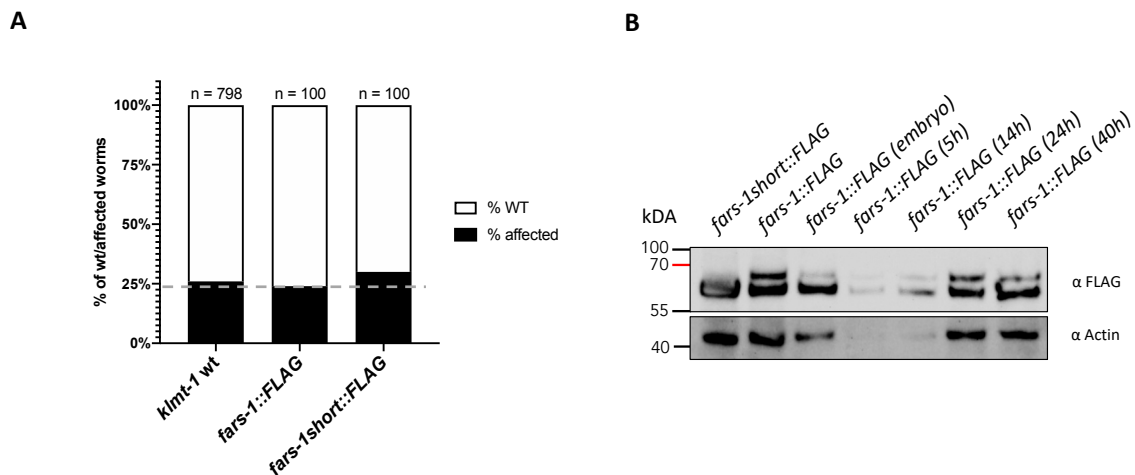


Figure 14. Validation of *fars-1::FLAG* and *fars-1short::FLAG* transgenic lines. (A) Cross between QX2343 and EG6180 (control), *fars-1::FLAG* or *fars-1short::FLAG* shows, 26%, 24% and 30% developmental defects in their F2 progeny, respectively. Dotted line represents the expected number of 25% affected offspring for a single TA element. (B) Western blot using anti-FLAG antibody on whole worm lysate on *fars-1short::FLAG* strain and whole worm, embryo lysates and timepoint (5h, 14h, 24h, 40h) specific lysates after synchronization on *fars-1::FLAG* strain. The expected size of 56kDa for *fars-1short::FLAG* strain and two fragments of the size 56kDa and 62.5kDa for *fars-1::FLAG* strain are visible. Additionally, anti- β -actin antibody was used to control the amount of protein loaded and show the expected fragment sizes of 45kDa.

To test if FARS-1 shares the same localization as its putative target KLMT-1, we performed IF on a *fars-1::FLAG* tagged strain in *C. tropicalis*, which shows a consistent staining in the cytoplasm throughout all stages during embryogenesis (Fig. 15). The early stages of embryonic development can be distinguished by counting the individual cells/nuclei, which also corresponds to the intensity of the DAPI staining. Additionally, later stages can be distinguished by the change in the morphological shape. During this morphogenesis the worm converts from a "bean" (*) shape into a longer, thinner animal, which continues through the comma stage, 1.5-fold stage and to the 3-fold stage (49). We observed a slight decrease in FARS-1 intensity during embryonic development, which could be the result of maternal FARS-1 degradation or a reduced rate of zygotic expression (Fig. 15B). While the maternally deposited *fars-1* and *de novo* translation of *fars-1* after zygotic activation would correspond to the higher intensities in early embryonic development, the decrease in intensity in later stages might be explained by the maternal protein degradation during the Egg-to-Embryo transition (50). Although this was studied in *C. elegans*, this mechanism might also occur in its sister species *C. tropicalis*.

It is currently unknown what is the physiological role that the FARS-1 long isoform may play. However, our results clearly show that if FARS-1 is the target of KLMT-1, then, the long isoform is dispensable for the toxicity of the selfish element. Alternatively, FARS-1 may not be the target of KLMT-1, in which case this is a trivial result. FARS-1 is ubiquitously present in the cytoplasm in embryos, which overlaps with the localization of KLMT-1. Thus, in principle, maternally deposited KLMT-1 could interact with FARS-1.

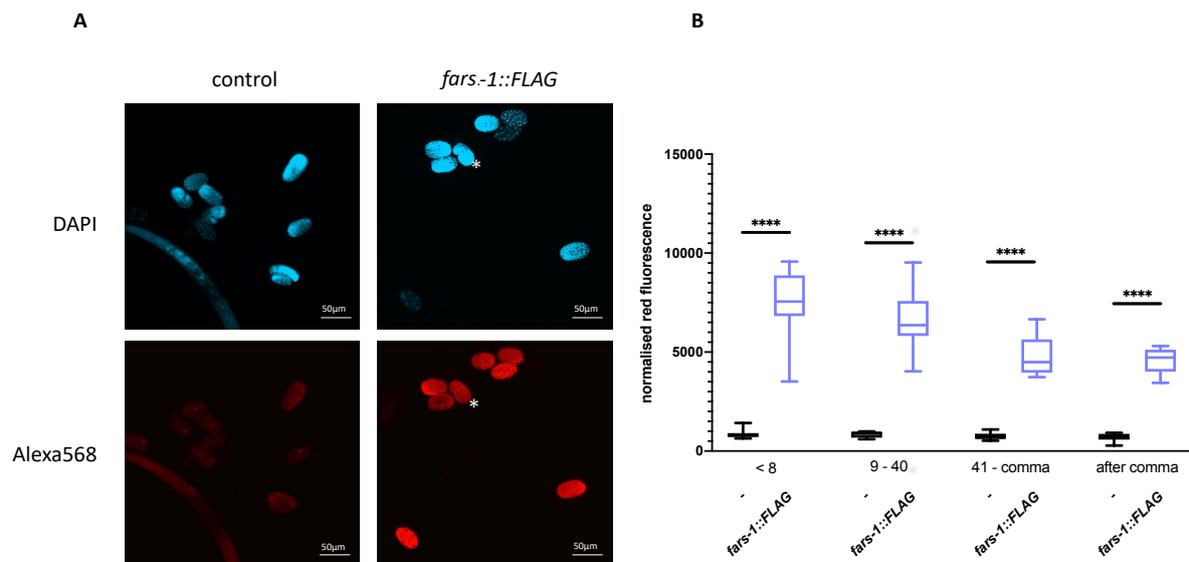


Figure 15. FARS-1 is ubiquitously present in the embryo. (A) Representative images of QX2343 (control) and *fars-1::FLAG* strain embryos stained with anti-FLAG antibody. DAPI and Immunofluorescence images of early, middle and late developed embryos. Bean-like embryo is indicated with a '*'. (B) Embryos were grouped into four broad developmental categories based on their number of nuclei (DAPI staining) and the normalized red fluorescence was quantified using ImageJ. *p*-values are Bonferroni corrected ($p < 0.0001$).

4.1.4. KSS-1 might be involved in KLMT-1 degradation

In our working model the antidote, KSS-1, binds KLMT-1 as part of the SCF complex. The binding of the SCF complex then mediates KLMT-1 ubiquitination, which triggers proteasomal degradation. We initially generated a transgenic line that has KLMT-1 tagged with mNeonGreen to follow the spatio-temporal expression of KLMT-1. Unfortunately, the addition of the fluorescent tag impairs the toxicity of KLMT-1. We hypothesized that the tag interferes with the target recognition of KLMT-1, but this does not mean that the recognition of its antidote *kss-1* is impaired, too. Therefore, we hypothesize that KSS-1 is able to interact with KLMT-1. To test this, we created a knockout mutation (KO) in *kss-1* in the background of the *klmt-1::2Ty::mNG* strain. Usually a KO mutation of KSS-1 would result in lethal offspring, because it cannot counteract the deadly effect of the toxin KLMT-1. However, using this strain enabled the opportunity to indirectly investigate the function of the antidote KSS-1 on KLMT-

1 by introducing a KO mutation into *kss-1*. The KO mutation was established by a frameshift mutation as a result of deleting four nucleotides from position 16 to 19, resulting in a premature stop codon. In the presence of KSS-1, the fluorescence signal of KLMT-1::2Ty::mNG is decreasing during embryonic development from 60min to 120min (Fig. 16). KO of KSS-1 results in a stable KLMT-1 fluorescence signal (Fig. 16). Whether the clear increase in KLMT-1 fluorescence signal is achieved through the lack of degradation of KSS-1 or by another mechanism (e.g. lack of repression through KSS-1), remains elusive. However, in the context of KSS-1 having the predicted F-box domain and FBA domain and with the fast decreasing fluorescent signal of KLMT-1 in the background of a functional antidote KSS-1, we speculate that KSS-1 might be involved in targeting KLMT-1 for degradation through binding KLMT-1 as part of a SCF complex.

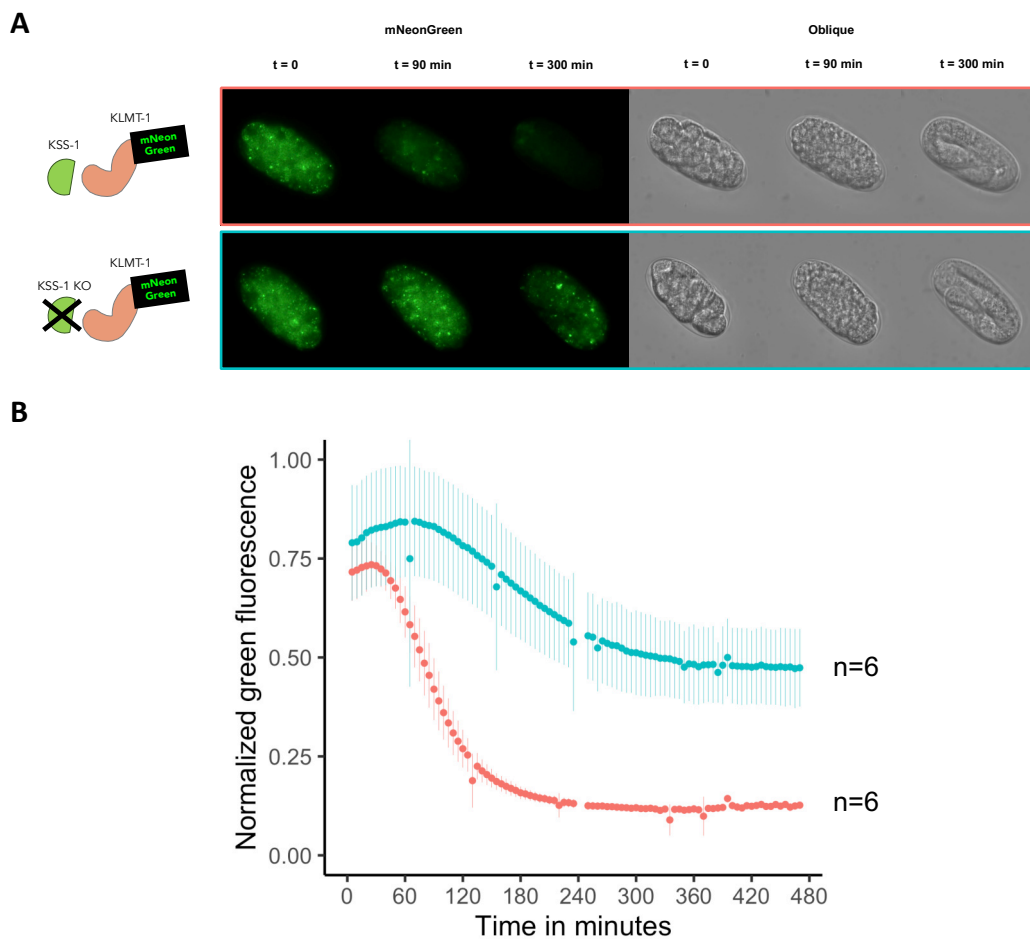


Figure 16. KSS-1 targets KLMT-1 for degradation – Time-lapse Imaging. (A) Cartoon representing active KSS-1 (top) and frameshift induced KO of KSS-1 (bottom) in the background of *klmt-1::2Ty::mNG*. In both transgenic lines, KLMT-1 is not toxic. Representative images of *klmt-1::2Ty::mNG* (top) and *kss-1* KO in *klmt-1::2Ty::mNG* (bottom). In the beginning of time-lapse imaging ($t=0$) embryos were already developed until 10 cell stage. Time-lapse imaging was performed in the CD7 using 20x magnification. (B) Normalized green fluorescence was

quantified using ImageJ. After 90min, *klmt-1::2Ty::mNG* embryos (red) show a strong decrease in fluorescence signal while *kss-1* KO embryos (blue) signal remains stable.

As previously described in section 4.1.1. for the *klmt-1::2Ty::mNG*, we also see the formation of small aggregates in the *kss-1* KO strain (Fig. 16A, 17). Although further investigations have to be made, our preliminary results indicate that in the *kss-1* KO strain, the KLMT-1::mNG aggregates are present in the soma. Interestingly, these aggregates seem to be very stable within the soma since they remain visible throughout the whole life of a worm. In contrast, when *kss-1* is active, KLMT-1::2Ty::mNG signal is never observed in the soma of the larvae or adult worms (Fig. 17).

Overall, our results indicate that KSS-1 might target KLMT-1 for ubiquitin-mediated protein degradation, as part of a SCF complex.

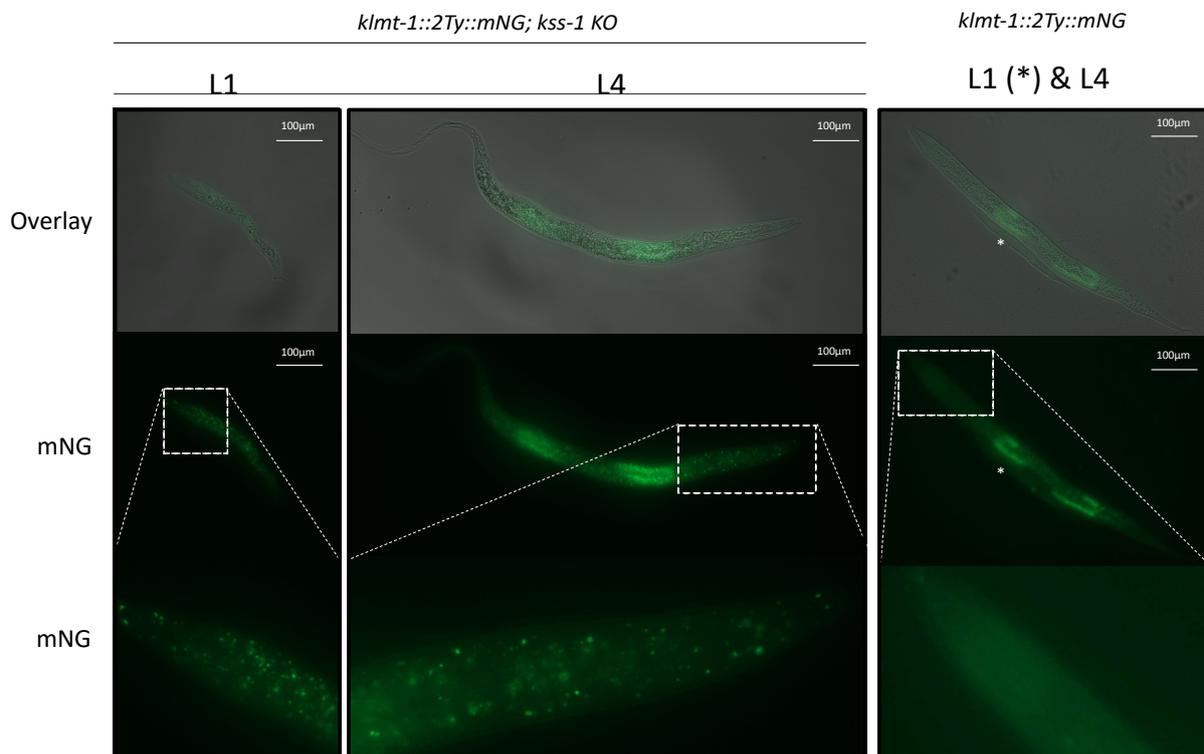


Figure 17. KLMT-1::mNG aggregates are present in the soma in the background of *kss-1* KO. Images representing L1 (left) and L4 (middle) worms of frameshift induced *kss-1* KO in the background of *klmt-1::2Ty::mNG* strain and a L1 (*) and L4 worm of *klmt-1::2Ty::mNG* strain (right). Inset shows magnification of the head of the worms. While KLMT-1::2Ty::mNG aggregates are visible in the *kss-1* KO strain in the soma, they are not visible in *klmt-1::2Ty::mNG* strain which carries a functional antidote *kss-1* when comparing L4 stages. Top row images show overlay of DAPI and green fluorescence signal; bottom row images show green fluorescence signal.

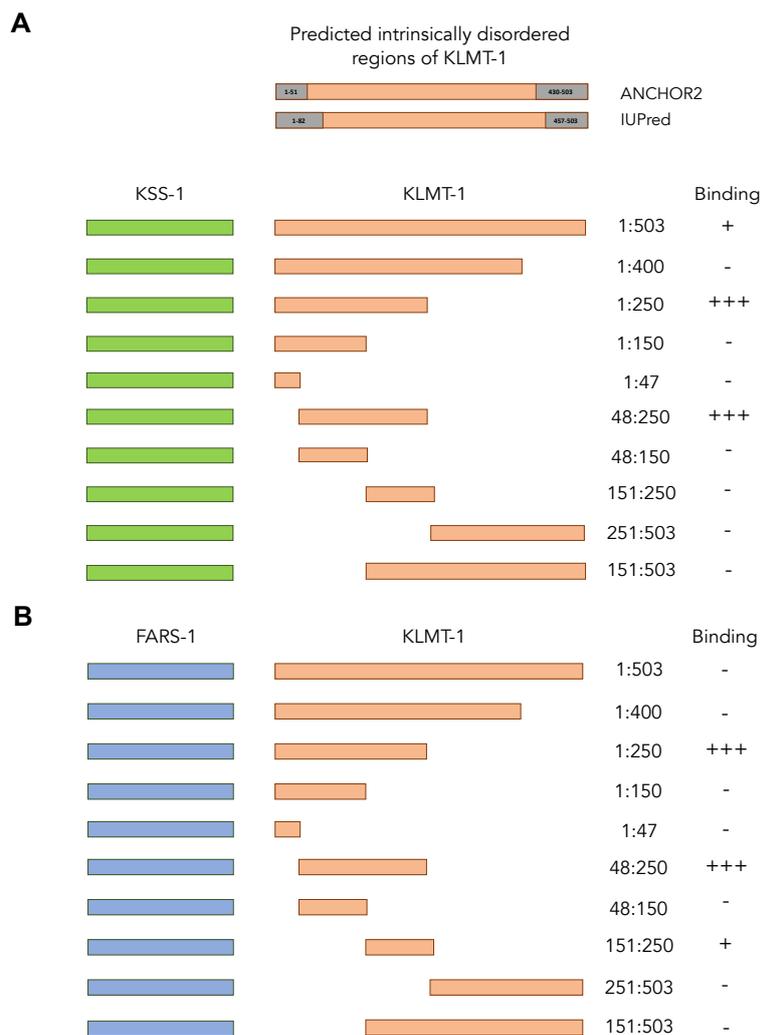
4.1.5. Characterization of protein-protein interaction of the KLMT-1/KSS-1 TA using a Yeast-2-Hybrid system

Our results suggest that KSS-1 targets KLMT-1 for ubiquitin-mediated protein degradation. Furthermore, pull-down assays performed by Manuel Hunold and Stefania Valeria in our lab indicate that KLMT-1 and FARS-1 physically interact *in vitro* (51). To validate interaction partners and further dissect the interactions between KLMT-1, KSS-1, FARS-1 we performed a yeast-two-hybrid assay. Y2H is a molecular biology technique to investigate physical interactions between two proteins or protein-DNA interactions (52). The key mechanism behind Y2H is that most eukaryotic transcription factors (tf) contain an activating domain (AD) and a DNA-binding domain (DBD), which can exert their function by being in close proximity to each other, without direct binding. The AD is the domain responsible for activation of transcription while DBD is responsible for binding to the upstream activating sequence. In Y2H, this property is used to split a transcription factor into two separate fragments, AD and DBD, which are then separately fused to the protein of interest. An interaction between the two proteins of interest can be tested by the activation of a downstream reporter gene, activated by the tf. A common Y2H system uses the GAL4 tf, which activates the reporter gene *lacZ* encoding for an enzyme called β -galactosidase. Activation of the *lacZ* reporter gene can be tested by using the substrate X-gal, which is cleaved by β -galactosidase, resulting in an intense blue product that is easy to identify. We cloned *klmt-1* into pGADT7 prey plasmid containing the AD and *kss-1* or *fars-1* into pGBKT7 bait plasmid which contains the DBD. These plasmids were transformed into Y2H Gold strain according to Supplementary Table 3, to investigate the interaction of KLMT-1 with its antidote KSS-1 or its putative target FARS-1. As a positive control of interaction, we used components of *C. tropicalis* PheRS complex, FARS-1 and FARS-3. Upon growing the transformants on X-gal containing plates, our data shows a blue coloration in yeast expressing KLMT-1 and KSS-1, suggesting an interaction between these two. Interestingly, no interaction between full-length KLMT-1 with its putative target FARS-1 could be detected. With the background of previous findings, it is conceivable that KLMT-1 is possibly modified or processed before it can bind to FARS-1, thereby exerting its toxic effect. Also, it always comes with the risk that the fusion of AD or DBD domains changes the folding properties or masks important binding domains, thereby impairing the binding between KLMT-1 and FARS-1.

Based on the highly disordered KLMT-1 domains predicted by IUPred2A algorithm, we hypothesize that post translational modifications could result in cleavage or conformational change, which may change the binding properties of KLMT-1 to its putative target. To dissect the importance of the predicted intrinsically disordered regions for interactions, we used truncated versions of KLMT-1 (Supplementary Table 3). Truncated version of KLMT-1 1:250AA preserves the interaction with KSS-1 and FARS-1 (Fig. 18). In addition, we performed a Western blot using anti-KLMT-1 antibody on total yeast protein lysates to investigate if the constructs of KLMT-1 are expressed (Fig. 19). Our result shows, that all fragments are expressed and correspond to the expected sizes (Fig. 19B). Moreover, our results show that the minimal necessary region for an interaction between KLMT-1 and KSS-1 or FARS-1 is 48:250 amino acids, indicating that the unstructured regions may prevent its binding ability to FARS-1 (Fig. 18). It is conceivable that the ability for KLMT-1 to interact with FARS-1 to exert its toxic effect is facilitated by a modification of KLMT-1, which results in a truncated version. Unfortunately, we don't have to date any strong piece of evidence supporting the notion that KLMT-1 is cleaved *in vivo*. In addition, it could be possible that KSS-1 only interacts with the truncated version of KLMT-1 in order to target it for degradation. Therefore, it would be interesting to test, if binding of KLMT-1 to FARS-1 increases the binding affinity of KSS-1. While all proteins used in the Y2H assay were fused with the AD or DBD to their N-terminus, it would be interesting to test if the binding properties changes by adding the fusion proteins to the C-terminus.

Our result of the sequence conservation analysis of KSS-1 revealed the presence of a F-Box and FBA domain. Based on this prediction, we speculated, that KSS-1 binds KLMT-1 as part of the SCF complex and mediates ubiquitination, resulting in proteasomal degradation. Previous studies reported that the SCF complex consists of common components such as Skp1, Cul1, Rbx1 and various variable components known as F-box proteins, which are expected to be substrate specific (39). In yeast and mammals, Skp1 functions as an adaptor that links Cul1 and the F-box protein (39). While in yeast and mammals only one *Skp1* gene has been detected, the genome of *C. elegans* has been reported to have 21 homologs of the human Skp1, which are named Skp1-related protein (SKR) (39) and are also present in *C. tropicalis*. To test if KSS-1 is involved in ubiquitin-mediated proteolysis, we performed additional Yeast-two-hybrid assay. Therefore, we have separately cloned SKR-1, SKR-7, SKR-20 into pGADT7 plasmids and CUL-1, CUL-6 and SEL-10 into pGBKT7 plasmids, all members of the SCF complex

(Supplementary Table 4). We note that all proteins were N-terminally fused to either AD or DBD. Since the interaction between components of the SCF complex was previously reported, we decided to use the interaction between adaptor SKR proteins and scaffold proteins CUL as a control (39). In addition SEL-10 is reported to mediate the degradation of Notch, a receptor important for development, through binding with its F-box domain to the adaptor protein SKR-1, which also serves as a positive control (53). Equivalent to SEL-10 and SKR-1 interaction, we would assume KSS-1 to interact with SKR family proteins, in order to bring KLMT-1 to the SCF-complex resulting in its degradation. We managed to recapitulate interaction between SKR-1 and SEL-10 and furthermore observed an interaction between KSS-1 and SKR-1 and SKR-7 (Fig. 20), indicating that it binds to a component of the SCF-complex. This supports our hypothesis, that it could play a role in KLMT-1 degradation. Unfortunately, we could not recapitulate the interaction between SKR-1, SKR-7, SKR-20 and CUL-1, CUL-6 proteins (39). However, this does not discredit the interaction between KSS-1 and SKR-1 and SKR-7.



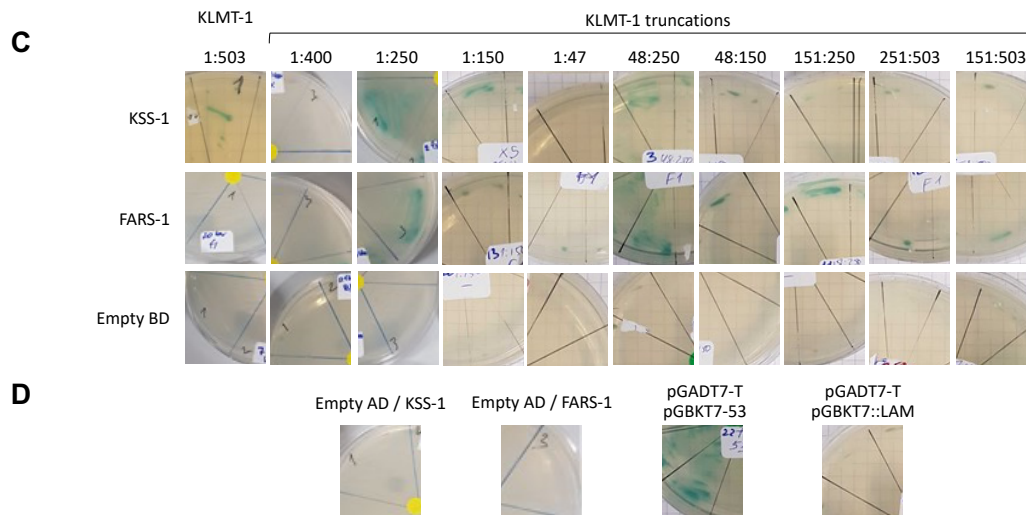


Figure 18. KLMT-1 interacts with KSS-1 and FARS-1 in Y2H assay. (A) Schematic representation of Y2H assay with all KLMT-1 fragments paired with KSS-1. Predicted intrinsically disordered regions of KLMT-1 using are schematically represented (top). (B) Schematic representation of Y2H assay with all KLMT-1 fragments paired with FARS-1. (C) Representative images of β -galactosidase assay. Transformed yeast colonies were streaked on synthetically defined (SD) medium lacking tryptophan and leucine but containing X-Gal and Aureobasidin A (SD/-Trp/-Leu/X-Gal/AbA). The blue coloration indicates a positive interaction, which was detected between DBD-KSS-1 and AD-KLMT-1 1:503, 1:250 and 48:250. Interaction between DBD-FARS-1 and AD-KLMT-1 1:250, 48:250 and 151:250 was also detected. No auto-activation was observed. Positive control was measured using pGBKT7-53 and pGADT7-T which encode for tumor suppressor p53 protein (53) and SV40 large T-antigen (T) (52). Negative control was measured using pGADT7-T and pGBKT7-LAM (human lamin C₍₆₆₋₂₃₀₎ protein). Plates were imaged 48 hours after streaking.

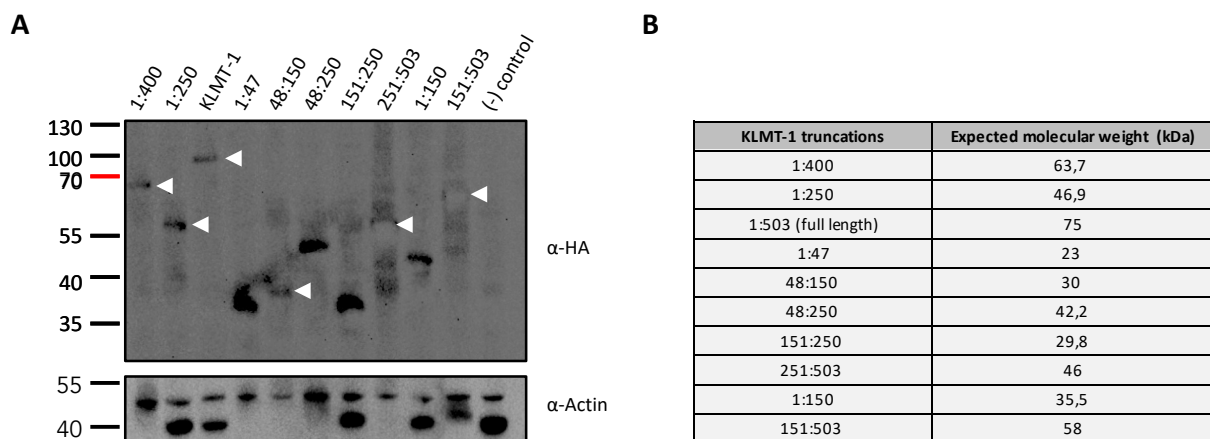


Figure 19. Western Blot showing the expression of KLMT-1 truncations in Y2H assay. (A) Western Blot of yeast protein lysates using anti-HA antibody showing that the KLMT-1 truncations are successfully expressed in the Y2H assay. Additionally, anti-b-actin antibody was used to control the amount of protein loaded and show the expected fragment sizes of 45kDa. Arrows indicate the bleached fragments. (B) Table showing the expected molecular weight of KLMT-1 truncations.

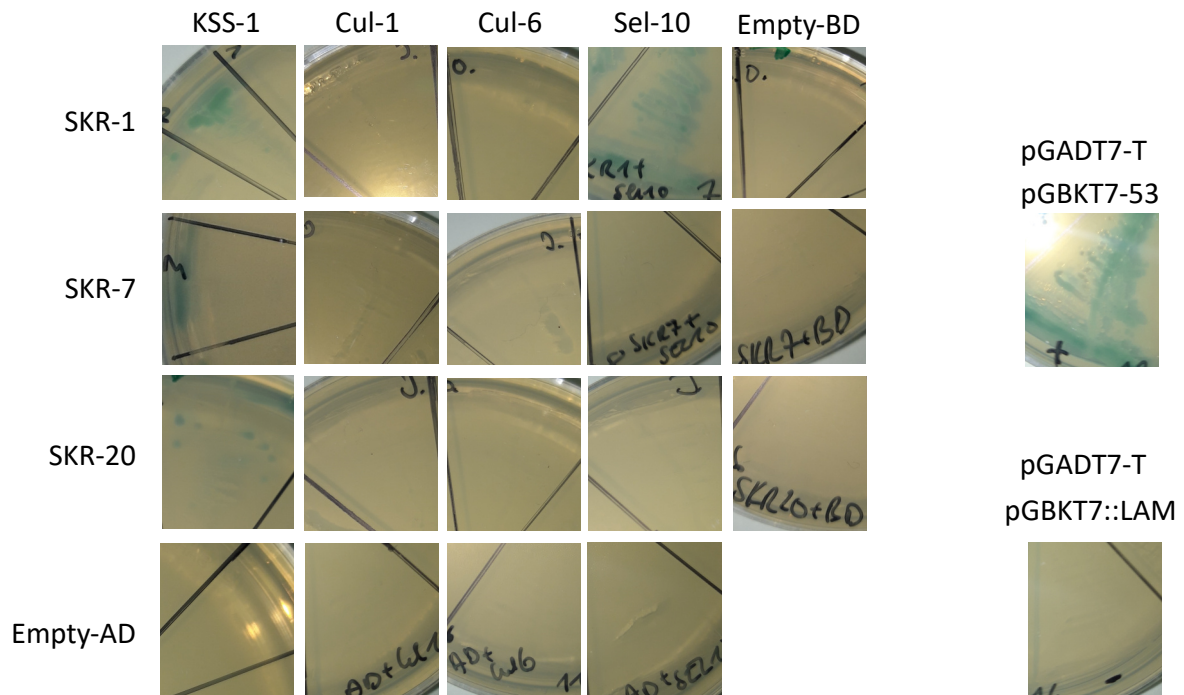


Figure 20. KSS-1 interacts with SKR-1 and SKR-7 in Y2H assay. Representative images of β -galactosidase assay. Transformed yeast colonies were streaked on synthetically defined (SD) medium lacking tryptophan and leucine but containing X-Gal and Aureobasidin A (SD/-Trp/-Leu/X-Gal/AbA). The blue coloration indicates a positive interaction, which was detected between DBD-KSS-1 and AD-SKR-1 and AD-SKR-7. Furthermore, we could recapitulate the interaction between DBD-Sel-10 and AD-SKR-7, which shows a blue coloration. No auto-activation was observed. Positive control was measured using pGBKT7-53 and pGADT7-T which encode for tumor suppressor p53 protein (53) and SV40 large T-antigen (T) (52). Negative control was measured using pGADT7-T and pGBKT7-LAM (human lamin C₍₆₆₋₂₃₀₎ protein). Images were taken 48 hours after streaking.

4.2. Aim 2: Specificity and evolutionary conservation of KLMT-1 toxicity

The evolution of the toxin, KLMT-1, from a highly essential and conserved enzyme that is required for aminoacylation of tRNA^{Phe}, offers a unique opportunity to investigate the molecular mechanism of a eukaryotic TA element and potentially provides insight into the evolution of TA elements and their impact on speciation. Although its putative target FARS-1 is highly conserved, we don't know whether KLMT-1 is toxic to other species.

4.2.1. Can KLMT-1 kill *Ceanorhabditis elegans*?

C. elegans and *C. tropicalis* are as divergent at the genetic level as human and mice. To investigate if *C. tropicalis* toxin KLMT-1 can poison its distant relative, we have generated a *C. elegans* transgenic line expressing KLMT-1 under a heat-shock-inducible promoter.

We generated this line by a cross between a transgenic line carrying *mCherry* flanked by two Frt sites and followed by *klmt-1*, all under a heat-shock promoter to a second transgenic line carrying a *flippase* recombinase (FLP) under the germline specific promoter *mex-5* (Fig. 21A)

(54). This allows for spatiotemporal expression of *klmt-1* in the germline and results in a heat shock-inducible *klmt-1* cassette (Fig. 21A). After inducing heat-shock in early embryos for 1h at 37C, we observed 2% (n=140) embryonic lethality in the control strain (N2), 11% (n=270) in the *mCherry* control transgenic line (before FLP mediated recombination), whereas 78% (n=371) in the heat-shock-inducible KLMT-1 transgenic line showed embryonic lethality and 21% (n=371) L1 arrest (Fig. 21C). When embryos were given 3 hours of development before exposing to the heat-shock, inducing overexpression of KLMT-1, drastically reduces the embryonic lethality to 34%, suggesting that the toxicity is stage-dependent (Fig. 21D). Furthermore, when applying a heat-shock in adult worms, we did not observe any severe effects after following them for 24h.

In addition, to confirm the heat-shock-inducible expression of *klmt-1*, we performed a Western Blot using protein lysates of embryos and mixed worm stages. While we did not observe any signal in the non-heat shock controls, we observed the expected pattern of 56.8 kDa in the worms and embryos that were exposed to a heat-shock, showing the successful induction of *klmt-1* expression (Fig. 21B). Interestingly, when comparing the three fragments on the Western blot of mixed worms and embryos that were exposed to a heat-shock, we observed that the mixed worms protein lysate shows a higher abundance of the middle fragment, while this middle fragment seems to be less abundant in the embryo protein lysate. Our results show that *klmt-1* is not only able to kill its distant relative *C. elegans*, but that the toxic effect is embryo specific and seems to be stronger when the expression is induced early in embryogenesis.

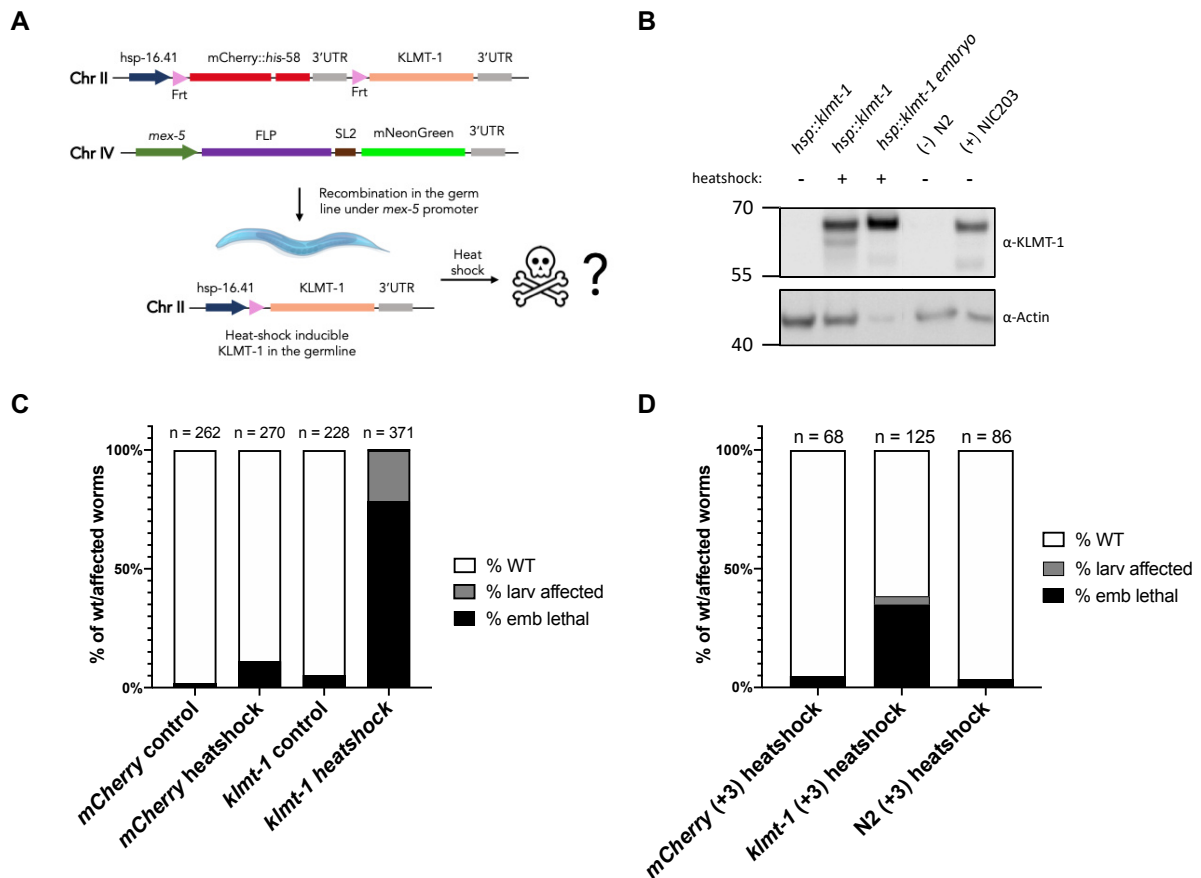


Figure 21. KLMT-1 expression in *C. elegans* is toxic for early embryos. (A) Schematic representation of mCherry reporter and *klmt-1* transgene integrated by MosSCI into chromosome II, and constructs expressing germline specific FLP recombinase inserted into chromosome IV. After recombination in germline, the downstream transgene *klmt-1* is under control of the heat-inducible promoter. (B) Western Blot using monoclonal *klmt-1* antibody showing the expression of KLMT-1 in total worm lysate and embryo extract upon heat shock (1 hour, 37°C). In addition, anti- β -actin antibody was used to control the amount of protein loaded and shows the expected fragment sizes of 45kDa. N2 (-), NIC203 (+). (C) Heat-induced expression of KLMT-1 in *C. elegans* compared to heat-induced expression of mCherry. (D) HS induction after embryos were given 3h of development reduces the toxic effect of *klmt-1* in embryos.

4.2.2. Can KLMT-1 kill *Saccharomyces cerevisiae*?

In our previous experiment we could show that KLMT-1 is able to poison *C. elegans*, a sister species to *C. tropicalis*. To decipher the toxic effect of KLMT-1 in another and even more distant eukaryotic species, we conducted experiments using *Saccharomyces cerevisiae*.

In *S. cerevisiae*, we have complemented the endogenous FRS1 (*YLR060W*) and FRS2 (*YFL022C*) with the homologous *fars-1* and *fars-3* from *C. tropicalis*. Complementation was accomplished by cloning *fars-1* and *fars-3* into a dual gene expression vector (pCEV-G2-Km) under two constitutive active *PGK1* and *TEF1* promoters and subsequently transformed into temperature sensitive (ts) *S. cerevisiae* strains. These strains carry mutant alleles of either FRS1 (*YLR060W*) or FRS2 (*YFL022C*) which are encoding for the subunits of the PheRS. FRS1

(*YLR060W*) and *FRS2* (*YFL022C*) strains were generated via diploid shuffle, a method for generating ts alleles for essential genes in *S. cerevisiae* (55). Growing these strains on 37°C allows precise conditional loss of the endogenous PheRS. As expected, after we incubated the ts strains in their restrictive temperature at 37°C for 2 days no growths could be detected (Fig. 22A, 23). However, this phenotype was rescued after the transformation of the *C. tropicalis* PheRS complex via a vector, expressing *fars-1* and *fars-3*. This suggests that the PheRS from *C. tropicalis* is capable to charge tRNA^{Phe} with L-phenylalanine in *S. cerevisiae* (PheRS-rescue) (Fig. 22A).

To test if KLMT-1 can interfere with the enzymatic activity of the PheRS, we cloned *klmt-1* into a galactose inducible gene expression vector (*p42::pGAL1-10::klmt-1*) into the PheRS-rescue strain. Unfortunately, after transforming *p42::pGAL1-10::klmt-1* into PheRS-rescue and incubation at 37°C for 2 days, no difference in growth could be detected on plates and in liquid media (Fig. 22B), suggesting the lack of potential co-factors or PTMs. Alternatively, this could indicate that FARS-1/FARS-3 is not the target of KLMT-1. In order to induce the conditional knockout of the PheRS, cells were grown at 37°C. While yeast tolerates these temperatures, *C. tropicalis* preferential temperature is 25°C. It is reasonable to suppose that the toxin KLMT-1 is sensitive to higher temperatures, abolishing its toxicity by misfolding. Regarding our hypothesis, KLMT-1 binds FARS-1 to exert its toxic effect, thereby competing with its binding partner FARS-3. It was previously reported that the *TEF1* promoter drives strong expression in galactose media (56). Since *TEF1* promoter drives the expression of FARS-3, one additional reason why KLMT-1 shows no effect in the PheRS-rescue yeast may be explained by the strong expression of FARS-3, resulting in a dosage problem between FARS-3 and KLMT-1. Therefore, it is conceivable that the toxic effect of KLMT-1 within the PheRS-rescue yeast is masked because of the high amount of functional PheRS, which are sufficient for the cells to survive. Expression of KLMT-1 was validated by Western Blot and shows the correct molecular weight of 56.9 kDa, after inducing its expression with galactose (Fig. 22C).

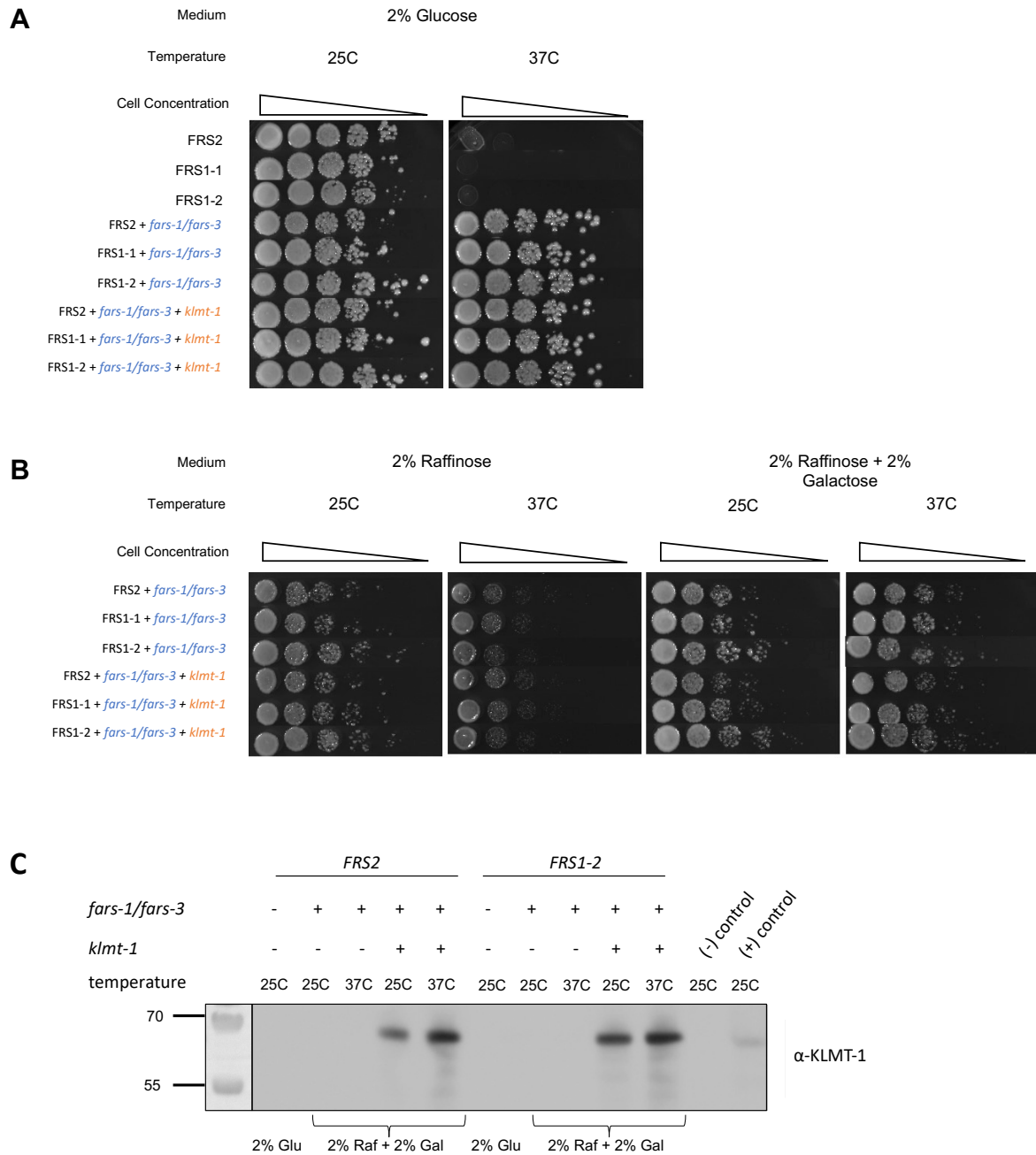


Figure 22. KLMT-1 overexpression has no effect in *PheRS* rescued yeast. Temperature sensitive *FRS1-1/FRS1-2* (YLR060W) or *FRS2* (YFL022C) strains were transformed with *pCEV-G2-Km::fars1::fars3* (blue) or with *pCEV-G2-Km::fars1::fars3* and *p42Nat::pGal1-10::klmt-1* (red). Each row represents a dilution series of 1:10 from a different yeast culture, starting with an OD600 of 0.1. The same volume of 5ul was used for each dilution spot. Yeast strains were incubated at 25°C (left) or at the restrictive temperature of 37°C (right). Growth was examined after 48 h. (A) *FARS-1* and *FARS-3* co-expression rescues the *ts* mutations. (B) Galactose induced overexpression of *KLMT-1* shows no change in growth behavior. Yeast strains were grown in 2% Raffinose YPD, before they were incubated on either 2% Raffinose (left) or 2% Raffinose/2% Galactose (right) plates. *KLMT-1* overexpression induced by Galactose shows no effect on growth behavior. (C) Western blot showing the expected pattern of 56.9 kDa of *KLMT-1* after inducing its overexpression by Galactose, while no expression was observed in only Glucose or Raffinose media.

A previous study has shown that loss of PheRS editing activity leads to accumulation of misaminoacylated tRNA^{Phe} and that PheRS editing activity is required for optimal growth during amino acid stress (57). Motivated by these findings we were interested if KLMT-1 impairs the PheRS editing activity. To simulate the conditions of an amino acid stress, we grew the PheRS-rescue strains, either with the galactose inducible KLMT-1 vector or an empty vector, in SDMM media supplemented with 1:400 or 400:400 Phe:Tyr (1 = 0.003 mM and 400 = 1.2 mM). The supplementation with an excess amount of Tyr over Phe, increases the chance of mis-aminoacylation of tRNA^{Phe} in yeast (54). While all PheRS-rescue strains grew on 25°C, the viability of the PheRS-rescue strains independent of KLMT-1 was reduced to zero when incubated at 37°C (Fig. 24).

Overall, no effect of KLMT-1 toxicity was observed in the PheRS-rescue strain.

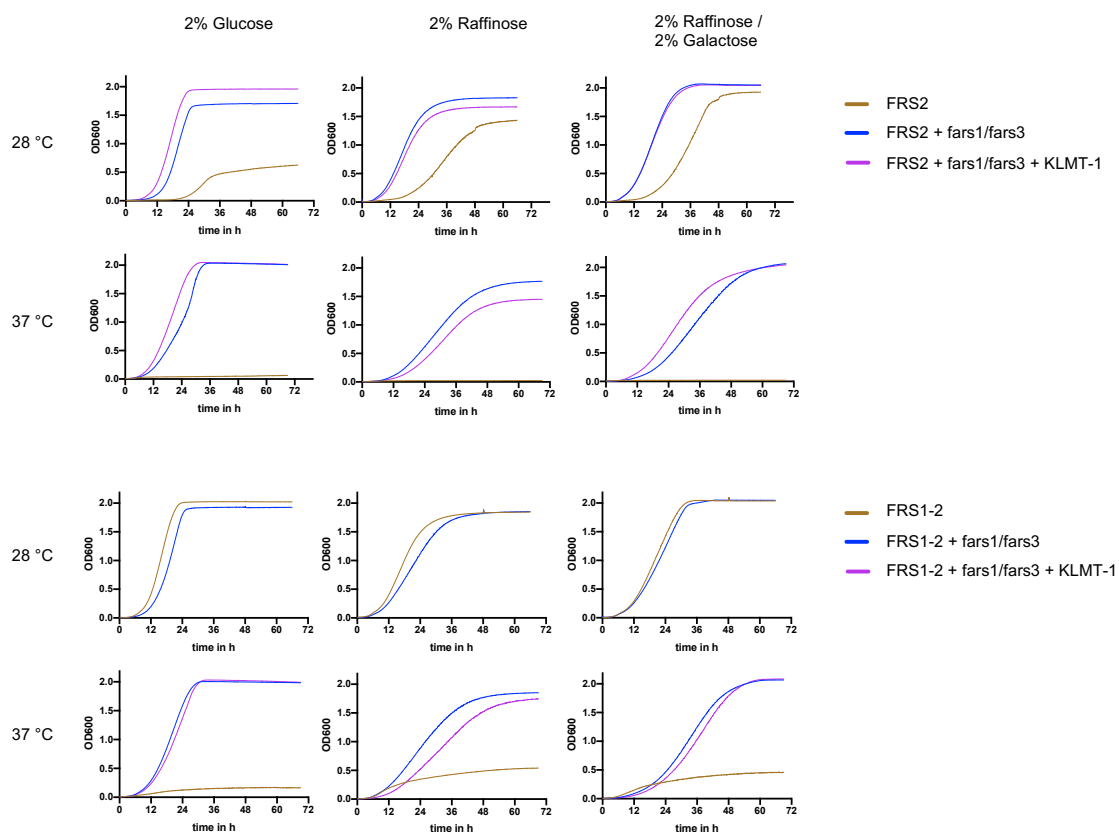


Figure 23. KLMT-1 overexpression has no effect in PheRS rescued yeast in liquid culture. Temperature sensitive FRS1-2 (YLR060W) or FRS2 (YFL022C) (yellow) strains were transformed with pCEV-G2-Km::fars1::fars3 (blue) or with pCEV-G2-Km::fars1::fars3 and p42Nat::pGal1-10::KLMT-1 (purple). Growth was monitored by measuring the absorbance at 600nm using a microplate spectrophotometer at either 28°C or 37°C for 72 h

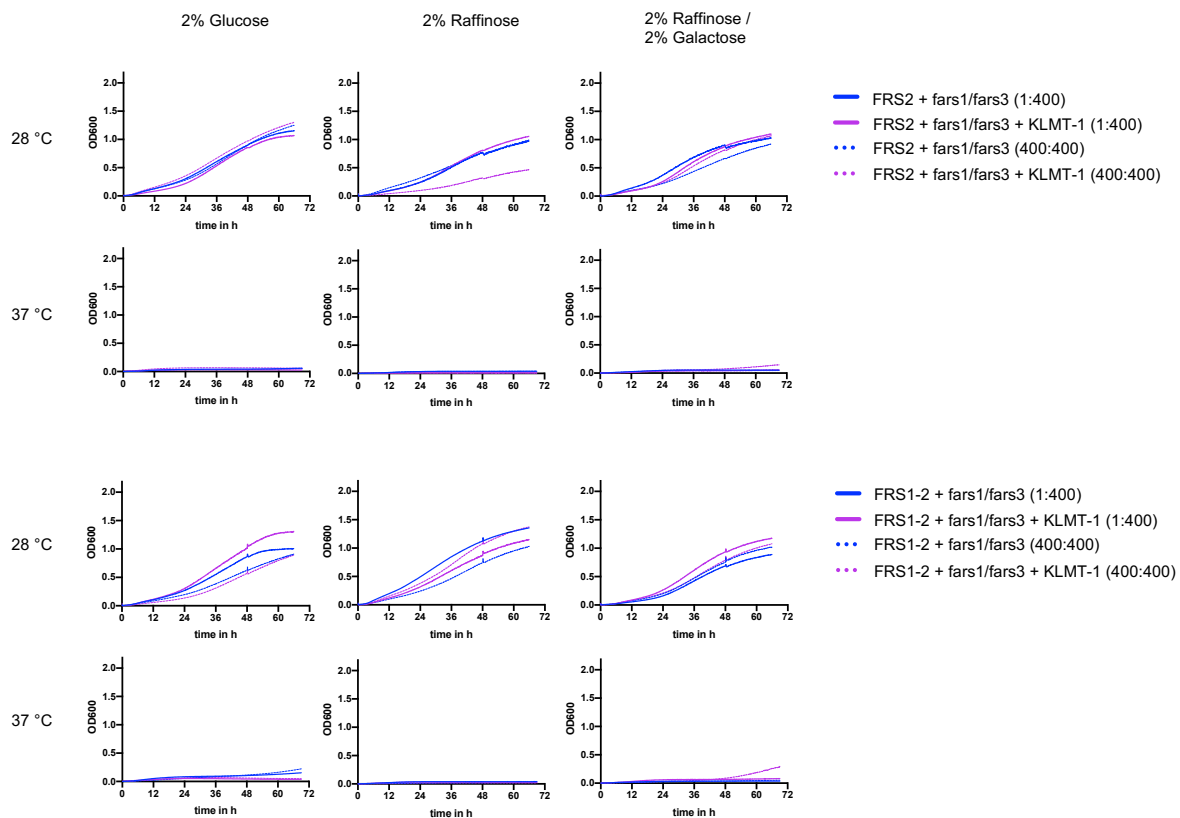


Figure 24. Tyrosine stress media shows no effect in *PheRS* editing ability in rescued yeast. Synthetic defined minimal medium (SDMM) was supplemented with 1:400 or 400:400, Phe:Tyr (1 = 0.003 mM and 400 = 1.2 mM) and inoculated with different yeast cultures to a starting OD₆₀₀ of 0.01. Growth was monitored by measuring the absorbance at 600nm using a microplate spectrophotometer at either 28°C or 37°C for 72 h.

5. Conclusion & future directions

TA-elements efficiently kill individuals that do not inherit them, guaranteeing their transmission to the next generation. Despite their simple genetic arrangement, they are capable of quickly spreading in natural populations. However, the molecular mechanism remains unclear. The present study outlines the first comprehensive characterization of the expression pattern of the *klmt-1/kss-1* TA element in *C. tropicalis*.

Our results indicate that KLMT-1 mRNA and protein are maternally deposited in eggs prior to fertilization, which matches the TA model inferred from our genetic crosses (Fig. 1). Later in embryonic development KLMT-1 is exclusively found in two cells, presumably the germline precursors (Z2 and Z3), which will give rise to the adult germline. Although we did not use any marker for co-localization of KLMT-1 with the germline cells, we tracked the mNG signal in the *klmt-1::2Ty::mNG* strain and observed that they will develop into the gonads, thereby supporting our assumption that KLMT-1 localizes in germline precursors in early embryos.

These observations suggest that *klmt-1* mRNA is expressed in the germline as early as embryonic development and that maternal-effect killing occurs through delivery of either oocyte-supplied transcripts or protein.

One important insight coming from this work is that we could for the first time observe that the antidote KSS-1 plays a role in the degradation of KLMT-1 in early development of embryos. While the stable KLMT-1::2Ty::mNG signal in the absence of KSS-1, could be a result of a lack of repression by KSS-1, we rather speculate that KSS-1 is involved in targeting KLMT-1 for degradation as a part of the SCF complex because of its predicted F-box and FBA domain. This interaction is also supported by our Y2H results, which strongly suggest that KSS-1 binds KLMT-1 as part of the SCF complex and that this interaction eventually results in KLMT-1 ubiquitination and proteasomal degradation. Although the mNG tag impairs the toxicity of KLMT-1, our data supports the hypothesis that the toxin KLMT-1 has two important interactions with (i) its target FARS-1 and (ii) its antidote KSS-1. Interestingly KLMT-1 degradation occurs in all cells except for the germline cells and this happens within a small time-window of approximately 30min. Based on this observation, we propose that there is a small burst-window of KSS-1 expression right after the transcriptional activation of the zygote. Furthermore, this raises the question how KLMT-1 can be present in the germline, without exerting its toxic effect. One possible explanation is the presence of factors that bind and inhibit KLMT-1 either directly or indirectly. Alternatively, KLMT-1 may need to be activated after fertilization. Interestingly, we observed the presence of foci and aggregates in our *in vivo* and IF images of *klmt-1::2Ty::mNG* strain. This surprising observation is interesting because it is rare that proteins with a fluorescent tag start forming aggregates. Moreover, we noticed that KLMT-1 tends to form aggregates when trying to purify it and this property seems to be enhanced with the fusion of mNG. Whether this is a property of KLMT-1 with any physiological relevance is still unknown. On the other hand, the ability to form aggregations may be one possible explanation of how KLMT-1 is toxic in embryos but non-toxic in the gonads of carrier mothers. This change in the quaternary structure of KLMT-1 might be a result of PTMS. Since we know that KLMT-1 exert its toxic effect in embryos, but we only observe aggregations of the inactive toxin tagged with mNG, we assume that the non-aggregation form is more likely the active form of KLMT-1.

While in previous *in vitro* studies, we observed an interaction between KLMT-1/FARS-1, no interaction between the full lengths KLMT-1 and FARS-1 could be detected via Y2H. Although

Y2H assays have been among the most powerful methods to detect binary protein-protein interactions, it is conceivable that the fusion of AD or DBD impairs the binding between KLMT-1 and FARS-1, resulting in false negative interaction. We found that the truncated KLMT-1 48:250AA is not only interacting with the antidote KSS-1, but also with its putative target FARS-1, suggesting the unstructured regions to be not necessary for interaction.

The ability of selfish elements to spread in populations could be applied as a potential synthetic gene drive controlling vector borne diseases. To be a potential candidate synthetic gene drive, it needs to be toxic in other species. To determine whether KLMT-1 can function as a toxin in *C. elegans*, KLMT-1 was expressed using a heat-shock promoter. Our results show that KLMT-1 is a potent killer in *C. elegans* embryos. Moreover, KLMT-1 not only induced embryonic lethality but also larval arrest phenotype, which is consistent with our observation in *C. tropicalis* crosses. The emergence of two phenotypes suggests that the toxic effect might be dosage depended. We speculate that those worms that may have experienced a lower level of KLMT-1 overexpression, or experienced it in later stages, are more likely to arrest in later stages of embryonic development.

To further characterize this effect in *C. elegans* we induced expression in embryos later in development and adults. Unlike in the TA *peel-1/zeel-1* found in *C. elegans*, no evidence of a toxin function outside of embryos was found. The fact that embryos were given 3 hours before inducing heat shock drastically increased their survival rate, implies that KLMT-1 needs to be present early in development to fulfill its toxic effect or later stages are less sensitive.

In order to investigate if KLMT-1/KSS-1 TA element is a universal killer, we successfully transformed the PheRS from *C. tropicalis* into yeast carrying ts mutations within its endogenous PheRS genes. Our results show that the PheRS-rescue yeast is able to survive when grown in the restrictive temperatures. Unfortunately, KLMT-1 overexpression shows no growth deficiency, suggesting the lack of potential co-factors or a dosage problem. In order to induce the conditional knockout of the PheRS, cells were grown at 37°C. While yeast tolerates these temperatures, *C. tropicalis* preferential temperature is 25°C. It is reasonable to suppose that the toxin KLMT-1 is sensitive to higher temperatures, abolishing its toxicity by misfolding. Another problem that possibly masks the toxic effect of KLMT-1 is the relative abundance of the overexpressed KLMT-1 and highly expressed FARS-1 and FARS-3, as a result of strong promoters and high plasmid copy numbers. To overcome these problems, we aim

to integrate *C. tropicalis fars-1* and *fars-3* into the yeast genome by replacing the endogenous FRS1 or FRS2 using homologous recombination. This will reduce the expression of *fars-1* and *fars-3* and eliminate the need to grow the strains on the restrictive temperatures.

One possible molecular mechanism of KLMT-1 toxicity could involve a drastic increase of tRNA misscharging errors. A previous study showed that under normal growth conditions mistranslation is well tolerated in yeast, while PheRS editing activity is required for optimal growth during amino acid stress (57). To challenge the editing activity, we exposed our yeast transformants to SDMM media supplemented with excess amount of L-Tyrosine, inducing amino acid stress and misincorporation. Although strains grew at 25°C, the additional exposure to 37°C while being grown in amino acid starving media supplemented with two different antibiotics, possibly negatively affecting the protein homeostasis in yeast, resulting in multifactorial stress induced cell death.

With our experiments, we have found strong support for our hypothesis that the toxin KLMT-1 exerts its toxicity in embryos by interaction with FARS-1, while the antidote KSS-1 is likely involved in its degradation through binding to the SCF-complex. To gain further insights in the molecular mechanism *in vivo*, we will continue truncating KLMT-1/KSS-1 and introduce mutations until we eventually find important regions for interaction at the single residue level. Furthermore, in this study we have generated and validated many transgenic lines, which allows us to implement standard molecular techniques in the future e.g. Immunoprecipitation (IP), which allows to identify protein–protein interactions, or evaluate protein PTMs. Future work will further dissect the spatio-temporal expression pattern by investigating *klmt-1/kss-1* mRNA in gonads, *kss-1* mRNA in embryos using smFISH and immunolabeling. We will further characterize the specific stage in development in which KLMT-1 is (i) toxic, (ii) not toxic anymore or (iii) toxic but resulting in larval arrest using time-lapse, which will also address the question the dosage dependency of KLMT-1 toxic effect. Furthermore, we aim to investigate PTMs on KLMT-1 and its disordered regions by using phosphatases and deacetylases that are involved in PTMs on KLMT-1 protein extracts, which might play a crucial role in the activity and localization of the toxin.

In addition, we aim to elaborate on the *C. elegans* strain carrying an inducible KLMT-1 transgene by rescuing the toxic effect by KLMT-1. This will be accomplished by introducing transgenes or extrachromosomal arrays which conditionally express *kss-1* or overexpress

fars-1 and *fars-3*, which will not only help us to understand the molecular mechanism but also helps to find the necessary key players for the design of synthetic gene drive.

Our current model does not involve co-factors, therefore we are aiming to perform IP in *C. elegans* carrying inducible KLMT-1 transgene and *C. tropicalis* with subsequent liquid chromatography and mass spectrometry, which enables the identification of potential co-factors. In addition, we will perform mutagenesis suppressor screens by mutagenizing *C. elegans* worm carrying inducible KLMT-1 transgene and applying additional selection by heat shock. We expect to see mutations within toxin itself, mutations in co-factors, mutation in target of toxin.

If we have success in finding potential co-factors, we will clone and transform them into our PheRS-rescue yeast. This will unravel the minimal necessary components which are important for the toxic activity of KLMT-1 in other species and will push the research on its ability to be a potential synthetic gene drive.

To verify the involvement of the ubiquitin-mediated proteolysis in the mechanism of action of *klmt-1/kss-1*, we will assess whether the KLMT-1 toxin is ubiquitinated *in vivo* by implementation of bortezomib, a potent inhibitor of the 26S proteasome.

KLMT-1/KSS-1 is not only an interesting target to understand the molecular mechanism of a TA element, it will also contribute to the understanding of how conserved proteins may turn into killing machines. Furthermore, due to the protein structure of KLMT-1, this TA element will also expand the current knowledge on the effect and mechanism of action of disordered regions within a protein. Understanding how TAs work will greatly enhance our current knowledge of their contribution to evolution and speciation.

6. Acknowledgements

Foremost, I would like to express my sincere gratitude to my advisor Dr. Alejandro Burga for the continuous support of my Master studies and research, for his patience, motivation, enthusiasm, and immense knowledge. His guidance helped me during all the time of research and writing of this thesis. I could not have imagined having a better advisor and mentor for my Master studies.

Besides my advisor, I would like to thank my lovely fellow lab mates at IMBA in Alejandro Burgas Group: for the stimulating discussions, for the sleepless nights we were working together, and for all the fun we have had in the last year. You are the best!

I would also like to thank the IMP/IMBA Core Facilities, especially the cutting edge service offered by the BioOptic Facility and the Molecular Biology Service, who supported me with the experimental design and helped to implement novel technologies.

I would like to thank my girlfriend, Natalie Özgen, for always being supportive and all the fruitful discussions. I am very grateful to have you in my life.

Last but not the least, I would like to thank my family, especially my mother Rita Hüfing and my stepfather Ralf Hüfing for supporting me spiritually throughout my life. The support you gave me cannot be put into words.

7. References

1. Schnabel H, Schnabel R. An Organ-Specific Differentiation Gene, *pha-1*, from *Caenorhabditis elegans*. *Science*. 1990 Nov 2;250(4981):686–8.
2. Beeman R, Friesen K, Denell R. Maternal-effect selfish genes in flour beetles. *Science*. 1992 Apr 3;256(5053):89–92.
3. Doolittle, W.F., and Sapienza, C. (1980). Selfish genes, the phenotype paradigm and genome evolution. *Nature* 284, 601–603.
4. Burt, A., and Trivers, R. (2006). *Genes in Conflict: The Biology of Selfish Genetic Elements* (Harvard University Press).
5. Orgel, L.E., and Crick, F.H.C. (1980). Selfish DNA: the ultimate parasite. *Nature* 284, 604–607.
6. Hickey DA. Selfish DNA: a sexually-transmitted nuclear parasite. *Genetics*. 1982 Aug;101(3–4):519–31.
7. Lyttle TW. Segregation Distorters. *Annu Rev Genet*. 1991 Dec;25(1):511–81.
8. Werren JH. BIOLOGY OF *WOLBACHIA*. *Annu Rev Entomol*. 1997 Jan;42(1):587–609.

9. Brennecke J, Malone CD, Aravin AA, Sachidanandam R, Stark A, Hannon GJ. An Epigenetic Role for Maternally Inherited piRNAs in Transposon Silencing. *Science*. 2008 Nov 28;322(5906):1387–92.
10. Yang J, Zhao X, Cheng K, Du H, Ouyang Y, Chen J, et al. A Killer-Protector System Regulates Both Hybrid Sterility and Segregation Distortion in Rice. *Science*. 2012 Sep 14;337(6100):1336–40.
11. Zanders SE, Eickbush MT, Yu JS, Kang J-W, Fowler KR, Smith GR, et al. Genome rearrangements and pervasive meiotic drive cause hybrid infertility in fission yeast. *eLife*. 2014 Jun 24;3:e02630.
12. Collins JP. Gene drives in our future: challenges of and opportunities for using a self-sustaining technology in pest and vector management. *BMC Proc*. 2018 Jul;12(S8):9.
13. Yamaguchi Y, Park J-H, Inouye M. Toxin-Antitoxin Systems in Bacteria and Archaea. *Annu Rev Genet*. 2011 Dec 15;45(1):61–79.
14. Seidel HS, Rockman MV, Kruglyak L. Widespread Genetic Incompatibility in *C. Elegans* Maintained by Balancing Selection. *Science*. 2008 Feb 1;319(5863):589–94.
15. Lorenzen MD, Gnirke A, Margolis J, Garnes J, Campbell M, Stuart JJ, et al. The maternal-effect, selfish genetic element *Medea* is associated with a composite Tc1 transposon. *Proc Natl Acad Sci*. 2008 Jul 22;105(29):10085–9.
16. Ben-David E, Burga A, Kruglyak L. A maternal-effect selfish genetic element in *Caenorhabditis elegans*. *Science*. 2017 Jun 9;356(6342):1051–5.
17. Ben-David E, Pliota P, Widen SA, Koreshova A, Lemus-Vergara T, Verpukhovskiy P, et al. Ubiquitous selfish toxin-antidote elements in *Caenorhabditis* species [Internet]. *Genomics*; 2020 Aug [cited 2021 Apr 1]. Available from: <http://biorxiv.org/lookup/doi/10.1101/2020.08.06.240564>
18. Burga A, Ben-David E, Kruglyak L. Toxin-Antidote Elements Across the Tree of Life. *Annu Rev Genet* [Internet]. 2020 Sep 4 [cited 2020 Oct 20]; Available from: <https://doi.org/10.1146/annurev-genet-112618-043659>
19. Brenner S. The genetics of *Caenorhabditis elegans*. *Genetics*. 1974 May;77(1):71–94.
20. Stevens L, Félix M-A, Beltran T, Braendle C, Caurcel C, Fausett S, et al. Comparative genomics of 10 new *Caenorhabditis* species. *Evol Lett*. 2019 Apr;3(2):217–36.
21. Gimond C, Jovelin R, Han S, Ferrari C, Cutter AD, Braendle C. OUTBREEDING DEPRESSION WITH LOW GENETIC VARIATION IN SELFING *CAENORHABDITIS* NEMATODES: OUTBREEDING DEPRESSION IN SELFING NEMATODES. *Evolution*. 2013 Nov;67(11):3087–101.

22. Muehlbauer GJ, Specht JE, Thomas-Compton MA, Staswick PE, Bernard RL. Near-Isogenic Lines—A Potential Resource in the Integration of Conventional and Molecular Marker Linkage Maps. *Crop Sci.* 1988 Sep;28(5):729–35.
23. Wade MJ, Beeman RW. The population dynamics of maternal-effect selfish genes. *Genetics.* 1994 Dec;138(4):1309–14.
24. Dokshin GA, Ghanta KS, Piscopo KM, Mello CC. Robust Genome Editing with Short Single-Stranded and Long, Partially Single-Stranded DNA Donors in *Caenorhabditis elegans*. *Genetics.* 2018 Nov 1;210(3):781–7.
25. Roy H, Ibba M. Phenylalanyl-tRNA Synthetase Contains a Dispensable RNA-Binding Domain that Contributes to the Editing of Noncognate Aminoacyl-tRNA[†]. *Biochemistry.* 2006 Aug;45(30):9156–62.
26. Ling J, Yadavalli SS, Ibba M. Phenylalanyl-tRNA synthetase editing defects result in efficient mistranslation of phenylalanine codons as tyrosine. *RNA.* 2007 Sep 5;13(11):1881–6.
27. Lu J, Bergert M, Walther A, Suter B. Double-sieving-defective aminoacyl-tRNA synthetase causes protein mistranslation and affects cellular physiology and development. *Nat Commun.* 2014 Dec;5(1):5650.
28. Bullwinkle TJ, Ibba M. Emergence and Evolution. In: Kim S, editor. *Aminoacyl-tRNA Synthetases in Biology and Medicine* [Internet]. Dordrecht: Springer Netherlands; 2013 [cited 2021 Apr 2]. p. 43–87. (Topics in Current Chemistry; vol. 344). Available from: http://link.springer.com/10.1007/128_2013_423
29. Finarov I, Moor N, Kessler N, Klipcan L, Safro MG. Structure of Human Cytosolic Phenylalanyl-tRNA Synthetase: Evidence for Kingdom-Specific Design of the Active Sites and tRNA Binding Patterns. *Structure.* 2010 Mar;18(3):343–53.
30. Sanni A, Mirande M, Ebel JP, Boulanger Y, Waller JP, Fasiolo F. Structure and expression of the genes encoding the alpha and beta subunits of yeast phenylalanyl-tRNA synthetase. *J Biol Chem.* 1988 Oct 25;263(30):15407–15.
31. Erdős G, Dosztányi Z. Analyzing Protein Disorder with IUPred2A. *Curr Protoc Bioinforma* [Internet]. 2020 Jun [cited 2021 Apr 8];70(1). Available from: <https://onlinelibrary.wiley.com/doi/abs/10.1002/cpbi.99>
32. Mészáros B, Erdős G, Dosztányi Z. IUPred2A: context-dependent prediction of protein disorder as a function of redox state and protein binding. *Nucleic Acids Res.* 2018 Jul 2;46(W1):W329–37.
33. Dosztányi Z, Csizmók V, Tompa P, Simon I. The Pairwise Energy Content Estimated from Amino Acid Composition Discriminates between Folded and Intrinsically Unstructured Proteins. *J Mol Biol.* 2005 Apr;347(4):827–39.

34. Mészáros B, Simon I, Dosztányi Z. Prediction of Protein Binding Regions in Disordered Proteins. Casadio R, editor. PLoS Comput Biol. 2009 May 1;5(5):e1000376.
35. Dyson HJ, Wright PE. Intrinsically unstructured proteins and their functions. Nat Rev Mol Cell Biol. 2005 Mar;6(3):197–208.
36. Jaakkola P, Mole DR, Tian YM, Wilson MI, Gielbert J, Gaskell SJ, et al. Targeting of HIF- α to the von Hippel-Lindau ubiquitylation complex by O₂-regulated prolyl hydroxylation. Science. 2001 Apr 20;292(5516):468–72.
37. Bu Z, Callaway DJE. Proteins MOVE! Protein dynamics and long-range allostery in cell signaling. In: Advances in Protein Chemistry and Structural Biology [Internet]. Elsevier; 2011 [cited 2021 Apr 3]. p. 163–221. Available from: <https://linkinghub.elsevier.com/retrieve/pii/B9780123812629000057>
38. Kipreos ET, Pagano M. The F-box protein family. Genome Biol. 2000;1(5):reviews3002.1.
39. Zheng N, Schulman BA, Song L, Miller JJ, Jeffrey PD, Wang P, et al. Structure of the Cul1-Rbx1-Skp1-F boxSkp2 SCF ubiquitin ligase complex. Nature. 2002 Apr 18;416(6882):703–9.
40. Raj A, Rifkin SA, Andersen E, van Oudenaarden A. Variability in gene expression underlies incomplete penetrance. Nature. 2010 Feb 18;463(7283):913–8.
41. Porta-de-la-Riva M, Fontrodona L, Villanueva A, Cerón J. Basic Caenorhabditis elegans Methods: Synchronization and Observation. J Vis Exp. 2012 Jun 10;(64):4019.
42. Kushnirov VV. Rapid and reliable protein extraction from yeast. Yeast Chichester Engl. 2000 Jun 30;16(9):857–60.
43. Dickinson DJ, Goldstein B. CRISPR-Based Methods for Caenorhabditis elegans Genome Engineering. Genetics. 2016 Mar;202(3):885–901.
44. Einhauer A, Jungbauer A. The FLAGTM peptide, a versatile fusion tag for the purification of recombinant proteins. J Biochem Biophys Methods. 2001 Oct;49(1–3):455–65.
45. Shaner N., Lambert, G., Chammas, A. et al. A bright monomeric green fluorescent protein derived from Branchiostoma lanceolatum. Nat Methods 10, 407–409 (2013). <https://doi.org/10.1038/nmeth.2413>.
46. Hostettler L, Grundy L, Käser-Pébernard S, Wicky C, Schafer WR, Glauser DA. The Bright Fluorescent Protein mNeonGreen Facilitates Protein Expression Analysis *In Vivo*. G3 GenesGenomesGenetics. 2017 Feb 1;7(2):607–15.
47. Pazdernik N, Schedl T. Introduction to germ cell development in Caenorhabditis elegans. Adv Exp Med Biol. 2013;757:1–16.
48. Waters KA, Reinke V. Extrinsic and intrinsic control of germ cell proliferation in *Caenorhabditis elegans*: GERM CELL PROLIFERATION IN *C. ELEGANS*. Mol Reprod Dev. 2011 Mar;78(3):151–60.

49. Hall DH, Herndon LA, Altun Z. WormAtlas Embryo Handbook - Introduction to *C. elegans* Embryo Anatomy. WormAtlas [Internet]. 2017 Nov [cited 2021 Oct 21]; Available from: <http://www.wormatlas.org/embryo/introduction/EIntroframeset.html>
50. Pellettieri J, Reinke V, Kim SK, Seydoux G. Coordinate Activation of Maternal Protein Degradation during the Egg-to-Embryo Transition in *C. elegans*. *Dev Cell*. 2003 Sep;5(3):451–62.
51. Masterthesis, Titel der Masterarbeit / Title of the Master's Thesis „Protein purification of a novel toxin-antidote selfish element in *Caenorhabditis tropicalis*“ submitted by Manuel David Hunold, BSc, 2020.
52. Yu D, Liao L, Zhang J, Zhang Y, Xu K, Liu K, et al. A novel, easy and rapid method for constructing yeast two-hybrid vectors using In-Fusion technology. *BioTechniques*. 2018 May;64(5):219–24.
53. Killian DJ, Harvey E, Johnson P, Otori M, Mitani S, Xue D. SKR-1, a homolog of Skp1 and a member of the SCFSEL-10 complex, regulates sex-determination and LIN-12/Notch signaling in *C. elegans*. *Dev Biol*. 2008 Oct;322(2):322–31.
54. Muñoz-Jiménez C, Ayuso C, Dobrzynska A, Torres-Mendéz A, Ruiz P de la C, Askjaer P. An Efficient FLP-Based Toolkit for Spatiotemporal Control of Gene Expression in *Caenorhabditis elegans*. *Genetics*. 2017 Aug 1;206(4):1763–78.
55. Ben-Aroya S, Coombes C, Kwok T, O'Donnell KA, Boeke JD, Hieter P. Toward a Comprehensive Temperature-Sensitive Mutant Repository of the Essential Genes of *Saccharomyces cerevisiae*. *Mol Cell*. 2008 Apr;30(2):248–58.
56. Vickers CE, Bydder SF, Zhou Y, Nielsen LK. Dual gene expression cassette vectors with antibiotic selection markers for engineering in *Saccharomyces cerevisiae*. *Microb Cell Factories*. 2013;12(1):96.
57. Mohler K, Mann R, Bullwinkle TJ, Hopkins K, Hwang L, Reynolds NM, et al. Editing of misaminoacylated tRNA controls the sensitivity of amino acid stress responses in *Saccharomyces cerevisiae*. *Nucleic Acids Res*. 2017 Apr 20;45(7):3985–96.

8. Supplementary Data

A

Description	Scientific Name	Max Score	Total Score	Query Cover	E value	Per. Ident	Acc. Len	Accession
Phenylalanine--tRNA ligase beta subunit [Caenorhabditis elegans]	Caenorhabditis elegans	343	343	70%	9e-108	50.83%	591	NP_495785.1
hypothetical protein GCK72_004979 [Caenorhabditis remanei]	Caenorhabditis remanei	332	332	70%	2e-103	50.83%	591	KAF1765028.1
CRE-FARS-3 protein [Caenorhabditis remanei]	Caenorhabditis remanei	332	332	70%	4e-103	50.97%	606	XP_003117512.1
hypothetical protein CAEBREN_17714 [Caenorhabditis brenneri]	Caenorhabditis brenneri	325	325	70%	1e-100	49.72%	592	EGT60199.1
hypothetical protein CAEBREN_24660 [Caenorhabditis brenneri]	Caenorhabditis brenneri	325	325	70%	1e-100	49.72%	592	EGT52316.1
hypothetical protein B9Z55_004800 [Caenorhabditis nigoni]	Caenorhabditis nigoni	324	324	70%	1e-100	50.00%	591	PIC44431.1
C. briggsae CBR-FRS-2 protein [Caenorhabditis briggsae]	Caenorhabditis briggsae	324	324	70%	2e-100	50.00%	591	XP_002630211.1
unnamed protein product [Caenorhabditis bovis]	Caenorhabditis bovis	318	318	69%	4e-98	48.60%	591	CAB3410924.1
hypothetical protein Y032_0016g2912 [Ancylostoma ceylanicum]	Ancylostoma ceylanicum	279	279	70%	4e-83	43.21%	593	EYC22719.1
hypothetical protein WR25_15973 [Diploscapter pachys]	Diploscapter pachys	283	283	70%	4e-83	44.48%	756	PAV80470.1

B

Phenylalanine--tRNA ligase beta subunit [Caenorhabditis elegans]

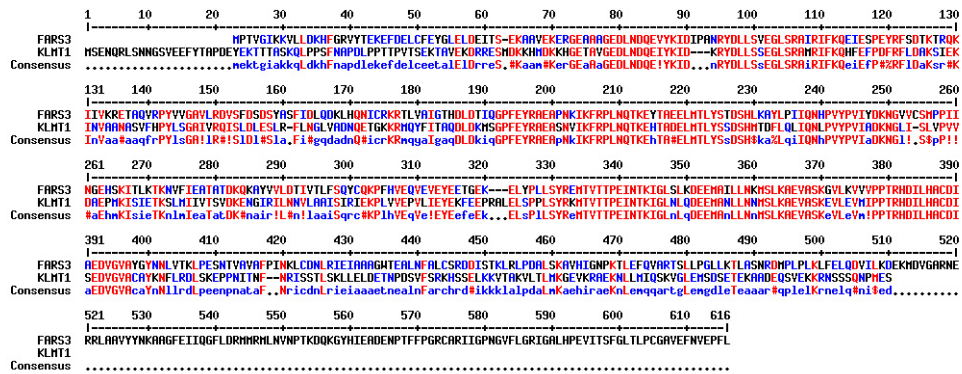
Sequence ID: [NP_495785.1](#) Length: 591 Number of Matches: 1

[See 2 more title\(s\)](#) [See all Identical Proteins \(IPG\)](#)

Range 1: 38 to 382 [GenPept](#) [Graphics](#) [Next Match](#) [Previous Match](#)

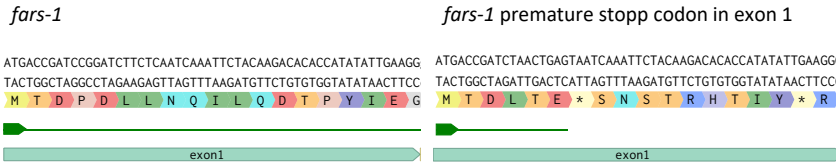
Score	Expect	Method	Identities	Positives	Gaps
343 bits(880)	9e-108	Compositional matrix adjust.	184/362(51%)	241/362(66%)	24/362(6%)
Query 48	VTSEKTAVEKDRRESMDKKHMDKKHGETAVGEDLNDQEIYKID---KRYDLLSSEGLSRA	104			
Sbjct 38	+TSEK AVEK++ T DNDQIE+YKID RYDLLS EGL+RA ITSEKAAVEKEQG-----TRAASDLNDQIEVYKIDIPANRYDLLSVEGLARA	83			
Query 105	MRIFKQHFEPDFRFLDA---KSTIEKINVAANASVFHYPYLSGAVRQISLDLESL--RFLNG	161			
Sbjct 84	+RIFKQ P+++D ++KI V + P++ GA++R IS D+S F++ IRIFKQEIIPSPAYKADVPKTLGKQIIVKKEAQAQVRFVAVLRDISFDADSYASFDL	143			
Query 162	LVDNQETGKKRMQYFITAQDLKMGSPFEYRAEASNVIKFRPLNQTKEHTADELMTLYS	221			
Sbjct 144	+Q +KR I DLD + GPFEYRAEA IKF+PLNQTKE+TA+ELMTLYS QDKLHQNICRKRTLVAIGTHDLDITQGFPEYRAEAPKDKFPLNQTKEYTAELMTLYS	203			
Query 222	SDSHMTDFLQIQNLVPPYVIADKNGLI--SLVPVDAEPMKISIEKSLMIIIVSDKEN	280			
Sbjct 204	+DSH+ +L+IQN PVPYVI DKNQ++ S+ P+++ E KI++ TK++ I T+ DK+ TDSHLKAYLPIIQNHPPYVPIYDKNQVVCMPPIINGEHSKTLNTKNVFEATATDKQK	263			
Query 281	GIRLNNVLAASIRIEKPLVVEPVLIEYEKFEPRALESPPLSYRKMVTITPEINTKI	340			
Sbjct 264	+L+ ++ S KP +E V + YE E EL P LSYR+MTVITPEINTKI AFVVLDTIVTLFSQYCAKPFITIEQVEVVE---ETGVKELYPLSYREMTVITPEINTKI	320			
Query 341	GLNLQDEEMANLNNMSLKAIEVASKEVLEVMIPPTRHDIHACDISEDVGVACAYKNFLR	400			
Sbjct 321	G+NL+DEEMA LLN MSLKAIEVA+KE L++++PPTRHDIHACDI+EDVGVA Y N + GINLQDEEMATLNNMSLKAIEVAEKETLKIIVPPTRHDIHACDI+EDVGVAFGYNLLIT	380			
Query 401	DL 402				
Sbjct 381	L 382				

C

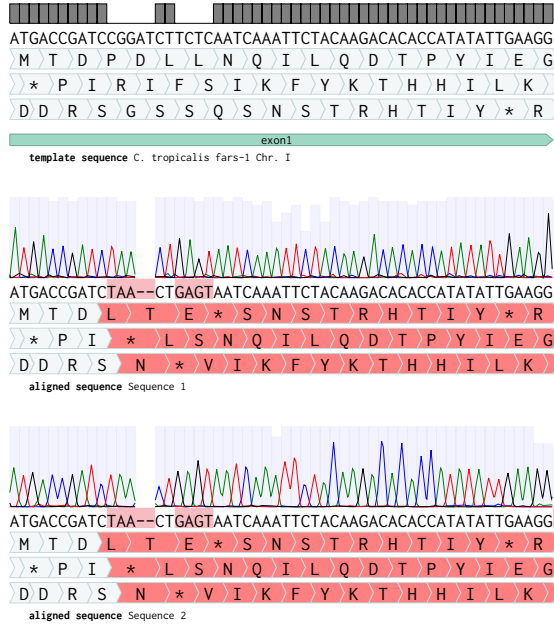


Supplementary Figure 1. A) Summary of sequences results that produced significant alignments to KLMT-1 peptide sequence using BLAST algorithm. B) Most significant alignment shows that KLMT-1 has homology to FARS-3 which is the beta subunit of the phenylalanine-tRNA synthetase. C) KLMT-1 and FARS-3 reveals sequence similarity within core region and differences in the N- and C-termini. Using the MultiAlin software visualizes the similarity of the paralogous KLMT-1 to FARS-3, the subunit of the phenylalanine-tRNA-synthetase. Letters in red reveal sequences with high consensus value (>90%), blue letters stand for low consensus value (<50%). The N- and C-termini of KLMT-1 show low sequence similarities to FARS-3, which also showed a high probability of disorder (Fig. 5). Resource: <http://multalin.toulouse.inra.fr/multalin/multalin.html> "Multiple sequence alignment with hierarchical clustering" F. CORPET, 1988, Nucl. Acids Res., 16 (22), 10881-10890.

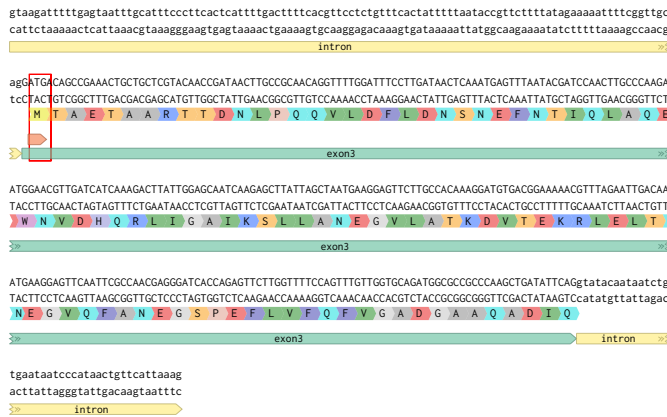
A



B



C



Supplementary Figure 2. A) Nucleotide and peptide sequence of the first exon of *fars-1*. A mutation in the first exon leads to a premature stop codon, which allows the transcription of only the short isoform. The premature stop codon is indicated with a star (*). B) Top row is showing the reference sequence of the first exon of *fars-1*. The two sequences below are sequencing results of 2 independent aligned sequences using Sanger Sequencing which are showing the mutations of *fars-1* in the first exon. C) Exon 3 and two flanking introns of *fars-1* are shown. The alternative transcription start site (TSS) of *fars-1* is indicated with a red square, showing the codon ATG, which allows the translation of *fars-1* short isoform.

Protein sequences

KLMT-1

MSENQRLSNNGSVVEEYFYTAPDEYEKTTTASQQLPPSFNAPDLPTTPVTSEKTAVEKDRRESMDKKHMD
KKHGETAVGEDLNDQEIYKIDKRYDLLSSEGLSRAMRIFKQHFEPDFRFLDAKSIEKINVAANASVFHPYL
SGAIVRQISLDLESLRFLNGLVADNQETGKKRMQYFITAQDLDKMSGPFYRAEASNVIKFRPLNQTKEH
TADELMTLYSSDSHMTDFLQLIQNLVPVPIADKNGLISLVPVDAEPMKISIETKSLMIIVTSVDKENGIRI
LNNVLAASIRIEKPLVVEPVLIEYEKFEPRALESPPLSYRKMTVTTPEINTKIGLNLQDEEMANLLNMS
LKAEVASKEVLEVMIPPTRHDILHACDISEDVGVACAYKNFLRDLDSKEPPNITNFRISSTLSKLELDETNP
DSVFSRKHSSELKKVTAKVLTLMKGEVKRAEKLLMIQSKVGLEMSDSETEKAADEQSVEKKRNSSSQNP
MES*

KSS-1

MEFPLIRLPDVPKIQIQLMSIGERIKLALSSRKMENYLAWVFKNRTLDAVYTIELRGDTSTFIGIDTKTWVLC
MNHFKPECKKPGYISVEELKPWIDEKWTMMERTFNVFIRLQKVLPCVMTNLCVTLKTEPTPILKILSYPCV
ANLTGVHFYGGTVERNELDAIMEWRKENTIQYISVTDNEIPLDYRHPNAFRFTGVVYGDARWISLEDLLS
MRNFYRPIFGKNRFTTKDLNTFIKYWINCDENMFTYLVIDYKDINISELMKDITVLKGRSEKPFYLIASNST
ENQILLTIQLIEHTEPQIRNVLDFSIQYANEPHKFRGGTVPAWTREYRILGRLARKRWLEEMITVGISIEE
IKELDDLEELTVVEVRIIDGIMTVQEKL*

FARS-1

MTDPDLLNQILQDTPYIEGFSGPSAVDFSTKASIKEKDLKGREHLQRWFFHLNSFEMTAETAARTTDNLP
QQVLDFLDNSNEFNITQLAQEWNVDHQRLIGAIAKSLLANEGVLATKDVTEKRELTNEGVOFANEGSPEF
LVFQVFGADGAAQADIQKQPFKIGMSKAMQFKWVSVDKGRVVRQTAEVVDSTRKQLESRLGSDDV
NENEKELKKRKLISEVNIKGLVVSKGSSFTTSLAKQEADLTPEMIASGSWKEKQFKYNFESLGVPSSGH
LHPLMKVRSEFRQIFFSMGFSEMATNRYVESSFWNFDAFQPPQHPARDAHDTFFVSDPAISVKFPEDY
LERVKTVHSGGGYGSAGYNYDWKIEEAQKNVLRHTTAVSARQLYQLAQEGFRPSKLFSDRVFRNETLD
ATHLAEFHQVEGVIAEKNSLAHLIGIFTEFFKLGITDLRFKPTYNPYTEPSMEIFAYHKGLAKWVEIGNSG
MFRPEMLLPMGLPADVNVAGYGLSLERPTMIKYGINNIRDLFGSKIDLEVYNNPICRLDK*

FARS-1 short isoform

MTAETAARTTDNLPQQVLDFLDNSNEFNITQLAQEWNVDHQRLIGAIIKSLLANEGVLATKDVTEKRLELT
NEGVQFANEGSPEFLVFQFVGADGAAQADIQKQPFQKIGMSKAMQFKWVSVDKGRVVRQTAEVVDS
TRKQLESRLGSDDVNENEKELKKRKLISEVNIKGLVVSKGSSFTTSLAKQEADLTPEMIASGSWKEKQFK
KYNFESLGVVPSGHLHPLMKVRSEFRQIFFSMGFSEMATNRYVESSFWNFDALFQPQQHPARDAHDT
FFVSDPAISVKFPEDYLERVKTVHSKGGYGSAGYNYDWKIEEAQKNVLRTHHTTAVSARQLYQLAQEGFRP
SKLFSIDRVFRNETLDATHLAEFHQVEGVIAEKNSLAHLIGIFTEFFKKGITDLRFKPTYNPNYTEPSMEIFA
YHKGLAKWVEIGNSGMFRPEMLLPMGLPADVNVAGYGLSLERPTMIKYGINNIRDLFSGSKIDLEVYNN
PICRLDK*

FARS-3

MPTVGIKKVLLDKHFGRVYTEKEFDELCEYGLELDEITSEKAAVEKERGEAAAGEDLNDQEVYKIDIPANR
YDLSVEGLSRAIRIFKQEIESPEYRFSDTKTRQKIIVKRETAQVRPYVVGAVLRDVFSFSDSYASFIDLQDKL
HQNICRKRTLVAIGTHDLDTIQGPFYRAEAPNKIKFRPLNQTKEYTAEELMTLYSTDShLKAYLPPIQNHP
VYPVIYDKNGVVCSMPPIINGEHSKITLTKNVFIEATATDKQKAYVVLDTIVTLFSQYCQKPFHVEQVEVE
YEETGEKELYPLLSYREMTVTTPEINTKIGLSLKDEEMAILLNKMSLKAEVASKGVLKVVVPTRHDILHAC
DIAEDVGVAYGYNLVTKLPESENTVAVAFPINKLCDNLRIEIAAAGWTEALNFALCSRDDISTKLRLPDALS
KAVHIGNPKTLEFQVARTSLLPGLLKTLASNRDMPLPLKLFELQDVILKDEKMDVGARNERRLAAYYNNK
AAGFEIIQGFLDRMMRMLNVNPTKDQKGYHIEADENPTFFPGRCARIIIGPNGVFLGRIGALHPEVITSFG
LTLPCGAVEFNVEPFL*

2Ty

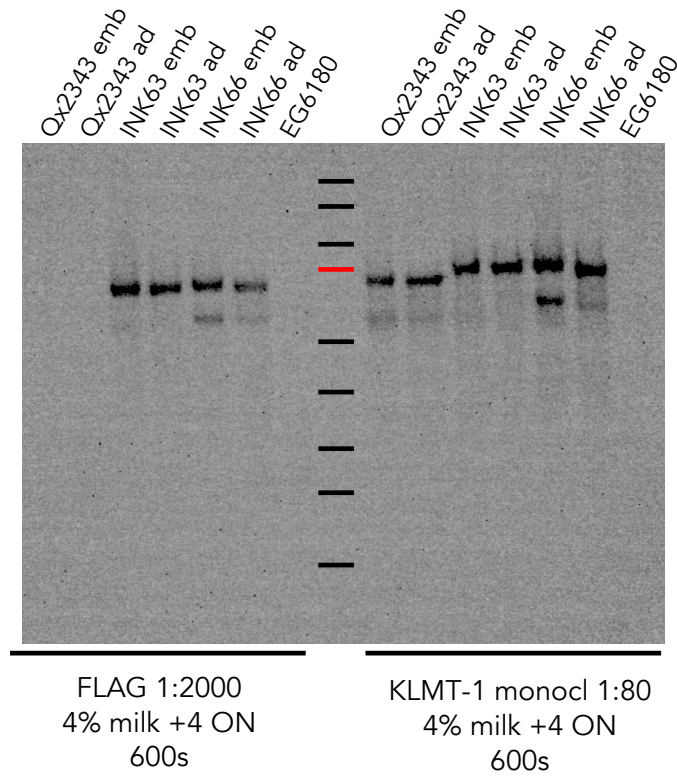
GEVHTNQDPLDEVHTNQDPLDGT

mNeonGreen

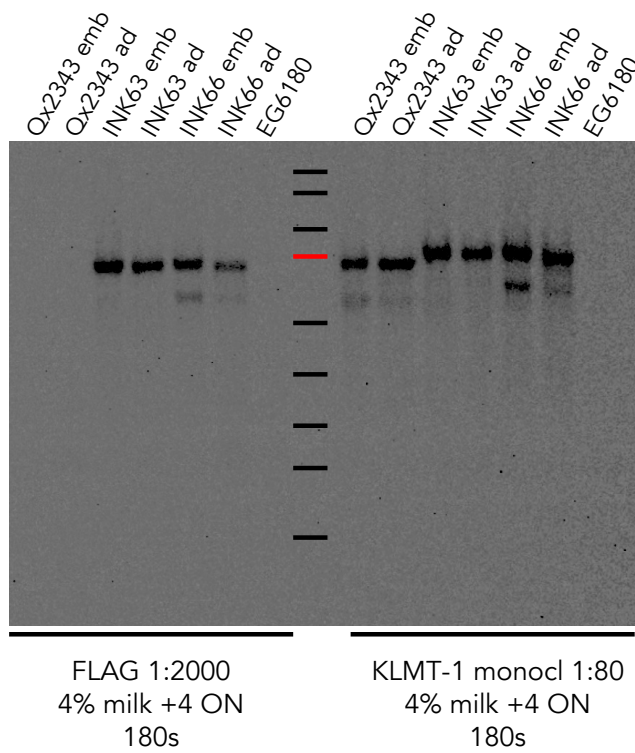
MVSKGEEDNMASLPATHELHIFGSINGVDFDMVGQGTGNPNDGYEELNLKSTKGDQLQFSPWILVPHIG
YGFHQYLPYPDGMSPFQAAMVDGSGYQVHRTMQFEDGASLTVNYRYTYEGSHIKGEAQVKGTGFPAD
GPVMTNSLTAADWCRSKKTYPNDKTIISTFKWSYTTGNGKRYRSTARTTYTFAKPMAANYLKNQPMYV
FRKTELKHSKTELNFKEWQKAFTDVMGMDELYK

Supplementary Figure 3. Amino acid sequences of KLMT-1, KSS-1, FARS-1, FARS-1 short isoform, FARS-3, 2Ty linker and mNeonGreen. Shown are the full sequences of the proteins used in this study. The start of the short isoform in FARS-1 is indicated with a bold M for methionine.

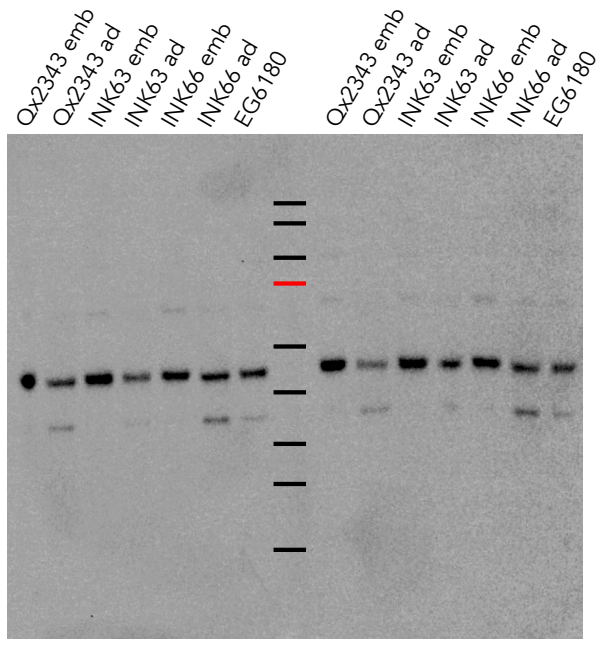
Raw Western Blots



Western Blot belongs to Figure 6B and 6C

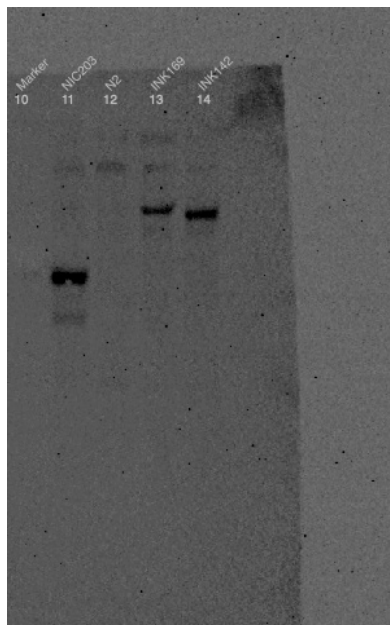


Western Blot belongs to Figure 6B and 6C

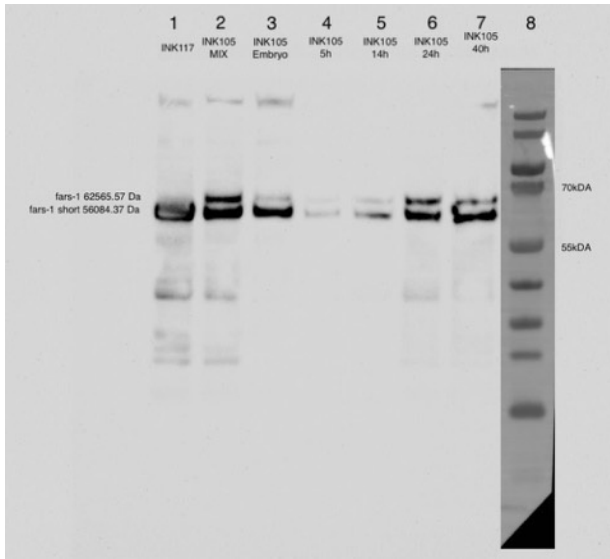


Actin 1:2000
 4% milk +4 ON
 30s (new HRP kit)

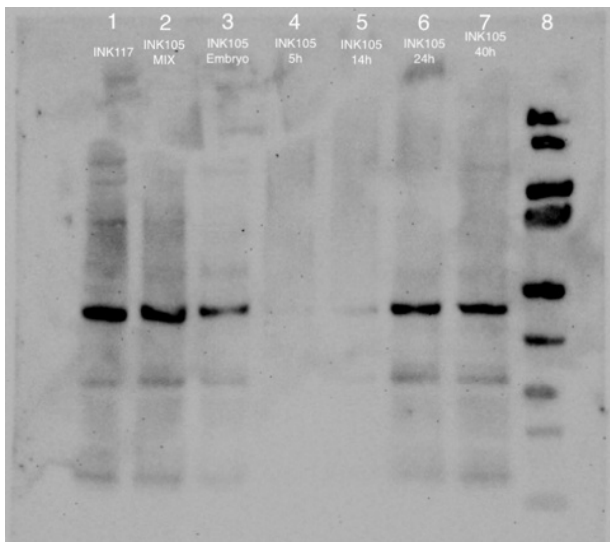
Western Blot belongs to Figure 6B and 6C



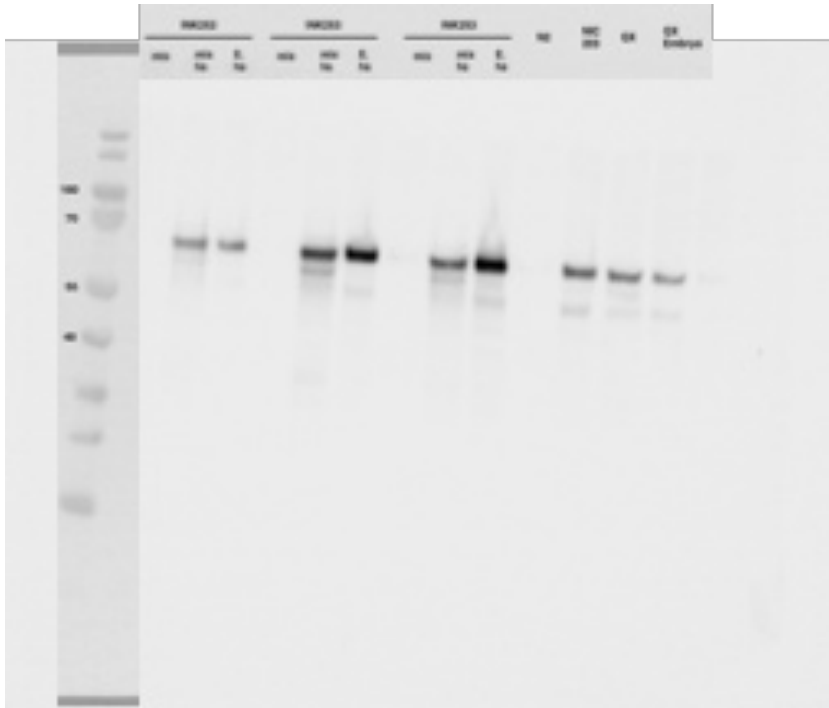
Western Blot belongs to Figure 11B



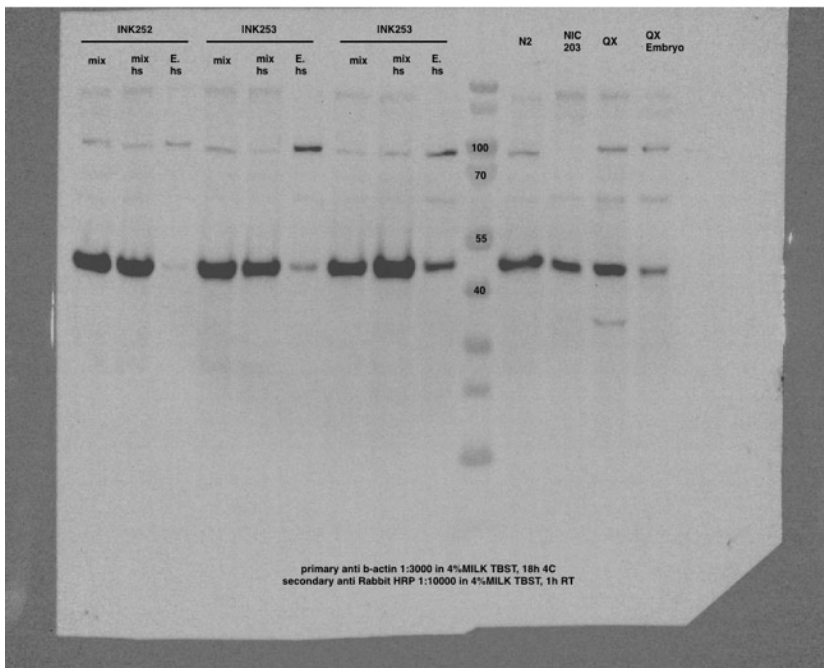
Western Blot belongs to Figure 17B



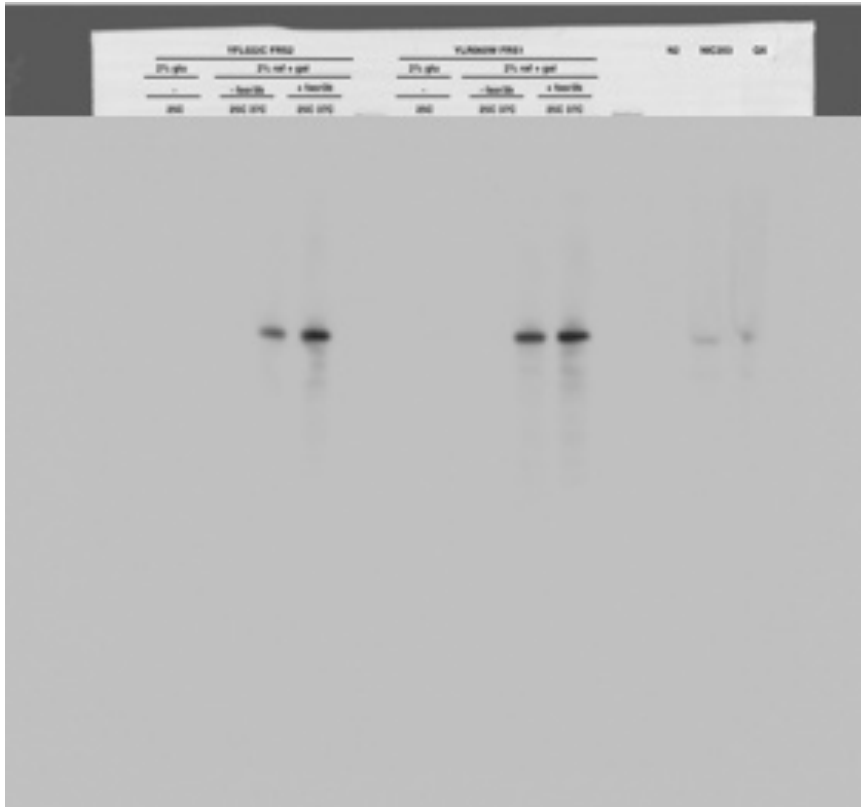
Western Blot belongs to Figure 17B



Western Blot belongs to Figure 21B



Western Blot belongs to Figure 21B



Western Blot belongs to Figure 22C

Supplementary Tables

Strain Name	Species	Genotype	Description	Source
EG6180	<i>C. tropicalis</i>	<i>wild type</i>	Wild isolate from El Yunque, Puerto Rico. Lat 18.3 Lon -65.8. Found in rotting fruit by M. Allison and E. Jorgensen	Christian Braendle
NIC203	<i>C. tropicalis</i>	<i>wild type</i>	Wild isolate from Capesterre Belle-Eau, Guadeloupe. Lat 16.05 Lon -61.63. Found in rotting flowers by N. Pouillet and C. Braendle	Christian Braendle
OX2343	<i>C. tropicalis</i>	<i>qqIR47(V:1.3-1.8 Mb; NIC203 > EG6180); EG6180 Mito</i>	NIL carrying NIC203 TA element Chr. V in a EG6180 background	Ubiquitous Selfish Toxin-Antidote
INK103	<i>C. tropicalis</i>	<i>kss-1(abu52[N-HA tag::kss-1]) V; kImt-1(abu35[kImt-1::C-FLAGtag]) V</i>	NIL carrying EG6180 TA element Chr. V in a NIC203 background; <i>kImt-1</i> tagged with FLAG on its C-terminus; <i>kss-1</i> tagged with HA on its N-terminus	This Study
INK105	<i>C. tropicalis</i>	<i>fars-1(abu48[fars-1::C-FLAGtag]) I</i>	NIL carrying EG6180 TA element Chr. V in a NIC203 background; <i>fars-1</i> tagged with FLAG	This Study
INK117	<i>C. tropicalis</i>	<i>fars-1(abu63[fars-1::C-FLAGtag, c.1A->G]) I</i>	NIL carrying EG6180 TA element Chr. V in a NIC203 background; <i>fars-1</i> tagged with FLAG; substitution of c.1A->G creates a stop codon in the first exon, resulting in the expression of the short variant of <i>fars-1</i>	This Study
INK144	<i>C. tropicalis</i>	<i>fars-1(abu63[fars-1::C-FLAGtag, c.1A->G]) I</i>	<i>fars-1</i> tagged with FLAG in EG6180 background; substitution of c.1A->G creates a stop codon in the first exon, resulting in the expression of the short variant of <i>fars-1</i>	This Study
INK169	<i>C. tropicalis</i>	<i>kImt-1(abu107[kImt-1::linker::mNeonGreen]) V</i>	NIL carrying EG6180 TA element Chr. V in a NIC203 background; <i>kImt-1</i> tagged with C-terminal linker 2Ty and mNeonGreen.	This Study
INK207	<i>C. tropicalis</i>	<i>kImt-1(abu107[kImt-1::linker::mNeonGreen]) V; kss-1(abu126[kss-1 c.16-19del]) V</i>	NIL carrying EG6180 TA element Chr. V in a NIC203 background; <i>kImt-1</i> tagged with C-terminal linker 2Ty and mNeonGreen. <i>kss-1</i> frameshift mutation c.16-19del	This Study
INK235	<i>C. tropicalis</i>	<i>kImt-1(abu107[kImt-1::linker2xTy::C-mNeonGreen]) V; kss-1(abu141[kss-1::mScarlet]) V</i>	NIL carrying EG6180 TA element Chr. V in a NIC203 background; <i>kImt-1</i> tagged with C-terminal linker 2Ty and mNeonGreen; <i>kss-1</i> tagged with mScarlet	This Study
INK63	<i>C. tropicalis</i>	<i>kImt-1(abu32[N-FLAGtag::kImt-1]) V</i>	NIL carrying EG6180 TA element Chr. V in a NIC203 background; <i>kImt-1</i> tagged with FLAG on its N-terminus	This Study
INK66	<i>C. tropicalis</i>	<i>kImt-1(abu35[kImt-1::C-FLAGtag]) V</i>	NIL carrying EG6180 TA element Chr. V in a NIC203 background; <i>kImt-1</i> tagged with FLAG on its C-terminus	This Study

Supplementary Table 1. Nematode strains used in this study.

Strain Name	Species	Genotype	Description	Source
Y2H Gold	<i>S. cerevisiae</i>	MATa, trp1-901, leu2-3, 112, ura3-52, his3-200, gal4a, gal80a, LYS2:: GAL1UAS-Gal1TATA-His3, GAL2UAS-Gal2TATA-Ade2, URA3:: MEL1UAS-Mel1TATA, AUR1-CMEL1	parental strain used for Y2H	Takara Bio Europe, SAS

Supplementary Table 2. Strain which was used to perform the transformation of Y2H experiments.

Internal Name	AD	Internal Name2	BD
pAB0035	pGADT7-AD::KLMT-1(10.2)	pAB0044	pGBKT7-BD::KSS-1-ant(9.1)
pAB0058	pGADT7-AD::KLMT-1[1:400]	pAB0044	pGBKT7-BD::KSS-1-ant(9.1)
pAB0059	pGADT7-AD::KLMT-1[1:250]	pAB0044	pGBKT7-BD::KSS-1-ant(9.1)
pAB0062	pGADT7-AD::KLMT-1 [1:47]	pAB0044	pGBKT7-BD::KSS-1-ant(9.1)
pAB0063	pGADT7-AD::KLMT-1 [48:150]	pAB0044	pGBKT7-BD::KSS-1-ant(9.1)
pAB0064	pGADT7-AD::KLMT-1 [48:250]	pAB0044	pGBKT7-BD::KSS-1-ant(9.1)
pAB0065	pGADT7-AD::KLMT-1 [151:250]	pAB0044	pGBKT7-BD::KSS-1-ant(9.1)
pAB0066	pGADT7-AD::KLMT-1 [251:503]	pAB0044	pGBKT7-BD::KSS-1-ant(9.1)
pAB0067	pGADT7-AD::KLMT-1 [1:150]	pAB0044	pGBKT7-BD::KSS-1-ant(9.1)
pAB0068	pGADT7-AD::KLMT-1 [151:503]	pAB0044	pGBKT7-BD::KSS-1-ant(9.1)
pGADT7 (empty)	cont empty	pAB0044	pGBKT7-BD::KSS-1-ant(9.1)
pAB0035	pGADT7-AD::KLMT-1(10.2)	pAB0041	pGBKT7-BD::NICfars1(6.7)
pAB0058	pGADT7-AD::KLMT-1[1:400]	pAB0041	pGBKT7-BD::NICfars1(6.7)
pAB0059	pGADT7-AD::KLMT-1[1:250]	pAB0041	pGBKT7-BD::NICfars1(6.7)
pAB0062	pGADT7-AD::KLMT-1 [1:47]	pAB0041	pGBKT7-BD::NICfars1(6.7)
pAB0063	pGADT7-AD::KLMT-1 [48:150]	pAB0041	pGBKT7-BD::NICfars1(6.7)
pAB0064	pGADT7-AD::KLMT-1 [48:250]	pAB0041	pGBKT7-BD::NICfars1(6.7)
pAB0065	pGADT7-AD::KLMT-1 [151:250]	pAB0041	pGBKT7-BD::NICfars1(6.7)
pAB0066	pGADT7-AD::KLMT-1 [251:503]	pAB0041	pGBKT7-BD::NICfars1(6.7)
pAB0067	pGADT7-AD::KLMT-1 [1:150]	pAB0041	pGBKT7-BD::NICfars1(6.7)
pAB0068	pGADT7-AD::KLMT-1 [151:503]	pAB0041	pGBKT7-BD::NICfars1(6.7)
pGADT7 (empty)	cont empty	pAB0041	pGBKT7-BD::NICfars1(6.7)
pAB0035	pGADT7-AD::KLMT-1(10.2)	pGBKT7	cont empty
pAB0058	pGADT7-AD::KLMT-1[1:400]	pGBKT7	cont empty
pAB0059	pGADT7-AD::KLMT-1[1:250]	pGBKT7	cont empty
pAB0062	pGADT7-AD::KLMT-1 [1:47]	pGBKT7	cont empty
pAB0063	pGADT7-AD::KLMT-1 [48:150]	pGBKT7	cont empty
pAB0064	pGADT7-AD::KLMT-1 [48:250]	pGBKT7	cont empty
pAB0065	pGADT7-AD::KLMT-1 [151:250]	pGBKT7	cont empty
pAB0066	pGADT7-AD::KLMT-1 [251:503]	pGBKT7	cont empty
pAB0067	pGADT7-AD::KLMT-1 [1:150]	pGBKT7	cont empty
pAB0068	pGADT7-AD::KLMT-1 [151:503]	pGBKT7	cont empty
pGADT7-T	cont	pGBKT7-53	cont
pGADT7-T	cont	pGBKT7::LAM	cont

Supplementary Table 3. Combination of plasmids used for Y2H experiment to investigate interaction between KLMT-1, including truncations, and KSS-1 or FARS-1.

Internal Name	AD	Internal Name2	BD
pAB0069	pGADT7-AD::SKR-1(C.tr)	pAB0072	pGBKT7-BD::CUL-1(C.tr)
pAB0070	pGADT7-AD::SKR-7(C.tr)	pAB0072	pGBKT7-BD::CUL-1(C.tr)
pAB0071	pGADT7-AD::SKR-20(C.tr)	pAB0072	pGBKT7-BD::CUL-1(C.tr)
pAB0069	pGADT7-AD::SKR-1(C.tr)	pAB0073	pGBKT7-BD::CUL-6(C.tr)
pAB0070	pGADT7-AD::SKR-7(C.tr)	pAB0073	pGBKT7-BD::CUL-6(C.tr)
pAB0071	pGADT7-AD::SKR-20(C.tr)	pAB0073	pGBKT7-BD::CUL-6(C.tr)
pAB0069	pGADT7-AD::SKR-1(C.tr)	pAB0074	pGBKT7-BD::SEL-10(C.tr)
pAB0070	pGADT7-AD::SKR-7(C.tr)	pAB0074	pGBKT7-BD::SEL-10(C.tr)
pAB0071	pGADT7-AD::SKR-20(C.tr)	pAB0074	pGBKT7-BD::SEL-10(C.tr)
pGADT7 (empty)	cont empty	pAB0072	pGBKT7-BD::CUL-1(C.tr)
pGADT7 (empty)	cont empty	pAB0073	pGBKT7-BD::CUL-6(C.tr)
pGADT7 (empty)	cont empty	pAB0074	pGBKT7-BD::SEL-10(C.tr)
pGADT7-T	cont	pGBKT7-53	cont
pGADT7-T	cont	pGBKT7::LAM	cont
pAB0069	pGADT7-AD::SKR-1(C.tr)	pAB0044	pGBKT7-BD::KSS-1-ant(9.1)
pAB0070	pGADT7-AD::SKR-7(C.tr)	pAB0044	pGBKT7-BD::KSS-1-ant(9.1)
pAB0071	pGADT7-AD::SKR-20(C.tr)	pAB0044	pGBKT7-BD::KSS-1-ant(9.1)

Supplementary Table 4 Combination of plasmids used for Y2H experiment to investigate interaction between members of the SCF complex and KSS-1.

Strain ID	Species	Genotype	Genotype (internal Plasmid names)	Parental Strain
YAB0001	<i>S. cerevisiae</i>	pGADT7-AD::KLMT-1[1:400] and pGBKT7-BD::KSS-1-ant(9.1)	pAB0058:pAB0044	Y2HGold
YAB0002	<i>S. cerevisiae</i>	pGADT7-AD::KLMT-1[1:250] and pGBKT7-BD::KSS-1-ant(9.1)	pAB0059:pAB0044	Y2HGold
YAB0005	<i>S. cerevisiae</i>	cont AD and pGBKT7-BD::KSS-1-ant(9.1)	pGADT7:pAB0044	Y2HGold
YAB0006	<i>S. cerevisiae</i>	pGADT7-AD::KLMT-1[1:400] and cont BD	pAB0058:pGBKT7	Y2HGold
YAB0007	<i>S. cerevisiae</i>	pGADT7-AD::KLMT-1[1:250] and cont BD	pAB0059:pGBKT7	Y2HGold
YAB0012	<i>S. cerevisiae</i>	pGADT7-AD::KLMT-1[1:400] and pGBKT7-BD::NICfars1(6.7)	pAB0058:pAB0041	Y2HGold
YAB0013	<i>S. cerevisiae</i>	pGADT7-AD::KLMT-1[1:250] and pGBKT7-BD::NICfars1(6.7)	pAB0059:pAB0041	Y2HGold
YAB0014	<i>S. cerevisiae</i>	pGADT7-AD::KLMT-1(10.2) and pGBKT7-BD::NICfars1(6.7)	pAB0035:pAB0041	Y2HGold
YAB0015	<i>S. cerevisiae</i>	cont AD and pGBKT7-BD::NICfars1(6.7)	pGADT7:pAB0041	Y2HGold
YAB0016	<i>S. cerevisiae</i>	pGADT7-AD::KLMT-1 [1:47] and pGBKT7-BD::KSS-1-ant(9.1)	pAB0062:pAB0044	Y2HGold
YAB0017	<i>S. cerevisiae</i>	pGADT7-AD::KLMT-1 [48:150] and pGBKT7-BD::KSS-1-ant(9.1)	pAB0063:pAB0044	Y2HGold
YAB0018	<i>S. cerevisiae</i>	pGADT7-AD::KLMT-1 [48:250] and pGBKT7-BD::KSS-1-ant(9.1)	pAB0064:pAB0044	Y2HGold
YAB0019	<i>S. cerevisiae</i>	pGADT7-AD::KLMT-1 [151:250] and pGBKT7-BD::KSS-1-ant(9.1)	pAB0065:pAB0044	Y2HGold
YAB0020	<i>S. cerevisiae</i>	pGADT7-AD::KLMT-1 [251:503] and pGBKT7-BD::KSS-1-ant(9.1)	pAB0066:pAB0044	Y2HGold
YAB0021	<i>S. cerevisiae</i>	pGADT7-AD::KLMT-1 [1:150] and pGBKT7-BD::KSS-1-ant(9.1)	pAB0067:pAB0044	Y2HGold
YAB0022	<i>S. cerevisiae</i>	pGADT7-AD::KLMT-1 [151:503] and pGBKT7-BD::KSS-1-ant(9.1)	pAB0068:pAB0044	Y2HGold
YAB0023	<i>S. cerevisiae</i>	pGADT7-AD::KLMT-1 [1:47] and pGBKT7-BD::NICfars1(6.7)	pAB0062:pAB0041	Y2HGold
YAB0024	<i>S. cerevisiae</i>	pGADT7-AD::KLMT-1 [48:150] and pGBKT7-BD::NICfars1(6.7)	pAB0063:pAB0041	Y2HGold
YAB0025	<i>S. cerevisiae</i>	pGADT7-AD::KLMT-1 [48:250] and pGBKT7-BD::NICfars1(6.7)	pAB0064:pAB0041	Y2HGold
YAB0026	<i>S. cerevisiae</i>	pGADT7-AD::KLMT-1 [151:250] and pGBKT7-BD::NICfars1(6.7)	pAB0065:pAB0041	Y2HGold
YAB0027	<i>S. cerevisiae</i>	pGADT7-AD::KLMT-1 [251:503] and pGBKT7-BD::NICfars1(6.7)	pAB0066:pAB0041	Y2HGold
YAB0028	<i>S. cerevisiae</i>	pGADT7-AD::KLMT-1 [1:150] and pGBKT7-BD::NICfars1(6.7)	pAB0067:pAB0041	Y2HGold
YAB0029	<i>S. cerevisiae</i>	pGADT7-AD::KLMT-1 [151:503] and pGBKT7-BD::NICfars1(6.7)	pAB0068:pAB0041	Y2HGold
YAB0030	<i>S. cerevisiae</i>	pGADT7-AD::KLMT-1 [1:47] and empty cont	pAB0062:pGBKT7	Y2HGold
YAB0031	<i>S. cerevisiae</i>	pGADT7-AD::KLMT-1 [48:150] and empty cont	pAB0063:pGBKT7	Y2HGold
YAB0032	<i>S. cerevisiae</i>	pGADT7-AD::KLMT-1 [48:250] and empty cont	pAB0064:pGBKT7	Y2HGold
YAB0033	<i>S. cerevisiae</i>	pGADT7-AD::KLMT-1 [151:250] and empty cont	pAB0065:pGBKT7	Y2HGold
YAB0034	<i>S. cerevisiae</i>	pGADT7-AD::KLMT-1 [251:503] and empty cont	pAB0066:pGBKT7	Y2HGold
YAB0035	<i>S. cerevisiae</i>	pGADT7-AD::KLMT-1 [1:150] and empty cont	pAB0067:pGBKT7	Y2HGold
YAB0036	<i>S. cerevisiae</i>	pGADT7-AD::KLMT-1 [151:503] and empty cont	pAB0068:pGBKT7	Y2HGold
YAB0037	<i>S. cerevisiae</i>	pGADT7-AD::SKR-7(C.tr) and pGBKT7-BD::KSS-1-ant(9.1)	pAB0070:pAB0044	Y2HGold
YAB0038	<i>S. cerevisiae</i>	pGADT7-AD::SKR-20(C.tr) and pGBKT7-BD::KSS-1-ant(9.1)	pAB0071:pAB0044	Y2HGold
YAB0039	<i>S. cerevisiae</i>	pGADT7-AD::SKR-1(C.tr) and empty cont	pAB0069:pGBKT7	Y2HGold
YAB0051	<i>S. cerevisiae</i>	pGADT7-AD::SKR-1(C.tr) and pGBKT7-BD::KSS-1-ant(9.1)	pAB0069:pAB0044	Y2HGold
YAB0052	<i>S. cerevisiae</i>	pGADT7-AD::SKR-1(C.tr) and pGBKT7-BD::CUL-1(C.tr)	pAB0069:pAB0072	Y2HGold
YAB0053	<i>S. cerevisiae</i>	pGADT7-AD::SKR-7(C.tr) and pGBKT7-BD::CUL-1(C.tr)	pAB0070:pAB0072	Y2HGold
YAB0054	<i>S. cerevisiae</i>	pGADT7-AD::SKR-20(C.tr) and pGBKT7-BD::CUL-1(C.tr)	pAB0071:pAB0072	Y2HGold
YAB0055	<i>S. cerevisiae</i>	pGADT7-AD::SKR-1(C.tr) and pGBKT7-BD::CUL-6(C.tr)	pAB0069:pAB0073	Y2HGold
YAB0056	<i>S. cerevisiae</i>	pGADT7-AD::SKR-7(C.tr) and pGBKT7-BD::CUL-6(C.tr)	pAB0070:pAB0073	Y2HGold
YAB0057	<i>S. cerevisiae</i>	pGADT7-AD::SKR-20(C.tr) and pGBKT7-BD::CUL-6(C.tr)	pAB0071:pAB0073	Y2HGold
YAB0058	<i>S. cerevisiae</i>	pGADT7-AD::SKR-1(C.tr) and pGBKT7-BD::SEL-10(C.tr)	pAB0069:pAB0074	Y2HGold
YAB0059	<i>S. cerevisiae</i>	pGADT7-AD::SKR-7(C.tr) and pGBKT7-BD::SEL-10(C.tr)	pAB0070:pAB0074	Y2HGold
YAB0060	<i>S. cerevisiae</i>	pGADT7-AD::SKR-20(C.tr) pGBKT7-BD::SEL-10(C.tr)	pAB0071:pAB0074	Y2HGold
YAB0061	<i>S. cerevisiae</i>	empty cont and pGBKT7-BD::CUL-1(C.tr)	pGADT7:pAB0072	Y2HGold
YAB0062	<i>S. cerevisiae</i>	empty cont and pGBKT7-BD::CUL-6(C.tr)	pGADT7:pAB0073	Y2HGold
YAB0063	<i>S. cerevisiae</i>	empty cont and pGBKT7-BD::SEL-10(C.tr)	pGADT7:pAB0074	Y2HGold

Supplementary Table 5. Complete list of yeast strains used for Y2H experiments.

Plasmid ID	Name	Description	Benchmarking Link
pGADT7-AD	pGADT7-AD	Yeast two-hybrid "prey" vector for expressing proteins fused to the GAL4 activation domain.	https://benchmarking.com/s/seq-Yt1UjpiE.Lu0OTfSL1.qsp
pGBK7-BD	pGBK7-BD	Yeast two-hybrid "bait" vector for expressing proteins fused to the GAL4 DNA-binding domain.	https://benchmarking.com/s/seq-hCQyW6HM3YwQ1ohf29
pGBK7-53	pGBK7-53	H2P Gal4-DNA-BD fused with murine p53	https://www.lifescience-market.com/plasmid-c-94/pgbk7lam-p-63758.html
pGADT7-T	pGADT7-T	H2P pGADT7-T encodes a fusion of the SV40 large T-antigen (a.a. 86-708) and the GAL4 AD (a.a. 768-881).	https://www.lifescience-market.com/plasmid-c-94/pgbk7lam-p-63758.html
pGBK7-LAM	pGBK7-LAM	Y2H for negative control interaction	https://www.lifescience-market.com/plasmid-c-94/pgbk7lam-p-63758.html

Supplementary Table 6. Plasmids used for cloning in Y2H experiments.

Plasmid ID	Name	Description	Benchling Link
pAB0041	pGBK7-BD::NICfars1(6.7)	from NIC203 cDNA	https://benchling.com/s/seq-u0bTm7TSsKbOjWUnAx
pAB0044	pGBK7-BD::KSS-1-ant(9.1)	from NIC203 cDNA	https://benchling.com/s/seq-bzCSJQnO0vAETnRhg
pAB0035	pGAD7-AD::NIC203-KLMT-1(10.2)	from NIC203 cDNA	https://benchling.com/s/seq-22EFkvGLPuPOSDUBCW
pAB0058	pGAD7-AD::KLMT-1[1:400]	from pAB0035	https://benchling.com/s/seq-7AIFU4eF8BtL1fNnPHI
pAB0059	pGAD7-AD::KLMT-1[1:250]	from pAB0035	https://benchling.com/s/seq-vvC8KXPdyKAEXYtXCSG
pAB0062	pGAD7-AD::KLMT-1[1:47]	from pAB0035	https://benchling.com/s/seq-9BrespXgkyHOFd9mdCe
pAB0063	pGAD7-AD::KLMT-1[48:150]	from pAB0035	https://benchling.com/s/seq-158BHVzFMkd7WrcsdF
pAB0064	pGAD7-AD::KLMT-1[48:250]	from pAB0035	https://benchling.com/s/seq-BD9R5B3iNz2vF9zbl
pAB0065	pGAD7-AD::KLMT-1[151:250]	from pAB0035	https://benchling.com/s/seq-g1h8NkAPjWYm1QXwGkpf
pAB0066	pGAD7-AD::KLMT-1[251:503]	from pAB0035	https://benchling.com/s/seq-19rC2aWnxZLU70K3v
pAB0067	pGAD7-AD::KLMT-1[1:150]	from pAB0035	https://benchling.com/s/seq-qz0suGno86vH8M5Fcoz
pAB0068	pGAD7-AD::KLMT-1[151:503]	from pAB0035	https://benchling.com/s/seq-gWide1c6CpdYmDRtUt

Supplementary Table 7. Plasmids that were created in this study for Y2H experiments.

Plasmid ID	Name	Description	Benchling Link
pAB0069	pGAD7-AD::SKR-1(C.tr)	from NIC203 cDNA	https://benchling.com/s/seq-Nsu3FCILAh3VTvshAFxp
pAB0070	pGAD7-AD::SKR-7(C.tr)	from NIC203 cDNA	https://benchling.com/s/seq-1Cxnz726rbo3iUS7up
pAB0071	pGAD7-AD::SKR-20(C.tr)	from NIC203 cDNA	https://benchling.com/s/seq-kBg2UFeAUL7PqWz3aAF
pAB0072	pGBK7-BD::CUL-1(C.tr)	from NIC203 cDNA	https://benchling.com/s/seq-dtAq8Kbg8v40hRbXybi
pAB0073	pGBK7-BD::CUL-6(C.tr)	from NIC203 cDNA	https://benchling.com/s/seq-TpdxYpCkps25vnxzUvA
pAB0074	pGBK7-BD::SEL-10(C.tr)	from NIC203 cDNA	https://benchling.com/s/seq-i491p0E5j3LMm08B51v
pAB0076	pGAD7-AD::CUL-3(C.tr)	from pAB0072	https://benchling.com/s/seq-UJCPmwoGCF99mz5Nv
pAB0077	pGAD7-AD::CUL-6(C.tr)	from pAB0073	https://benchling.com/s/seq-JQISABINwN0QkqwU
pAB0078	pGAD7-AD::SEL-10(C.tr)	from pAB0074	https://benchling.com/s/seq-j6vYFreKlp0PvAdjtZ
pAB0079	pGBK7-BD::SKR-1(C.tr)	from pAB0069	https://benchling.com/s/seq-8BpZ5lmAkG8hqiBWuolb
pAB0080	pGBK7-BD::SKR-7(C.tr)	from pAB0070	https://benchling.com/s/seq-JHELLazolFuJh6i6can
pAB0081	pGBK7-BD::SKR-20(C.tr)	from pAB0071	https://benchling.com/s/seq-9QniWDV6PuhfzRnUDXF

Supplementary Table 8. Plasmids that were created in this study for Y2H experiments.

Strain Name	Species	Genotype	Description	Source
BN711	<i>C. elegans</i>	<i>bq5171[mex-5P::FLP::SL2::mNG + unc-119(+)] IV.</i>	Constitutive co-expression of codon-optimised FLP and fluorescent mNeonGreen in the germ line. Reference: Macias-Leon J & Askjaer P. (2018). Efficient FLP-mediated germ-line recombination in <i>C. elegans</i> . Micropublication:biology. Dataset. https://doi.org/10.17912/W2G665	Peter Askjaer
N2	<i>C. elegans</i>	wild type	<i>C. elegans</i> var Bristol. Generation time is about 3 days. Brood size is about 350. Also CGC reference 257. Isolated from mushroom compost near Bristol, England by L.N. Staniland. Cultured by W.L. Nicholas, identified to genus by Gunther Osche and species by Victor Nigon; subsequently cultured by C.E. Dougherty. Given to Sydney Brenner ca. 1966. Subcultured by Don Riddle in 1973. <i>Caenorhabditis elegans</i> wild isolate. DR subclone of CB original (Tc1 pattern I). [NOTE: This stock might carry a ~1.8 kb deletion in <i>alh-2</i> in the background. (UPDATE: 03/26/2018 - a user reported the stock they received was homozygous for the <i>alh-2</i> (ot588) mutation.)]	CB
INK252	<i>C. elegans</i>	<i>abu157[hsp-16.41p::(Frt)::klmt-1(cDNA)::unc-54 3'UTR] II</i>	Heatshock induces expression of <i>klmt-1</i>	This Study
INK248	<i>C. elegans</i>	<i>abu153[hsp-16.41p::(Frt)::mCherry::his-58::let-8 3'UTR::(Frt)::klmt-1(cDNA)::unc-54 3'UTR] II</i>	Heatshock produces red nuclei	This Study

Supplementary Table 9. Worm strains used for investigating the toxic effect of KLMT-1 in *C. elegans*.

Strain Name	Species	Genotype	Description	Source
YLRO60W (FRS1-1)	<i>S. cerevisiae</i>	<i>MATA/α ura3Δ0/ura3Δ0 leu2Δ0/leu2Δ0 his3Δ1/his3Δ1 lys2Δ0/LYS2 met15Δ0/MET15 can1Δ::LEU2-MFA1pr::His3/CAN1 yfgΔ::KanMX/YFG</i>	https://benchling.com/s/seq-zxFGyH1tVnieIQZ14Td ; No growth at 34C (FRS1-1)	Ben-Aroya, S. et al. Mol Cell. 2008 30(2): 248-58
YLRO60W (FRS1-2)	<i>S. cerevisiae</i>	<i>MATA/α ura3Δ0/ura3Δ0 leu2Δ0/leu2Δ0 his3Δ1/his3Δ1 lys2Δ0/LYS2 met15Δ0/MET15 can1Δ::LEU2-MFA1pr::His3/CAN1 yfgΔ::KanMX/YFG</i>	https://benchling.com/s/seq-zxFGyH1tVnieIQZ14Td ; No growth at 32C (FRS1-2)	Ben-Aroya, S. et al. Mol Cell. 2008 30(2): 248-58
YFLO22C (FRS2)	<i>S. cerevisiae</i>	<i>MATA/α ura3Δ0/ura3Δ0 leu2Δ0/leu2Δ0 his3Δ1/his3Δ1 lys2Δ0/LYS2 met15Δ0/MET15 can1Δ::LEU2-MFA1pr::His3/CAN1 yfgΔ::KanMX/YFG</i>	https://benchling.com/s/seq-zxFGyH1tVnieIQZ14Td ; No growth at 37C	Ben-Aroya, S. et al. Mol Cell. 2008 30(2): 248-58

Supplementary Table 10. Temperature sensitive yeast strains used for the investigation of KLMT-1 toxicity in yeast.

Plasmid ID	Name	Description	Benchling Link
p42Nat	p42Nat	Multiplicity with clonNat resistance marker for single Gateway insertion	https://benchling.com/s/seq-HWDMwRdgwvIPGeZFru
pCEV-G2-Km	pCEV-G2-Km	TEF1 and PGK1 promoter controlled expression cassettes with G418 resistance for yeast transformation	https://benchling.com/s/seq-t0vL3yuZe3YU7mEwZ1zG
p406Gal1	p406Gal1	GALL1 promoter + polylinker + CYC1 terminator	https://benchling.com/s/seq-up6n2PrQUmZ1r0j25Bi
pAB0163	pCEV-G2-Km::fars1	<i>fars-1</i> short isoform from <i>C. trop.</i> , constitutive PGK1 promoter	https://benchling.com/s/seq-3GF6HwCFY504ka0UTG4u
pAB0164	pCEV-G2-Km::fars3	<i>fars-3</i> from <i>C. trop.</i> , constitutive TEF1 promoter	https://benchling.com/s/seq-3FTMG1KQNu7Upk0JuU
pAB0165	pCEV-G2-Km::fars1:fars3	<i>fars-1</i> short isoform from <i>C. trop.</i> , constitutive PGK1 promoter; <i>fars-3</i> from <i>C. trop.</i> , constitutive TEF1 promoter	https://benchling.com/s/seq-3GF6HwCFY504ka0UTG4u
pAB0166	p42Nat::pGal1-10::(C.trop)KLMT-1	galactose inducing KLMT-1 expression; pGal1-10 amplified from p406Gal1	https://benchling.com/s/seq-x3FTMG1KQNu7Upk0JuU

Supplementary Table 11 Plasmids used in this study to investigate KLMT-1 toxicity in FRS1/FRS2 ts yeast.

Strain Name	Species	Genotype	Description
DH5α	<i>E. coli</i>	<i>F-φ80lacZΔM15 Δ(lacZYA-argF)UJ169 recA1 endA1 hsdR17(rK-, mK+) phoA supE44 λ-thi-1 gyrA96 relA1</i>	Chemically competent <i>E. coli</i> cells ideal for construction of gene banks or generation of cDNA libraries using plasmid-derived vectors

Supplementary Table 12 *E. coli* strain used in this study for construction of gene banks for plasmids

Internal Name	Target	Sequence	Comment
500	<i>klmt-1</i>	GGGCTGAGGCGGCAAATTAAT	C-Flag check reverse primer
499	<i>klmt-1</i>	ACTGCCAAAGTGCTCACCTAA	C-Flag check forward primer
498	<i>klmt-1</i>	TTTTCGTATTCGTCCGGAGCct	N-Flag check reverse primer
497	<i>klmt-1</i>	ATCGCATGCGCCTTAATACCG	N-Flag check forward primer
170	EG6180 Indel Chr.V	CACTGTTTCGAAAGTGGACGTC	EG6180 Indel Chr.V forward primer
169	EG6180 Indel Chr.V	AGACACTCTGAAACGTGCGTTG	EG6180 Indel Chr.V reverse primer
562	<i>fars-1</i>	GGATTGTCGTAGAGCGTCCAAC	C-Flag check forward primer
563	<i>fars-1</i>	ACTCGGTGATTCGACAACAGCAAT	C-Flag check reverse primer
564	<i>fars-1</i>	TCCGCATTTCTGTGTTCCAGA	<i>fars-1</i> short C-Flag check forward primer
565	<i>fars-1</i>	AACTCTGGTGATCCCTCGTTGG	<i>fars-1</i> short C-Flag check reverse primer
502	<i>fars-1</i>	ACCTGTTGCGCAAGTTATCGGT	<i>fars-1</i> short primer for sequencing
575	<i>kss-1</i>	tatcccatctgccagtggtga	N-HA tag check reverse primer
576	<i>kss-1</i>	taccgatgaagagggtgctgcc	N-HA tag check forward primer
578	<i>kss-1</i>	acgaaatgtgctgacttctcg	C-terminal mScarlet check reverse primer
577	<i>kss-1</i>	gtcttgcatcttcaagcgtca	C-terminal mScarlet check forward primer
271	<i>hsp-16.41</i>	TTTTCCGTCTGCGTCTCTTTGC	forward primer heatshock promoter for INK248/252
272	<i>klmt-1</i>	GATCCTTTTCCACCGCCGTTTT	reverse primer for INK248/252 located in <i>klmt-1</i>
304	flanking INK248/252 transgene	CGAAAAGAGGCAGAATGTGA	forward chr.II mosci left arm outside; INK248/252
327	flanking INK248/252 transgene	AAGCGGAATGTGAAAAATCG	reverse chr.II mosci left arm outside; INK248/252
305	flanking INK248/252 transgene	TTTTACAAGGACTTGGATAAATGG	reverse chr.II mosci left arm inside; INK248/252
617	flanking BN711 transgene	CAGGAGAGCAAGGACCAAAG	forward chr.IV left arm outside ; BN711
618	flanking BN711 transgene	TCCGAATCAGTTTTGGGAAC	reverse chr.IV right arm outside ; BN711
619	FLP	GTGGCCTTTGGGTCTTGTA	forward FLP exon1; BN711
50	<i>klmt-1</i>	ATGCCGAAATCAGCGACTTT	forward primer
63	<i>klmt-1</i>	TTAACTTCCATTGGATTCTGTG	reverse primer
188	<i>klmt-1</i>	ACCGGGTAGACAGGAAGATT	reverse primer <i>klmt-1</i> inside
294	plasmid background	CCTGCGTTATCCCTGATTCTGTGG	plasmid background p42Nat
191	<i>fars-1</i>	GGCTCGTCAACTTTACCAAT	reverse primer <i>fars-1</i> inside
1054	<i>kanMX</i>	tgccagagttgtttctgaa	forward primer inside
1055	<i>kanMX</i>	agtgacgactgaatccggtga	reverse primer inside
1056	<i>kanMX</i>	tcggtgagttttctcttcat	forward primer inside
48	<i>fars-3</i>	ATGCCAACCGTGGGAATCAAGA	forward primer
49	<i>fars-3</i>	TTAGAGGAACGGTCCACGTTG	reverse primer
179	AD	TGAAGATACCCCAACCAACC	GAL4 DNA activation domain
301	ADH1 terminator	CAGGAAAGAGTTACTCAAGAATAAGAA	reverse primer used for genotyping pGADT7-AD/pGBKT7-BD and <i>fars-1</i> in pAB0165
178	BD	GTTGACTGTATCGCCGGAAT	GAL4 DNA binding domain

Supplementary Table 13 Primers used for genotyping and sequencing in this study

Internal Number	Target Gene	Name	Primers sequence	Target Plasmid	Benchmark link
728	<i>fars-1</i>	(728) FW_FARS-1_PGK1_gibson	tgttcaatctgaaatcaatgataatctactgtccagctcgacaaa	pCEV-g2-Km	https://benchmarking.com/s/seq-9P9cfq7zcp9pWx9dmik
729	<i>fars-1</i>	(729) RV_FARS-1_PGK1_gibson	actttttacaacaataaaacaagatGACA GCGAAACTGCTGCTGTACAAAC	pCEV-g2-Km	https://benchmarking.com/s/seq-Y7dW03FT5nQLcQV7UJ
730	<i>fars-1</i>	(730) FW_FARS-3_TEF1_gibson	gcaatcaatcaatgatttaataaacaagATGCCAACCGTGGGAAATCAAG	pCEV-g2-Km	https://benchmarking.com/s/seq-FngzPwV3Y2v6uf6H800
731	<i>fars-3</i>	(731) RV_FARS-3_TEF1_gibson	tggaaatcaactctgtttccatgTTA GAGAACCGTTCCACGT	pCEV-g2-Km	https://benchmarking.com/s/seq-W5sCSypvU2e6k16zmx
755	<i>pGal1:10</i>	(755) FW_FARS-3b_pGal1_homology	agctccaacggggtggggggggcctctctgaaagataagattgaagaccgccc	p42Nat	https://benchmarking.com/s/seq-xCoFnY4a8BG779P7Bx03
756	<i>pGal1:10</i>	(756) RV_pGal1_Fars-3B_homology	GTTGTTCCGAAAGTCGCTGATTTCCGACATGttttttctctgagcttaagat	p42Nat	https://benchmarking.com/s/seq-55jJM5t0d6vUM8j280I
757	<i>klmt-1</i>	(757) FW_FARS-3b_pGal1_homology	ctataacttaacgtcaaggagaaacaatGTCGAAAATCAAGCACTT	p42Nat	https://benchmarking.com/s/seq-F7co0hmHMF7zamET5MY
758	<i>klmt-1</i>	(758) RV_FARS-3b_p42Nat_homology	tta ca tga ct c at g a t t g a a t g a t a t a a c t t c c a t t g g a t t c g t g	p42Nat	https://benchmarking.com/s/seq-F7co0hmHMF7zamET5MY
803	<i>cul1</i>	FW_CUL1_pgADT7	GATTACGCTCATATGGCCATGGAGCCAGTGaaATGACAAACCCAGCCAG	pGADT7-AD	https://benchmarking.com/s/seq-dRaQ8kBg8v40hbRpxYbi
805	<i>cul6</i>	FW_Cul6_pgADT7	TTACGCTCATATGGCCATGGAGCCAGTGaaATGTTGGTCTCGGAAATGGCGA	pGADT7-AD	https://benchmarking.com/s/seq-TpXdyPcLkps25VnxLUA
807	<i>sel10</i>	FW_SEL10_pgADT7	TTACGCTCATATGGCCATGGAGCCAGTGaaATGTTGGTCTCGGAAATGGCGA	pGADT7-AD	https://benchmarking.com/s/seq-49i1p0E5j3JlMmn08BS17
798	<i>skr1</i>	FW_SKR1_pgBK17	TCTCAGAGGAGACTGCATATGGCCATGGCCGCTGCTGACTACTCTCACTGCT	pGBK17-BD	https://benchmarking.com/s/seq-Nsu3FCJLAh3VtvsHAFXp
799	<i>skr7</i>	FW_SKR7_pgBK17	CAGAGGAGACTGCATATGGCCATGGCCGCTGCTGACTACTCTCACTGCTT	pGBK17-BD	https://benchmarking.com/s/seq-1CcXnu726fbs3uS7up
801	<i>skr20</i>	FW_SKR20_pgBK17	TCAGAGGAGACTGCATATGGCCATGGCCGCTGCTGACTACTCTCACTGCTA	pGBK17-BD	https://benchmarking.com/s/seq-kBgZUFeAUl7PqWz3aAF
804	<i>cul1</i>	RV_CUL1_pgADT7	TGGGGGTTTTCA GATCTACGATTCATTCGCA GCTTAGCGGATGTA TTTGAGAC	pGADT7-AD	https://benchmarking.com/s/seq-dRaQ8kBg8v40hbRpxYbi
806	<i>cul6</i>	RV_Cul6_pgADT7	TGGGGGTTTTCA GATCTACGATTCATTCGCA GCTTAGCGGATGTA TTTGAGAC	pGADT7-AD	https://benchmarking.com/s/seq-TpXdyPcLkps25VnxLUA
808	<i>sel10</i>	RV_SEL10_pgADT7	AGTATCTACGATTCATTCGCA GCTTAGCGGATGTA TTTGAGAC	pGADT7-AD	https://benchmarking.com/s/seq-49i1p0E5j3JlMmn08BS17
799	<i>skr1</i>	RV_SKR1_pgBK17	TTATGCTAGTATGCGGCGCTGCAGGTTAACTCTCGCACAGCGCTT	pGBK17-BD	https://benchmarking.com/s/seq-Nsu3FCJLAh3VtvsHAFXp
800	<i>skr7</i>	RV_SKR7_pgBK17	GCTAGTATGCGGCGCTGCAGGTTAAAGGGAGACTGGTCTCTCCGAAATCTCAAG	pGBK17-BD	https://benchmarking.com/s/seq-Ccxnu726fbs3uS7up
802	<i>skr20</i>	RV_SKR20_pgBK17	TAGTATGCGGCGCTGCAGGTTAAAGGGAGACTGGTCTCTCCGAAATCTCAAG	pGBK17-BD	https://benchmarking.com/s/seq-kBgZUFeAUl7PqWz3aAF
155	<i>klmt-1</i>	(155) FW_NIC203_fars3b(TOX)_Gibson_AD	ACGCTCATATGGCCATGGAGCCAGTGaaATGTCGAAAATCAAGCACTT	pGADT7-AD	https://benchmarking.com/s/seq-9BrespXlkyHOFd9mdCe ; https://benchmarking.com/s/seq-qZosUjGno86vH8MjFcoz ;
744	<i>klmt-1</i>	(744) RV_FARS-3b[1:47]_Gibson_AD	GCGGGGTTTTCA GATCTACGATTCATTCGCA GCTTAGCGGATGTA TTTGAGG	pGADT7-AD	https://benchmarking.com/s/seq-9BrespXlkyHOFd9mdCe ; https://benchmarking.com/s/seq-158brHvfmKt7Wkcsdf ;
745	<i>klmt-1</i>	(745) Fw_fars-3b[48:250]_Gibson_AD	ACGCTCATATGGCCATGGAGCCAGTGaaATGTCGAAAATCAAGCACTT	pGADT7-AD	https://benchmarking.com/s/seq-9BrespXlkyHOFd9mdCe ; https://benchmarking.com/s/seq-158brHvfmKt7Wkcsdf ;
742	<i>klmt-1</i>	(742) RV_fars-3b[48:150]_Gibson_AD	GCGGGGTTTTCA GATCTACGATTCATTCGCA GCTTAGCGGATGTA TTTGAGG	pGADT7-AD	https://benchmarking.com/s/seq-9BrespXlkyHOFd9mdCe ; https://benchmarking.com/s/seq-158brHvfmKt7Wkcsdf ;
745	<i>klmt-1</i>	(745) Fw_fars-3b[48:250]_Gibson_AD	ACGCTCATATGGCCATGGAGCCAGTGaaATGTCGAAAATCAAGCACTT	pGADT7-AD	https://benchmarking.com/s/seq-9BrespXlkyHOFd9mdCe ; https://benchmarking.com/s/seq-158brHvfmKt7Wkcsdf ;
674	<i>klmt-1</i>	(674) RV_fars-3b[1:250]_Gibson_AD	GCGGGGTTTTCA GATCTACGATTCATTCGCA GCTTAGCGGATGTA TTTGAGG	pGADT7-AD	https://benchmarking.com/s/seq-9BrespXlkyHOFd9mdCe ; https://benchmarking.com/s/seq-158brHvfmKt7Wkcsdf ;
743	<i>klmt-1</i>	(743) Fw_fars-3b[151:250]_Gibson_AD	ACGCTCATATGGCCATGGAGCCAGTGaaATGTCGAAAATCAAGCACTT	pGADT7-AD	https://benchmarking.com/s/seq-9BrespXlkyHOFd9mdCe ; https://benchmarking.com/s/seq-158brHvfmKt7Wkcsdf ;
746	<i>klmt-1</i>	(746) Fw_FARS-3b[251:400]_Gibson_AD	ACGCTCATATGGCCATGGAGCCAGTGaaATGTCGAAAATCAAGCACTT	pGADT7-AD	https://benchmarking.com/s/seq-9BrespXlkyHOFd9mdCe ; https://benchmarking.com/s/seq-158brHvfmKt7Wkcsdf ;
156	<i>klmt-1</i>	(156) RV_NIC203_fars3b(TOX)_Gibson_AD	GCGGGGTTTTCA GATCTACGATTCATTCGCA GCTTAGCGGATGTA TTTGAGG	pGADT7-AD	https://benchmarking.com/s/seq-9BrespXlkyHOFd9mdCe ; https://benchmarking.com/s/seq-158brHvfmKt7Wkcsdf ;
675	<i>klmt-1</i>	(675) RV_fars-3b[1:400]_Gibson_AD	GCGGGGTTTTCA GATCTACGATTCATTCGCA GCTTAGCGGATGTA TTTGAGG	pGADT7-AD	https://benchmarking.com/s/seq-9BrespXlkyHOFd9mdCe ; https://benchmarking.com/s/seq-158brHvfmKt7Wkcsdf ;
/	<i>ksr-1</i>	FW_NIC203_GeneX(ANT)_Gibson_BD	GCTGATCTCAGAGGAGGACTGCATATGGCCATGGCCGCTGCTGCTTCAATTC	pGBK17-BD	https://benchmarking.com/s/seq-bzCSlQnQ00VAE1RRH8G
/	<i>ksr-1</i>	RV_NIC203_GeneX(ANT)_Gibson_BD	GGTATGCTAGTATGCGGCGCTGCAGCTAGAGTTGCTTCTTGAACAGTCA	pGBK17-BD	https://benchmarking.com/s/seq-bzCSlQnQ00VAE1RRH8G
/	<i>fars-1</i>	FW_NIC203_fars1_Gibson_BD	CTGATCTCAGAGGAGGACTGCATATGGCCATGGCCGCTGCTGCTTCAATTC	pGBK17-BD	https://benchmarking.com/s/seq-ubiTm7T5skbrOjWlUnAx
/	<i>fars-1</i>	RV_NIC203_fars1_Gibson_BD	GTTA TGCTAGTATGCGGCGCTGCAGGTTACTTGTCCAGTCCGAAATTTG	pGBK17-BD	https://benchmarking.com/s/seq-ubiTm7T5skbrOjWlUnAx

Supplementary Table 14. Primers used for cloning in this study